Research Square

Preprints are preliminary reports that have not undergone peer review.
They should not be considered conclusive, used to inform clinical practice,
or referenced by the media as validated information.

Phosphatidylethanolamine lipids secreted by CD8+ T cells mediate cytotoxic immunity

Chenqi Xu

cqxu@sibcb.ac.cn

Shanghai Institute of Biochemistry and Cell Biology https://orcid.org/0000-0002-4968-6782

Zhaolin Cheng

Shanghai Institute of Biochemistry and Cell Biology

Xinyu Ke

Shanghai Institute of Biochemistry and Cell Biology

Xi Chen

Interdisciplinary Research Center on Biology and Chemistry, Shanghai Institute of Organic Chemistry, Chinese Academy of Sciences, Shanghai https://orcid.org/0000-0001-5276-2013

Wei Wu

Institute of Biochemistry and Cell Biology, Chinese Academy of Sciences, Shanghai

Kexin Cao

State Key Laboratory of Molecular Biology, Shanghai Institute of Biochemistry and Cell Biology, Center for Excellence in Molecular Cell Science, Chinese Academy of Sciences

Haolin Xiong

Shanghai Institute of Organic Chemistry

Zhihan Zhang

Shanghai Institute of Biochemistry and Cell Biology

Ziyue Ma

Shanghai Institute of Immunity and Infection

Caiwan Xiong

Shanghai Institute of Immunity and Infection

Xiangyan Xu

Shanghai Institute of Biochemistry and Cell Biology

Zhengxu Ren

Shanghai Institute of Biochemistry and Cell Biology

Chengsong Yan

Shanghai Institute of Biochemistry and Cell Biology, Chinese Academy of Sciences

Haochen Yang

Shanghai Institute of Biochemistry and Cell Biology https://orcid.org/0000-0003-4273-5411

Xing He

Shanghai Institutes of Biochemistry and Cell Biology, Chinese Academy of Sciences
https://orcid.org/0009-0003-8209-3692

Lin Zheng
Shanghai Institutes of Biochemistry and Cell Biology, Chinese Academy of Sciences

Kexin Liu
Shanghai Institute of Biochemistry and Cell Biology, Chinese Academy of Sciences
https://orcid.org/0009-0008-3204-3140

Tao Liang
Hangzhou Institute for Advanced Study

Haopeng Wang
ShanghaiTech University

Guangchuan Wang
Chinese Academy of Sciences Center for Excellence in Molecular Cell Science https://orcid.org/0000-0001-5315-1599

Weiwei Yang
Chinese Academy of Sciences Center for Excellence in Molecular Cell Science

Hui Xiao
Institut Pasteur of Shanghai https://orcid.org/0000-0001-5304-243X

JIN ZHONG
Shanghai Institute of Immunity and Infection, Chinese Academy of Sciences

Catherine Wong
Department of Medical Research Center, State Key Laboratory of Complex Severe and Rare Diseases, Peking Union Medical College Hospital, Chinese Academy of Medical Science & Peking Union Medical Coll https://orcid.org/0000-0002-6855-2798

Zheng-Jiang Zhu
Shanghai Institute of Organic Chemistry https://orcid.org/0000-0002-3272-3567

Biological Sciences - Article

Keywords:

Posted Date: November 3rd, 2026

DOI: https://doi.org/10.21203/rs.3.rs-5625089/v1

License: This work is licensed under a Creative Commons Attribution 4.0 International License.
Read Full License

Additional Declarations: There is **NO** Competing Interest.

Phosphatidylethanolamine lipids secreted by CD8$^+$ T cells mediate cytotoxic immunity

ABSTRACT

Current understanding of T-cell immunity largely focuses on protein factors responsible for immune surveillance and regulation, with limited exploration of the roles played by other molecular types. While proteins such as perforin and granzymes are well-established mediators of CD8$^+$ T cell cytotoxicity[1-5], our study uncovers the cone-shaped phosphatidylethanolamine (PE) lipids as a new class of effector molecules with broad cytotoxic functions against tumor and infected cells. Upon activation, CD8$^+$ T cells upregulated the *de novo* biosynthesis pathway to produce substantial amounts of PE lipids carrying polyunsaturated or monounsaturated fatty acid sidechains. The newly synthesized PE lipids were packaged into vesicular compartments distinct from Lamp1$^+$ granules, rapidly polarized to immunological synapses, and secreted through the membrane fusion protein Munc13-4, generating PE$^+$ extracellular vesicles enriched in synaptic lipids and proteins. CD8-derived PE lipids were efficiently taken up by target cells and transported to the endoplasmic reticulum via Esyt1, where excessive PE loading induced ER stress-mediated cell death that is interconnected with other cell death pathways. The PE pathway functioned independently of conventional cytotoxic mechanisms and remained effective even when those pathways were absent. Manipulation of the PE-Esyt1-ER stress axis markedly altered T cell cytotoxicity, and ethanolamine pretreatment of T cells enhanced the efficacy of adoptive cell therapy. These findings introduce a new lipid-based mechanism of cytotoxic immunity and underscore the importance of non-protein molecules as immune effectors.

INTRODUCTION

T cells play crucial roles in immune surveillance and regulation, maintaining health and modulating disease responses[6,7]. The protein factors involved in T-cell immunity, including cytokines, chemokines, and toxins have been extensively characterized. Specifically, $CD8^+$ T cells utilize three primary protein-mediated pathways to exert cytotoxicity: the perforin/granzyme pathway, the Fas/FasL pathway and the cytokine-dependent pathways[1-5]. In the perforin/granzyme pathway, perforin proteins released by $CD8^+$ T cells form pores in the target cell membrane, allowing granzymes to enter and cleave procaspases or gasdermins to induce apoptosis or pyroptosis[8-10]. The Fas/FasL pathway involves FasL expressed on $CD8^+$ T cells binding to Fas on target cells, triggering Caspase 8 activation and leading to apoptosis[11,12]. In the cytokine pathways, IFNγ interacts with the IFNγ receptor 1 (IFNGR1)-IFNγ receptor 2 (IFNGR2) complex, initiating Janus Kinase activation and promoting ferroptosis[13]. Additionally, tumor necrosis factor (TNF) family members bind TNF receptor 1 (TNFR1) to induce cell death[14].

While the protein effectors of T-cell immunity are well understood, less is known about the potential immunological roles of non-protein molecules secreted by T cells. In contrast, non-protein molecules secreted by tumor cells have been recognized for their sophisticated immunoregulatory functions[15-19]. In this study, we sought to investigate the non-protein mechanisms of T-cell immunity, specifically focusing on lipid molecules secreted by $CD8^+$ T cells. Through mass spectrometry-based lipidomics, we identified phosphatidylethanolamine (PE) lipids as a new class of cytotoxic molecules. We then performed mechanistic studies to elucidate the vesicular secretion pathway of PE lipids and their cytotoxic effects on target cells. Finally, we assessed the functional relevance of PE-mediated cytotoxicity in the context of antitumor immunity.

MAIN

Activated $CD8^+$ T cells secrete phosphatidylethanolamine (PE) lipids with cytotoxic functions

To study the functional importance of unconventional effectors, we set up a toxin-null system to remove the conventional cytotoxic pathways, including perforin, IFNG, TNF, and FAS (Extended Data Fig. 1a). Perforin was knocked out in T cells and *Ifngr1/Tnfr1* were both knocked out in B16F10 tumor cells that have intrinsic deficiency of *Fas* (Extended Data Fig. 1b-c). Killing of B16F10 cells by $CD8^+$ T cells persisted even in the absence of conventional cytotoxic effectors (Extended Data Fig. 1d). Conditioned media collected from activated $CD8^+$ T cells (activated conditioned media, CD8 ACM) but not activated $CD4^+$ T cells exhibited evident cytotoxicity (Extended Data Fig. 1e). Importantly, CD8 ACM exerted cytotoxic functions under this toxin-null condition (Extended Data Fig. 1f). In addition to genetic manipulations, we also tried blockade antibodies to neutralize conventional cytotoxic pathways and obtained similar results of ACM killing (Extended Data Fig. 1g). Cell death induced by perforin-KO CD8 ACM occurred rapidly after 1 hour (Extended Data Fig. 1h-i). These data suggest that $CD8^+$ T cells might secret unconventional effectors to exert cytotoxic functions. Notably, lipid extracts from the CD8 ACM exerted robust cytotoxicity (Extended Data Fig. 1j). Consistently, non-specific depletion of lipids using fumed silica[20] markedly reduced the cytotoxicity of CD8 ACM (Extended Data Fig. 1k-l). We also analyzed conditioned media of human CAR-T cells derived from two donors. Like mouse $CD8^+$ T cells, CAR-T ACM induced tumor cell death, and lipid depletion reduced this effect (Extended Data Fig. 1m). These data support that activated $CD8^+$ T cells can secrete cytotoxic lipids to kill target cells.

To identify the lipid species responsible for cytotoxicity, we performed non-targeted LC-MS-based lipidomics analysis of ACM from mouse $CD8^+$ T cells stimulated by either tumor cells or CD3/CD28 antibodies (Fig. 1a, Supplementary Table 1 and 2). Conditioned media from naïve $CD8^+$ T cells (NCM) or tumor cells (Tumor CM) were collected as controls. Notably, Phosphatidylethanolamine (PE) lipids were specifically enriched in the CD8 ACM under both stimulation conditions, but not in the NCM or Tumor CM (Fig. 1a). Lipidomic analysis revealed that PE levels were markedly elevated in tumor interstitial fluid (TIF) of B16F10 tumor on C57BL/6 mice (~150 μM), when compared with PE levels in mouse serum (~50 μM) (Extended Data Fig. 2a). PE levels in CD8 ACM approached ~ 6 μM, which was much higher than blank medium (~ 0.5 μM) (Extended Data Fig. 2b). Notably, CD8 ACM represents a spatially averaged and diluted pool of secreted PE lipids, which likely accounts for the lower PE concentrations observed in ACM compared with TIF derived from tumors with densely compacted multicellular architecture. When applied at physiologically relevant concentrations (2.5-30 μg/mL, corresponding to ~3-40 μM)[21,22], PE lipids displayed significant cytotoxicity against tumor cells and cell death could occur rapidly (Fig. 1b, Extended Data Fig. 2c-d), though the PE uptake efficiency of solubilized PE treatment was lower than that of CD8 ACM treatment (Extended Data Fig. 2e). In contrast, other enriched lipids like PG, LPG, and HexCer exhibited limited cytotoxicity (Extended Data Fig. 2f). To further confirm the cytotoxic role of PE, we specifically depleted PE using duramycin[23-25], a widely used PE binding peptide (Extended Data Fig. 2g). Removal of PE led to an evident reduction in tumor killing by CD8 ACM (Fig. 1c).

More than 70% of PE lipids secreted by mouse $CD8^+$ T cells contained poly-unsaturated fatty acids (PUFAs), approximately 30% contained mono-unsaturated fatty acids (MUFAs), and less than 1% contained saturated fatty acids (Fig. 1d). These fatty acids were connected to the ethanolamine headgroup through either acyl or ether backbones. The intracellular PE compositions of activated mouse $CD8^+$ T cells mirrored this secretion profile: 84% PUFA-PE, 12% MUFA-PE, and 3% SFA-PE (Extended Data Fig. 3a). PE secretion appeared specific to activated $CD8^+$ T cells, as activated $CD4^+$ T cells did not secrete PE (Extended Data Fig. 3b-c). Human CAR-T cells also secreted PE lipids upon stimulation, with approximately 90% PUFA-PE and 10% MUFA-PE (Fig. 1e, Supplementary Table 3). It is worthy to mention that human CAR-T cells predominantly exhibit a $CD8^+$ phenotype during the early phase response[26]. Similarly, human NK cells secreted PE lipids, with 67% PUFA-PE and 33% MUFA-PE species (Extended Data Fig. 3d-e). We selected the most abundant PE species in CD8 ACM (PE P-18:0/20:4) and several other enriched PE species to cover structural diversity of natural PE (Extended Data Fig. 3f, Supplementary Table 4). Both PUFA-PE and MUFA-PE species (with either acyl or ether backbone) induced phosphatidylserine exposure (Annexin V^+) and cell death (Fig. 1f-g, Extended Data Fig. 3h-i), with PUFA-PEs showing more pronounced effects. In contrast, the most abundant PC species in CD8 ACM (PC 16:0/18:1 and 18:0/18:1), exhibited limited cytotoxicity (Fig. 1f-g, Extended Data Fig. 2f, Extended Data Fig. 3g). We also compared PC and PE lipids with matched sidechains and observed stronger cytotoxicity of PE (Extended Data Fig. 3j). Given the presence of tumor cells in both tissue and circulation[27], we evaluated the cytotoxicity of PE lipids on both attached and detached tumor cells. Broad antitumor functions of PE were observed for mouse and human tumor cells, either at attached or detached conditions (Fig. 1h-j, Extended Data Fig. 3k-m). Additionally, PE impaired sphere formation of detached tumor cells (Fig. 1k). Finally, we assessed the cytotoxic effects of PE lipids on virus-infected cells, observing target cell death and suppression of viral load (Extended Data Fig. 4a-c). Similar to perforin[28,29], PE also killed non-cancerous cells including T cells themselves, but the cytotoxic efficacy was markedly lower compared to tumor cells (Extended Data Fig. 4d-e).

CD8-secreted PE lipids are enriched in extracellular vesicles carrying lipids and proteins from the immunological synapse

Despite its high absolute abundance, plasma PE did not cause cytotoxicity, suggesting that PE toxicity is not solely determined by concentration. In plasma, PE are mainly present together with abundant PC lipids in lipoproteins and appropriate PE:PC ratio might prevent cytotoxicity[30]. We thus measured the PE:PC ratios of murine plasma, TIF, blank medium, and CD8 ACM. Murine plasma and blank medium displayed low PE:PC ratios (~1:40), whereas the ratios were substantially elevated in TIF (~1:5) and CD8 ACM (~1:6.5) (Extended Data Fig. 5a), consistent with the enrichment of PE relative to PC. To directly test whether the PE:PC ratio modulates PE cytotoxicity, we prepared liposomes with varying PE:PC ratios (Extended Data Fig. 5b). PE concentration was fixed at 6 μM, corresponding to that measured in CD8 ACM, while the PE:PC ratios were set at 1:40, 1:6.5, 1:5, 1:2.5, and 1:0. At a PE:PC ratio of 1:40, mimicking mouse plasma and blank medium conditions, the PE:PC liposome even promoted cell growth, likely by supplying more lipids as membrane building blocks. In contrast, increasing the PE:PC ratios beyond 1:6.5, corresponding to conditions relevant to CD8 ACM and TIF, resulted in evident cytotoxicity, with higher PE:PC ratios inducing stronger effects (Extended Data Fig. 5b). To understand the PE forms in CD8 ACM, we employed ultrafiltration to separate large particles and soluble fraction[31].The fraction > 100KD killed target cells (Extended Data Fig. 5c), while the fraction < 3KD had no cytotoxicity (Extended Data Fig. 5d). A kit purifying EVs/lipoprotein confirmed that cytotoxic PE lipids were enriched in large particles but not in soluble form (Extended Data Fig. 5e-f).

To further define the physicochemical properties and molecular compositions of PE-containing particles, we fractionated CD8 ACM according to size and density. Cultures were subjected to sequential centrifugation and PEG8000 precipitation to obtain small EV/lipoprotein fractions and large EV fractions. Each fraction was then separated into 14 subfractions (S1-14 and L1-14) by sucrose gradient ultracentrifugation (Extended Data Fig. 5g-h). PC lipids were mainly detected in subfractions S2-4 (~50 nm), together with cholesterol ester (CE) and triacylglycerol (TAG), the major components of LDL. The densities of these subfractions ranged from ~ 1.02033 to 1.07490 g/cm^3, which is comparable to that of LDL (~1.019-1.063 g/cm^3)[32]. PE lipids, however, were mainly enriched in S12-13 (~200 nm) and L14 (~950 nm) (Extended Data Fig. 5g-h, Extended Data Fig. 6a-b). L14 subfraction had the polymer dispersity index (PDI) value larger than 0.7, showing that large PE$^+$ EVs had substantial size variations. In contrast, S12-13 subfractions had the PDI values lower than 0.3, reflecting that small PE$^+$ EVs were more homogenous in size (Extended Data Fig. 6a-b). The small and large PE$^+$ EVs shared similar lipid compositions, including diacylglycerol (DAG), Hexosylceramides (HexCer), and PG (Extended Data Fig. 5g-h). Notably, PE, DAG, and HexCer are all enriched in T-cell immunological synapses[33-37]. Importantly, both small and large PE$^+$ EVs contained low levels of PC lipids and exhibited a high PE:PC ratio of approximately 1:2 (Extended Data Fig. 6a-b). Both small and large PE$^+$ EVs exhibited similar zeta potentials (~ -8mV) and densities (~1.2 g/cm^3) (Extended Data Fig. 6a-b). PE$^+$ EVs had higher densities than PC subfractions, suggesting a higher proportion of proteins. Consistent with the fractionation data, SIM imaging revealed that PE$^+$ EVs had the diameters ranging from sub-micrometer to micrometer (Extended Data Fig. 6c). Moreover, PE$^+$ EVs lacked Lamp1 and CD45 signals and they did not contain biomarkers of apoptotic bodies (Extended Data Fig. 6c-e).

We further characterized the protein profiles of CD8-secreted PE$^+$ EVs by duramycin capture and proteomics analysis. A total of 181 proteins were identified to be specifically enriched in CD8-derived PE$^+$ EVs, not in tumor-derived counterparts (Extended Data Fig. 7a, Supplementary Table 5). The protein list had minor overlap with the conventional supramolecular attacking particles (SMAP) complex[5,38,39] (Extended Data Fig.

7b, Supplementary Table 5). Importantly, the conventional cytotoxic proteins, such as perforin, granzyme, IFNγ, and TNFα, were not found in PE^+ EVs. Caspase family members were also absent. Instead, an enrichment of immunological synapse proteins was observed, including LFA-1 (integrin aLb2), CD3ζ, CD28, and CD2 (Extended Data Fig. 7c). CD45, which is excluded from the synapse[40], was not detected. The t-SNARE and v-SNARE complexes mediating membrane fusion[41,42] were also enriched in PE^+ EVs (Extended Data Fig. 7c). FACS analysis confirmed the presence of LFA-1 and the absence of cytotoxic proteins and phosphatidylserine (Extended Data Fig. 7d). LFA-1 interaction with the ligand ICAM is a major driving force of immunological synapse formation[43], which may also facilitate the cell targeting of PE^+ EVs. Some tumor cells naturally express ICAMs[44]. Moreover, IFNγ treatment induced ICAM expression in low-expressing tumor cells[45,46]. Blockade of LFA-1 substantially reduced the cytotoxicity of conditioned media of both mouse $CD8^+$ T cells and human CAR-T cells (Extended Data Fig. 7e-g). Thus, LFA-1-mediated cell targeting might serve as a tropism mechanism of PE^+ EVs during $CD8^+$ T cell killing.

PE vesicles are secreted at immunological synapse in a manner independent of conventional cytotoxic granules

We next investigated the mechanisms underlying PE lipid production in $CD8^+$ T cells. The *de novo* biosynthesis pathway in the endoplasmic reticulum (ER), known as the CDP-ETA pathway, contributes to the general cellular PE pool, whereas the salvage pathway, mediated by phosphatidylserine decarboxylase (Pisd), generates PE specifically within mitochondria[47] (Fig. 2a). Notably, mouse $CD8^+$ T cells expressed genes of the *de novo* pathway, whereas Pisd expression was minimal. Upon stimulation with anti-CD3/CD28 or anti-CD3 alone, *de novo* pathway genes were strongly upregulated, while Pisd remained at a minimal level (Fig. 2b, Extended Data Fig. 8a). Consistently, blockade of TCR signaling with the Src family kinase inhibitor PP2[48] significantly reduced PE secretion by mouse $CD8^+$ T cells (Extended Data Fig. 8b). Similarly, in human CAR-T cells stimulated by tumor cells, the *de novo* PE biosynthesis pathway was upregulated (Fig. 2c). By contrast, human tumors generally downregulate Pcyt2, a key enzyme in the CDP-ETA pathway, and some tumor types also downregulate Pisd (Extended Data Fig. 8c-d). Together, these findings reveal opposite patterns of PE production in activated $CD8^+$ T cells versus tumor cells.

The conventional cytotoxic effector molecules, such as perforin and granzymes, are loaded into $Lamp1^+$ cytotoxic granules and released at the immunological synapses[57]. In naive $CD8^+$ T cells, PE signals were typically at the plasma membrane (PM) (Fig. 2d left), consistent with its structural roles in building the cell membrane. After cell activation, PE signals were enriched to vesicular structures that did not colocalize with the $Lamp1^+$ granules (Fig. 2d right, Fig. 2e, Extended Data Fig. 8e). Apart from partial overlap with ER, PE^+ vesicles showed minimal colocalization with other organelles or canonical cytotoxic effectors in $CD8^+$ T cells (Extended Data Fig. 9a–f). Similar to $Lamp1^+$ granules, PE vesicles rapidly polarized to T–tumor contact sites within short time, thereby exhibiting reduced overlap with the ER (Fig. 2f, Extended Data Fig. 9g-i). TIRF microscopy of $CD8^+$ T cells stimulated on supported lipid bilayers further confirmed the polarization of PE vesicles at the immunological synapse (Fig. 2g). Notably, polarized PE vesicles and $Lamp1^+$ granules remained at different compartments, and knockout of perforin did not affect PE vesicle polarization (Extended Data Fig. 9j-k).

To further understand PE trafficking, we designed a strategy to identify PE-interacting proteins in $CD8^+$ T cells (Extended Data Fig. 10a). The PE headgroup contains a primary amino group, which can covalently crosslink with N-Hydroxy succinimide (NHS)[49]. Using this chemical reaction, we first coated NHS magnetic beads with three different types of PE lipids, including the most abundant PE (P-18:0/20:4) and two other

top species PE (18:0/20:4, P-18:0/18:1) in CD8 ACM (Extended Data Fig. 3f). Each type of PE-NHS magnetic bead was incubated with cell lysates of activated $CD8^+$ T cells or tumor cells to capture PE-binding proteins, which were subsequently analyzed by mass spectrometry (Extended Data Fig. 10b-c). The proteins interacting with all three types of PE beads were considered as common PE-binding proteins, and the experiment was repeated to validate the hits. After removing shared hits between $CD8^+$ T cells and tumor cells, 48 proteins were identified as PE-binding proteins specifically in $CD8^+$ T cell, including two proteins related to vesicles derived from endoplasmic reticulum (ER), i.e. Receptor expression-enhancing protein 3 (Reep3) and Reep4[50], and one protein involved in granule exocytosis and membrane fusion, Mammalian uncoordinated-13 Homolog 4 (Munc13-4)[51,52] (Fig. 2h, Supplementary Table 6-7). We observed colocalization of PE with Reep3 at vesicular structures, suggesting PE vesicles might originate from the ER (Fig. 2i-j, Extended Data Fig. 10d). However, Reep3 knockdown in OT-I T cells did not significantly impair PE levels in the ACM (Extended Data Fig. 10e). The killing function of Reep3-KD OT-I T cells was nearly similar to WT control (Extended Data Fig. 10f). Thus, Reep3 could serve as a biomarker but is dispensable for PE secretion. In contrast, inhibiting Munc13-4 by Bexin-1[53] decreased PE levels in CD8 ACM and concomitantly decreased PE abundance in CD8-derived EVs in a dosage-dependent manner (Fig. 2k, Extended Data Fig. 10g). Moreover, Bexin-1 treatment or Munc13-4 knockdown substantially impaired killing function of OT-I T cells (Extended Data Fig. 10h-i). While commercially available murine Munc13-4 antibody was not suitable for immunofluorescence imaging, we imaged Rab27a, a direct partner of Munc13-4 in mediating vesicle-membrane fusion[51,54]. A good colocalization of Rab27a and PE was observed in T cells, especially at the immunological synapse (Extended Data Fig. 10j). We next compared the secretion kinetics of perforin and PE and found that they accumulated in ACM within 4–8 hours after T cell stimulation (Extended Data Fig. 10k-l). Notably, ACM collected at 4 hours of T cell stimulation was already sufficient to induce tumor cell death, coinciding with PE release, and this effect was only modestly affected in perforin-deficient T cells (Extended Data Fig. 10m-n).

Intercellular transportation of CD8-derived PE lipids

Upon treatment of tumor cells with CD8 ACM, PE accumulation became detectable after 1 hour by mass spectrometry and progressively increased thereafter, largely independent of perforin (Extended Data Fig. 11a). To further examine the transportation of PE lipids from $CD8^+$ T cells to tumor cells, we designed a tracing experiment. $CD8^+$ T cells were first incubated with NBD-labeled ethanolamine, the precursor of PE synthesis, to fluorescently label the synthesized PE. After removal of residual NBD-ETA, $CD8^+$ T cells were co-cultured with tumor cells at varying effector-to-target cell ratios, followed by analysis of NBD fluorescence signals in both $CD8^+$ T cells and tumor cells using flow cytometry (Fig. 3a). The NBD fluorescence signal in tumor cells gradually increased with higher numbers of cocultured T cells, accompanied by a corresponding loss of NBD signals in T cells (Fig. 3b–d). Kinetic analysis revealed that NBD loss in T cells occurred as early as 1 hour, and NBD signals gradually accumulated in tumor cells (Extended Data Fig. 11b-c). In contrast, tumor cells cultured without T cells maintained stable NBD signals throughout the time course (Extended Data Fig. 11d). This fast kinetics of PE intercellular transportation was further corroborated by live-cell imaging (Extended Data Fig. 11e, Supplementary Movie 1). In the reciprocal experiment, NBD-labeled tumor cells retained their fluorescence after coculture with T cells. Correspondingly, T cells did not acquire NBD signals, even at a tumor-to-T cell ratio as high as 16:1 (Fig. 3e-h).

The directional transportation of PE lipids from $CD8^+$ T cells to tumor cells was confirmed by ^{13}C-isotype tracing. Detection of ^{13}C-PE lipids was performed by mass spectrometry, for which $CD8^+$ T cells and tumor

cells could not be simultaneously measured like flow cytometry. Therefore, a conditioned medium approach was employed to trace intercellular PE transportation (Fig. 3i, Extended Data Fig. 11f). $CD8^+$ T cells were activated by antibodies in the presence of ^{13}C-ETA, which was incorporated into the *de novo* synthesized PE (Figure. 3i-j). Lipidomic analysis of the conditioned medium confirmed the secretion of ^{13}C-PE lipids (Fig. 3k), and tumor cells treated with this conditioned medium exhibited robust ^{13}C-PE signals (Fig.3l). We also analyzed the transportation preference of newly synthesized PE from $CD8^+$ T cells to tumor cells, under the condition of target cell stimulation (Extended Data Fig. 11f). In $CD8^+$ T cells, 20-40% of intracellular PE lipids were synthesized *de novo* from ^{13}C-ETA (Extended Data Fig. 11g). Interestingly, labeled PE species accounted for approximately 60% of the total PE in CD8 ACM (Extended Data Fig. 11h). Moreover, ^{13}C-labeled PE in ACM were effectively taken up by tumor cells (Extended Data Fig. 11i). These results suggest that *de novo*-synthesized PE lipids are preferentially secreted compared with other PE pools.

Extended Synaptotagmin-1 (Esyt1) mediates PE cytotoxicity in target cells

To further understanding PE killing mechanism, we studied PE-binding proteins in tumor cells using the PE interactome assay described earlier (Extended Data Fig. 10a, Supplementary Table 8). Among the proteins commonly interacting with the three types of PE lipids, Esyt1 ranked the first for the enriched intensity (Fig. 4a). Previous studies have shown that Esyt1 is involved in the transportation of phospholipids, including PE lipids, from the PM to the ER[55-57]. To test its role in PE toxicity, we knocked down Esyt1 in B16F10 cells (Extended Data Fig. 12a). While Esyt1 deficiency did not affect cell proliferation (Extended Data Fig. 12b), it rendered tumor cells resistant to killing by PE lipids, CD8 ACM, and direct $CD8^+$ T cell attack, under both attached and detached conditions (Fig. 4b-e, Extended Data Fig. 12c-f). This resistance was consistent across PE lipids with different sidechains (Fig. 4f). In contrast, Esyt1-deficient tumor cells remained sensitive to staurosporine, an apoptosis inducer (Extended Data Fig. 12g). The importance of ESYT1 was further validated in human HCT116 colorectal cancer cells (Extended Data Fig. 12h), where ESYT1 deficiency conferred resistance to both PE lipids and MSLN-CAR-T cell–mediated killing (Extended Data Fig. 12i-j). Conversely, Esyt1-overexpressing (Esyt1-OE) cells displayed heightened sensitivity to PE lipids, CD8 ACM, and $CD8^+$ T cell–mediated killing (Fig. 4g–h, Extended Data Fig. 12k). Notably, Esyt1 deficiency also protected viral-infected cells from PE killing (Extended Data Fig. 12l).

In vivo studies further highlighted the role of Esyt1 (Fig. 4i). In a subcutaneous melanoma model, the Esyt1-deficient B16F10 tumor had accelerated progression compared to wild-type tumor in immunocompetent C57BL/6 mice (Fig. 4j), whereas the difference was minimal in immunodeficient B-NDG mice (Fig. 4k). Reversely, Esyt1 overexpression in B16F10 delayed the tumor growth (Fig. 4l). Although Esyt1 deficiency impaired the intrinsic migration and invasion of B16F10 cells (Extended Data Fig. 13a-d), it enhanced metastatic foci formation in a melanoma lung metastasis model (Fig. 4m). Notably, Esyt1-deficient tumors were resistant to killing by both wild-type and *Prf1*$^{-/-}$ OT-I T cells (Extended Data Fig. 13e). Under the toxin-null system, Esyt1 deficiency still accelerated tumor growth *in vivo* (Extended Data Fig. 13f-g). Together, these findings exclude a role for Esyt1 in conventional cytotoxic pathways and instead highlight its essential function in PE-mediated cytotoxicity.

Excessive PE induces endoplasmic reticulum (ER) stress in target cells

Previous studies find the PUFA-containing lipids, but not MUFA-containing lipids, can induce ferroptosis through lipid peroxidation, a process that can be enhanced by IFNγ[1,58,59]. Consistent with this framework, we found that PUFA-PEs enhanced lipid ROS levels in tumor cells (Extended Data Fig. 14a-b). Consistently, RSL3 or IFNγ-induced ferroptosis was sensitized by PUFA-PEs ((Extended Data Fig. 14c-e). Despite these

ferroptosis-sensitizing features, multiple lines of evidence show that PE-induced cell death is distinct from ferroptosis. Pharmacological inhibition of ferroptosis using ferrostatin-1, liproxstatin-1, or vitamin E[60] failed to rescue PE-induced cell death (Extended Data Fig. 15a-e). Similarly, overexpression of Gpx4 or Slc7a11, key mediator of ferroptotic resistance[61,62], did not alter tumor cell sensitivity to PE-induced cytotoxicity (Extended Data Fig. 15f-g). Morphologically, PE-treated cells displayed features that were distinguishable from RSL3-induced ferroptosis[63] or staurosporine-induced apoptosis[64] (Extended Data Fig. 15h). Furthermore, transcriptomic analysis revealed no induction of canonical ferroptosis signatures following PE treatment (Extended Data Fig. 15i). In addition, apoptosis biomarkers were not induced by PE treatment (Extended Data Figure 16a-c). Notably, canonical pyroptosis and necroptosis are unlikely to contribute to our system, as B16F10 cells lack caspase-1, Gsdmb/Gsdmd, and Ripk3 (Extended Data Figure 16d-e), rendering them intrinsically resistant to these two pathways. Gsdme/Gsdmc, mediators of noncanonical pyroptosis, were expressed but they were not activated upon PE treatment (Extended Data Figure 16f-g).

PE treatment of tumor cells induced rapid PE accumulation at the ER within 15-30 minutes (Fig. 5a–b), accompanied by colocalization of the PE signal with Esyt1 (Extended Data Fig. 17a-b). PE is a cone-shaped lipid species, owing to its smaller ethanolamine headgroup relative to its bulky acyl chains[65,66]. Consistent with previous studies showing PE induces curvature stress on the membrane[65], we found that PE-treated tumor cells had evident morphological changes of ER, including bended elongation and disordered distribution (Fig. 5c-d). Elevated signals from ER tracker staining further confirmed ER abnormalities in PE-treated cells, which could be rescued by Esyt1 deficiency (Fig. 5e).

Disturbed ER structure can trigger ER stress, which in turn activates pathways leading to cell death[67-70]. We next examined the contribution of ER stress in PE cytotoxicity. Transcriptional analysis of PE-treated tumor cells revealed gene signatures of ER stress and ER stress-induced cell death (Fig. 5f). Both MUFA-PE and PUFA-PE treatments resulted in similar changes (Extended Data Fig. 18a-b). The ER stress inhibitor Tauroursodeoxycholate (TUDCA)[71] effectively protected cells from PE-induced cell death (Fig. 5g). Similarly, tumor cells treated with CD8 ACM exhibited clear gene signatures of ER stress (Extended Data Fig. 18c). Blocking IFNγ, a cytokine known to induce ER stress in some tumor cells[72], mitigated typical IFNγ-responsive features, such as upregulation of Interferon Regulatory Factor 1 (IRF1) or antigen processing[73] (Extended Data Fig. 18d). However, blocking IFNγ did not alleviate the ER stress response induced by ACM (Extended Data Fig. 18c). Analysis of the ER stress-related genes showed that PE or CD8 ACM but not CD4 ACM treatment induced a dramatic upregulation of DNA damage-inducible transcript 3 protein (Chop), a key transcription factor in the process of cell death triggered by ER stress[74] (Fig. 5h, Extended Data Fig. 18c,e-f), which could be reversed by either global lipid or targeted-PE depletion (Extended Data Fig. 18g-j). PE treatment of tumor cells rapidly induced Chop expression, reaching a peak within 4–6 hours (Fig. 5i). Similarly, CD8 ACM triggered Chop expression as early as 1 hour (Extended Data Fig. 18k), consistent with the rapid kinetics of ACM-induced cell death (Extended Data Fig. 1h-i). Importantly, depletion of Chop rendered B16F10 cells more resistant to PE or ACM cytotoxicity (Fig. 5j, Extended Data Fig. 19a-c). Dual knockout of Esyt1 and Chop did not confer additional resistance to PE treatment beyond that observed in single knockouts (Extended Data Fig. 19d), supporting that Esyt1 and Chop function within the same pathway rather than in parallel pathways. This connection was further recapitulated in immune-competent mice (Extended Data Fig. 19e). Tumor-specific knockdown of either Esyt1 or Chop led to augmented tumor growth, while dual knockdown did not show an additional effect (Extended Data Fig. 19e).

Chop is induced primarily through three ER stress sensors: eukaryotic translation initiation factor 2-alpha

kinase 3 (Perk)[74,75], serine/threonine-protein kinase/endoribonuclease (Ire1α), and cyclic AMP-dependent transcription factor 6 (Atf6). Notably, Perk has been implicated as a lipid sensor[76,77], and the recruitment of Esyt1 by Perk was reported earlier[78]. *Perk*-knockdown tumor cells exhibited resistance to both PE- and ACM-induced cytotoxicity (Extended Data Fig. 19f-h), which was accompanied by diminished induction of Chop and Gadd34 in response to ACM (Extended Data Fig. 19i-j). Consistently, Esyt1 ablation abolished PE- or ACM-induced Chop and Gadd34 upregulation, whereas enforced Esyt1 expression further augmented Chop induction (Fig. 5k-l, Extended Data Fig. 20a-c). These data together established a mechanistic connection within the Esyt1-Perk-Chop axis. Notably, PE also induced ER stress in non-cancerous cells (Extended Data Fig. 20d). However, the basal ER stress levels in the non-cancerous cells were substantially lower than those in tumor cells (Extended Data Fig. 20e). In addition, PE treatment robustly induced CHOP and GADD34 expression in HCT116 tumor cells, while the induction was significantly lower in non-cancerous 293FT cells (Extended Data Fig. 20f). This difference provides an explanation for the lower sensitivity of non-cancerous cells to PE-induced cytotoxicity (Extended Data Fig. 4d).

At time points slightly later than the onset of ER stress, we observed mitochondrial dysfunction in ACM-treated tumor cells, characterized by increased mitochondrial ROS and decreased mitochondrial membrane potential (Extended Data Fig. 18k, Extended Data Fig. 21a-e). Inhibition of ER stress mitigated this mitochondrial dysfunction, supporting the upstream role of ER stress (Extended Data Fig. 21f-g). According to previous studies, ER stress is also coupled with ferroptosis in regulating cell death [79-81]. Chop knockdown markedly alleviated cell death induced by the ferroptosis inducer RSL3 or its combination with PE (Extended Data Fig. 21h). Furthermore, in Chop-deficient tumor cells, PE-induced cell death was partially rescued by ferroptosis or apoptosis inhibitor (Extended Data Fig. 21i).

Collectively, these findings indicate that PE lipids trigger ER stress-mediated cell death that is interconnected with other death pathways. When ER stress signaling is suppressed, alternative death programs become more prominent in mediating PE cytotoxicity.

PE cytotoxicity is crucial for T-cell antitumor immunity

To assess the physiological importance of PE cytotoxicity, we knocked down *Pcyt2* (Pcyt2-KD) to inhibit PE biosynthesis in mouse OT-I T cells (Extended Data Fig. 22a), which decreased both intracellular and secreted PE levels but did not affect cell proliferation (Extended Data Fig. 22b-d). Tumor killing of Pcyt2-KD OT-I T cells was significantly impaired, despite an increase in the production of conventional cytotoxic proteins (Extended Data Fig. 22e-f). Additionally, we used meclizine, a validated Pcyt2 inhibitor[82], to block PE biosynthesis in OT-I T cells, leading to reduced intracellular and secreted PE levels (Figure 6a, Extended Data Fig. 22g). Meclizine treatment attenuated ACM-induced ER stress and cytotoxicity in tumor cells (Figure 6b, Extended Data Fig. 22h-i). Meclizine treatment also impaired tumor killing in both mouse OT-I T cells and human MSLN CAR-T cells (Fig. 6c-d). *In vivo*, meclizine-pretreated OT-I cells exhibited diminished cytotoxicity against B16F10-OVA tumors (Extended Data Fig. 22j). Even in a toxin-null system where conventional cytotoxic pathways were absent, meclizine still suppressed T cell-mediated killing (Extended Data Fig. 22k-m).

A previous lipidomic study indicated that intratumoral $CD8^+$ T cells had reduced PE levels[83]. We therefore tested a strategy of pretreating T cells with ETA to enhance PE levels, before adoptive transfer therapy against solid tumors. OT-I T cells tolerated 1 mM ETA, which increased PE abundance while decreasing PC levels, shifting the PE:PC ratio from ~1:6.5 to ~1:2 (Extended Data Fig. 23a–b). In line with this, ETA-pretreated OT-I cells (ETA OT-I) secreted higher amounts of PE lipids upon activation (Fig. 6e), which led to more PE

uptake by tumor cells (Extended Data Fig. 23c). Conditioned medium from ETA OT-I cells induced stronger ER stress and tumor cell death than the untreated control (Fig. 6f, Extended Data Fig. 20a-c). ETA OT-I cells also displayed superior killing of B16F10-OVA cells (Fig. 6g), despite dampened TCR signaling and reduced amounts of TNFα and IFNγ (Extended Data Fig. 23d-f). Single-cell RNA sequencing and FACS analysis indicated a slight increase in T cell stemness following ETA treatment, although this was not evident in bulk RNA sequencing (Extended Data Fig. 24a-d). To exclude stemness as a major contributor, we measured T cell killing at 8 hours when stemness has minimal influence (Extended Data Fig. 24e-f). A substantial enhancement of acute cytotoxicity was observed, indicating that ETA primarily augments PE-mediated cytotoxicity. Notably, the augmenting effect of ETA persisted even in the absence of conventional cytotoxic molecules (Extended Data Fig. 24f-g). Mechanistically, the augmenting effect of ETA was critically dependent on Esyt1. Knockdown of Esyt1 largely abolished ETA-enhanced ER stress and tumor cell death (Extended Data Fig. 20a-b, Extended Data Fig. 25a), whereas Esyt1 overexpression further potentiated these responses (Extended Data Fig. 20c, Extended Data Fig. 25b). Extending this strategy to human MSLN CAR-T cells produced a similar enhancement in tumor killing (Fig. 6h). Finally, *in vivo* studies using ETA-pretreated OT-I or MSLN CAR-T cells in mouse melanoma and human colorectal cancer models demonstrated improved tumor control and prolonged survival (Fig. 6i-m). Notably, the *in vivo* augmentation effect of T-cell antitumor responses conferred by ETA pretreatment was abrogated in tumor models deficient in Esyt1 or Chop (Extended Data Fig. 25c-d). Collectively, these results highlight ETA pretreatment as a promising strategy to enhance T cell-mediated antitumor immunity.

DISCUSSION

Here, we uncover phosphatidylethanolamine (PE) lipids as a new class of cytotoxic effectors secreted by activated $CD8^+$ T cells, exhibiting broad cytotoxic effects against both tumor and infected cells. PE *de novo* biosynthesis is induced by TCR signaling. The newly synthesized PE lipids are packaged into vesicular compartments, secreted from immunological synapse via the membrane fusion protein Munc13-4, and transported to target cells efficiently. Esyt1 functions as a PE transporter in the target cells, mediating PE accumulation in the ER and triggering ER stress-induced cell death. Modulation of the PE-Esyt1-ER stress axis significantly impacts antitumor functions of T cells, influencing tumor progression in both mouse and human tumor models. Moreover, PE cytotoxicity could operate independently of the conventional cytotoxic pathways.

PE and PC are the most abundant phospholipids in mammalian cell membranes. PE has been shown to bind with membrane proteins such as CXCR5, regulating T cell differentiation[25]. Unlike PC that has a cylindrical shape, PE adopts a conical shape due to the difference in volume between its small head group and long, unsaturated sidechains[84]. PUFA sidechain can further expand lateral area[85], accentuating this conical geometry. When incorporated into membrane, PE induces negative curvature and membrane stress. Interestingly, tumor cells generally downregulate PE biosynthesis, leading to a reduction of PE lipids while an accumulation of the precursor phosphoethanolamine with pro-survival function under nutrient starvation[86]. In contrast, activated $CD8^+$ T cells synthesized and secreted PE^+ extracellular vesicles that are notably deficient of PC, which were efficiently transported to tumor cells and accumulated at ER through the PM/ER lipid transporter Esyt1. In tumor cells, the overloading of PE in the ER led to elongation and bending of the ER membrane, subsequently causing ER stress and cell death. Depletion of Esyt1, the ER stress sensor Perk, or the downstream effector Chop, could rescue tumor cells from PE cytotoxicity. Mitochondrial dysfunction was also observed during ACM killing, slightly later than ER stress. Inhibition

of ER stress alleviated mitochondrial dysfunction. While ER stress is crucial for the cytotoxicity of T-cell secreted PE lipids on wildtype tumor cells, alternative death pathways, particularly ferroptosis, make a more pronounced contribution when ER stress is compromised. Moreover, T-cell secreted PE lipids induce lipid peroxidation in tumor cells, which can sensitize other ferroptosis-inducing pathways in the tumor microenvironment[59,60,87,88]. Altogether, T cell-secreted PE lipids are capable of inducing multiple cell death pathways. Since tumor cells are highly heterogenous[88], these mechanisms might act together in the tumor microenvironment to mediate antitumor response.

PE lipids are synthesized via two pathways: the CDP-ETA *de novo* biosynthesis pathway contributing to cellular PE pool and the PSD salvage pathway specifically contributing to mitochondrial PE pool[47]. The *de novo* biosynthesis pathway, rather than salvage pathway, is highly expressed in activated $CD8^+$ T cells. Inhibition of Pcyt2, the rate-limiting enzyme in PE *de novo* biosynthesis, significantly reduced PE production and secretion, leading to markedly impaired cytotoxicity. The newly synthesized PE lipids were assembled into vesicular structures in T cells. Both PE vesicles and conventional cytotoxic granules polarized toward the immunological synapse with comparable kinetics, but they exhibited distinct spatial distributions. Cytotoxic granules are specialized lysosomal organelles enriched with perforin, granzymes, and the lysosome marker Lamp1[52]. In contrast, PE vesicles lacked Lamp1 signal, indicating non-lysosomal origin. Our interactome and imaging analyses revealed co-localization of PE vesicles with Reep3, a member of the Reep protein family, known for its role in ER-derived vesicles[50]. Since ER is the major site of PE biosynthesis, it is plausible that the newly synthesized PE lipids, with their conical shapes, could bud from the ER to form vesicles. Munc13-4, a mediator of membrane fusion[52], was also identified as a PE-binding protein in $CD8^+$ T cells. Both PE vesicles and conventional cytotoxic granules utilize the Munc13-4/Rab27a complex for membrane fusion. Secretion of cytotoxic granules is characterized by discharge of vesicular contents upon membrane fusion[51,54], while how PE lipids are secreted warrant further investigation. The enrichment of immunological synapse lipids and proteins within PE^+ EVs supports the notion that their membranes might originate from the synaptic membrane. Notably, previous reports show that T cells are capable of secreting vesicles that carry functional protein and RNA cargoes[89-92]. Here we reveal that functional lipids can also be secreted by the vesicular pathway. These PE-containing EVs varied in sizes while shared similar lipid compositions and physicochemical properties. The t-SNARE and v-SNARE complex enriched in PE^+ EVs might mediate vesicle-vesicle fusion to yield size heterogeneity[41,42,93,94]. PE lipids themselves could also promote vesicular fusion[95-98]. Importantly, PE^+ EVs carried LFA-1 with cell targeting functions. Blockade of LFA-1 significantly reduced ACM killing, supporting that PE^+ EVs have a tropism mechanism for cytotoxicity. The v-SNAREs might also promote vesicle fusion with target cells[42].

In summary, our study identifies a previously unrecognized pathway of lipid-mediated T cell immunity that functions independently of conventional protein-based cytotoxic mechanisms. By employing diversified cytotoxic strategies, T cells establish a comprehensive network to maintain effective immunosurveillance. Given that tumor and pathogen immune evasion from conventional cytotoxic pathways has been widely documented[99-103], the identification of this lipid-dependent mechanism provides a promising avenue for therapeutic intervention. Furthermore, our findings underscore the potential of lipid molecules as critical immune effectors with broad implications for health and disease.

Figures and legends

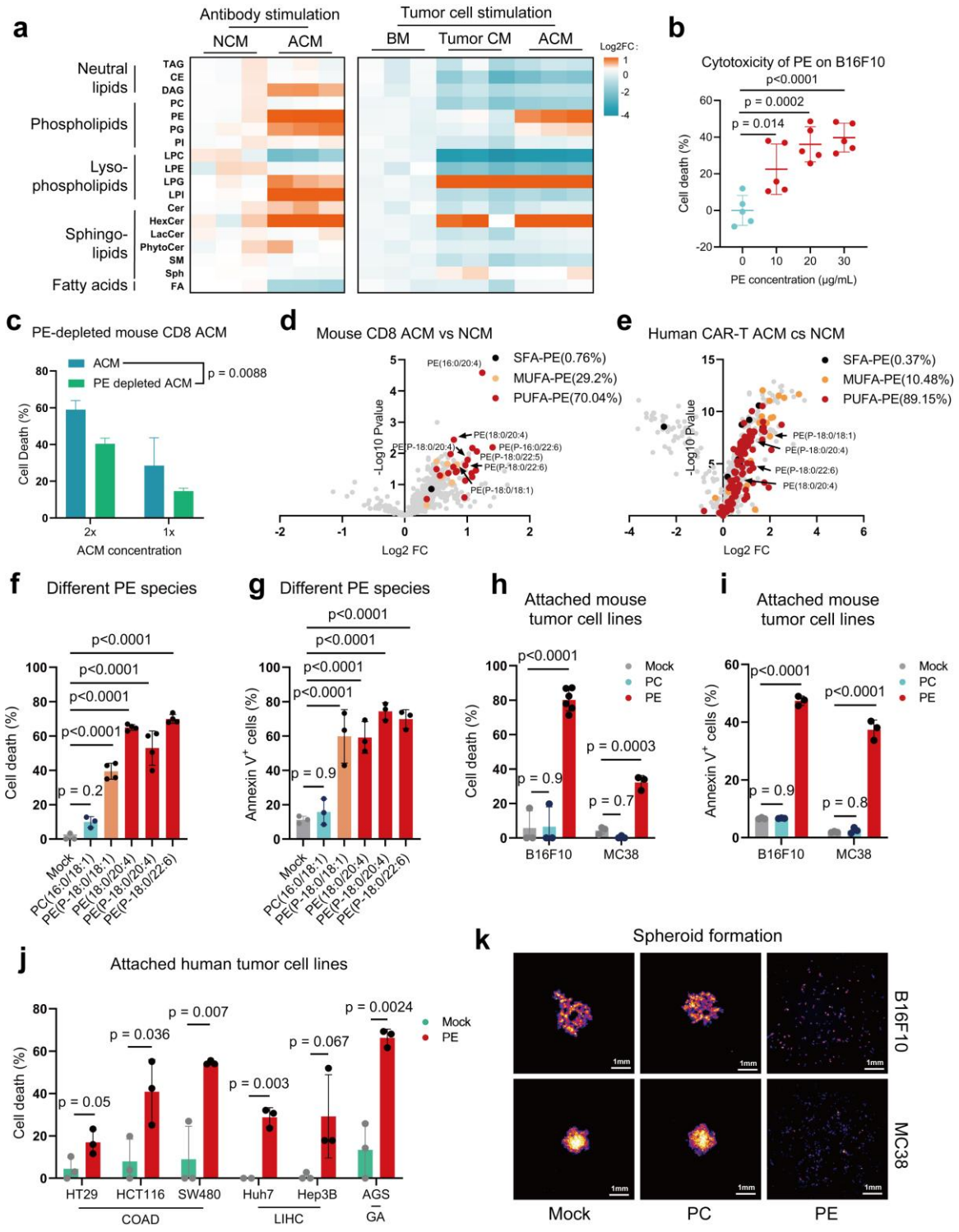


Figure 1. Phosphatidylethanolamine (PE) lipids secreted by CD8⁺ T cells had broad tumor killing functions

a, Relative abundance of lipid classes secreted by activated mouse CD8⁺ T cells, determined by LC-MS-based lipidomics. Class abundance, calculated as the summed ion counts of all lipid species within each class, is normalized to the controls. Identified lipid hits are categorized into 18 lipid classes and displayed in a heatmap. Each row represents a lipid class, and each column represents one sample. OT-I CD8⁺ T cells were either activated by tumor cells or antibodies and activated conditioned medium (ACM) were collected

for lipidomic and metabolic MS analysis. For the antibody stimulation, naïve $CD8^+$ T cells were isolated from mouse spleen, seeded onto the plate coated with anti-mCD3ε (10 μg/mL) and anti-mCD28 (10 μg/mL) and cultured in the fresh medium with IL-2 (10 ng/mL) for 48 hours, then the conditioned medium was collected. The control of antibody-stimulated CD8 ACM was medium collected from naïve $CD8^+$ T cells cultured with IL-7 (10 ng/mL) for 48 hours. For the condition of tumor cell stimulation, splenocytes from OT-I mice were firstly boosted with $OVA_{257–264}$ (N4) in the presence of IL-2 (10 ng/mL) for 48 hours to acquire pre-activated $CD8^+$ T cells. These cells were then mixed with B16F10-OVA cells at the effector cells: target cells (E:T) ratio = 2:1 in the fresh medium for 24 hours, followed by the collection of the conditioned medium. Tumor cell conditioned medium (Tumor CM) collected from B16F10-OVA cells cultured in fresh medium for 24 hours, and blank medium (BM) was used as a control. Medium samples were then analyzed via mass spectrometry (n = 3).

b, Cytotoxicity of phosphatidylethanolamine (PE) on attached B16F10 melanoma cells, at varied concentrations. After 24-hour treatment, cell death was evaluated by cell number count via flow cytometry (n = 5). Methanol was served as the solvent mock control.

c, Effect of PE depletion on the cytotoxicity of CD8 ACM. Mouse $CD8^+$ T cells were stimulated by target cells. ACM was collected and concentrated with 3KD ultrafiltration and incubated with 100 μM duramycin-biotin overnight. Streptavidin-magnetic beads were then added to capture and remove PE-duramycin-biotin complex. PE-depleted concentrates were diluted to one or half fold of the original ACM volume, i.e. 1x or 2x of the original ACM concentrations. B16F10 cells were seeded overnight and treated with PE-depleted concentrates for 24 hours. Cell death was evaluated by cell number count via flow cytometry (n = 3). The rat IgG antibody was served as a control in the PE depletion assay.

d-e, Secreted lipidome of activated mouse $CD8^+$ T cells and human CAR-T cells. Mouse CD8 T^+ cells were stimulated by anti-mCD3ε (10 μg/mL) and anti-mCD28 (10 μg/mL) antibodies with IL-2 (10 ng/mL) for 48 hours (**d)**, and human CD19.28Z CAR-T cells were stimulated by Raji cells at the 2:1 ratio for 48 hours (**e)**. ACM samples were collected and subjected to lipidomic analysis (mouse CD8 ACM, n = 3; human CAR-T ACM, n = 7). Non-stimulated T cell conditioned medium (NCM) was collected from control cells. The control cells in **d** were naïve $CD8^+$ T cells cultured in fresh medium with IL-7 (10 ng/mL) for 48 hours and those in **e** were human CAR-T cells cultured in fresh medium with IL-7 (10 ng/mL) and IL-15 (10 ng/mL) for 48 hours. PE lipids with different saturation levels were labelled by different colors and percentage shown in **Figure 1d-e** were calculated based on all PE lipids detected in ACM. The data were displayed by the numbers of Log2 (fold changes), labeled as Log2 FC, and the reverse numbers of Log10 (P- values), labeled as -Log10 P-value, between ACM and NCM.

f-g, Cytotoxicity of PE lipids with either polyunsaturated sidechains or monounsaturated sidechains on B16F10 cells. PC (16:0/18:1) was served as a control. B16F10 cells were treated with methanol (Mock), 30 μg/mL PC (16:0/18:1), PE (P-18:0/18:1), PE (18:0/20:4), PE (P-18:0/20:4) or PE (P-18:0/22:6) for 24 hours. P- represents ether bond. Cell death (**f,** n = 4) and apoptosis (**g,** n = 3) were evaluated by cell number count and Annexin V staining.

h-i, PE cytotoxicity on B16F10 and MC38 cells under the attachment condition. Cells were treated with methanol (Mock), 30 μg/mL PC (16:0/18:1) or 30 μg/mL PE (18:0/20:4) for 24 hours. Cell death was evaluated by cell number count (**h,** n = 3-6) and Annexin V staining (**i,** n = 3).

j, PE cytotoxicity on different species of human cancer cell lines under the attachment condition. Cells were treated with 30 μg/mL PE (18:0/20:4) for 24 hours. Cell death was evaluated by cell number count via flow cytometry (n = 2-3). COAD, Colorectal cancer; LIHC, Liver Hepatocellular Carcinoma; GA, gastric adenocarcinoma.

k, Effect of PE on the tumor spheroid formed by detached tumor cells. B16F10 or MC38 tumor spheroid was treated with methanol (Mock), 20 μg/mL PC (16:0/18:1) or 20 μg/mL PE (18:0/20:4) for 24 hours. Scale bar, 1 mm.

Data were shown as mean ± SD and were analyzed by unpaired Student's t-test (**d-e**), one-way ANOVA (**b, f-g**) or two-way ANOVA (**c, h-j**). Experiments were repeated seven (**a**), six (**d**), three (**k**), two (**b, f-g, h-i**) times.

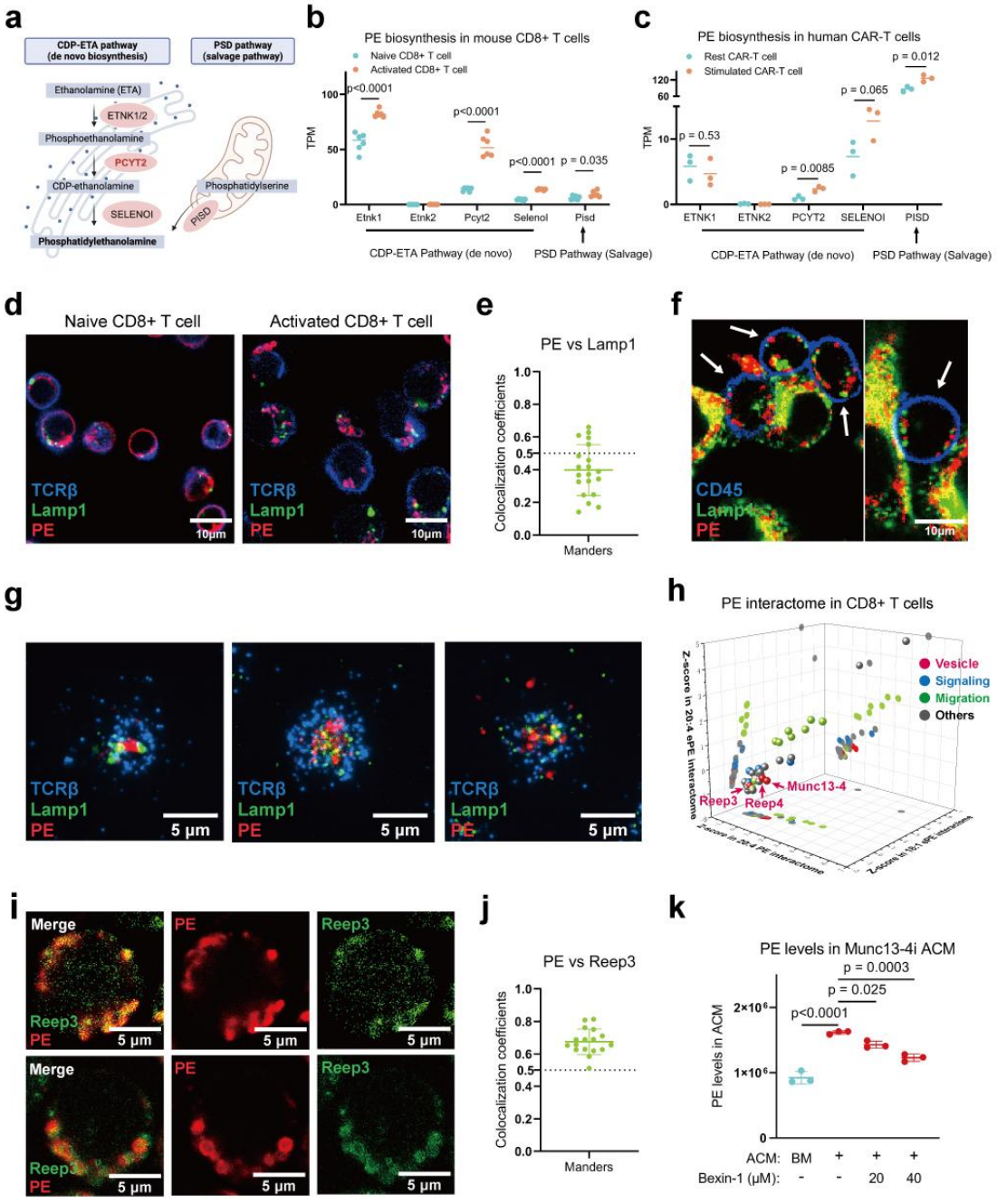


Figure 2. Biosynthesis and secretion of PE lipids by CD8$^+$ T cells.

a, A diagram of PE biosynthesis pathways. The *de novo* PE biosynthesis is through the Kennedy pathway, which begins with the phosphorylation of ethanolamine (ETA) to phosphoethanolamine (p-ETA) catalyzed by ETNK1/2. The rate-limiting enzyme PCYT2 catalyzes the conjugation of p-ETA with cytidine triphosphate (CTP), yielding CDP-ETA. Finally, PE is produced after the conjugation of CDP-ETA with diacylglycerol (DAG), which is catalyzed by SELENOI. Alternatively, PE can be generated via decarboxylation of phosphatidylserine (PS) by PISD.

b, Transcriptional levels of PE biogenesis enzymes in naive and activated mouse CD8$^+$ T cells. Naive CD8$^+$ T cells were isolated from mouse spleens and activated with anti-CD3ε (5 μg/mL), anti-CD28 (5 μg/mL) and 10 ng/mL IL-2 for 48 hours. Bulk RNA sequencing was performed, and transcriptional levels of PE biogenesis enzymes were displayed (n = 6).

c, Transcriptional levels of PE biogenesis enzymes in rest and activated human CD19.28z CAR-T cells. Rest CAR-T cells were cultured with human IL-7 (10 ng/mL) and IL-15 (10 ng/mL) for over 1 week. For the activation condition, CAR-T cells were co-cultured with Raji cells at the E:T ratio = 1:1 for 72 hours. Bulk RNA sequencing was performed, and transcriptional levels of PE biosynthesis enzymes were displayed (n = 3).

d-e, Representative confocal images of naïve and activated $CD8^+$ T cells with PE vesicles and $Lamp1^+$ cytotoxic granules (**d**). Mander's colocalization coefficients of PE to Lamp1 were measured with Coloc 2 algorithm in ImageJ (**e**). Dash line indicates the common cutoff value of 0.5. To generate activated $CD8^+$ T cells, splenocytes from OT-I mice were stimulated with $OVA_{257–264}$ (N4) in the presence of IL-2 (10 ng/mL) for 48 hours. Cells were seeded in poly-L-serine-coated plates for 30 minutes, fixed and stained with duramycin to indicate PE, anti-Lamp1 to indicate conventional cytotoxic granule, and anti-TCRβ to indicate cell membrane. Each dot represents a cell (n = 20).

f, Spatial distribution of PE vesicles and $Lamp1^+$ granules in $CD8^+$ T cells conjugated with tumor cells, imaged by confocal microscopy. B16F10-OVA cells were seeded on the poly-L-serine-coated plates overnight. Activated $CD8^+$ T cells were generated as in panel **d**. Activated $CD8^+$ T cells were added and co-incubated with tumor cells for 2 hours, and then fixed and stained with duramycin to indicate PE vesicles, anti-Lamp1 to indicate cytotoxic granules and anti-CD45 to indicate T-cell membrane. $CD8^+$ T cells ($CD45^+$ cells) are indicated by white arrows.

g, Spatial distribution of PE vesicles and $Lamp1^+$ granules at the immunological synapse, imaged by Total Internal Reflection Fluorescence (TIRF) Microscopy. Activated $CD8^+$ T cells were generated as in panel **d**. Cells were seeded onto the supported lipid bilayer (SLBs) coated with anti-CD3/anti-CD28 (5 μg/mL) and Icam-1 (10 nM) for 15 minutes and then fixed and stained with duramycin, anti-LAMP1, and anti-TCRβ, followed by TIRF imaging.

h, PE interaction proteins in activated $CD8^+$ T cells, identified by a PE interactome assay described in Extended Data Figure 9a. The PE interactome assay was performed with both $CD8^+$ T cells and B16F10 cells, and the hits shared by the two cell types were excluded from the CD8 list. The proteins interacting with 20:4 PE (PE 18:0/20:4), 18:1 ePE (PE P-18:0/18:1) and 20:4 ePE (PE P-18:0/20:4) specifically in CD8 T cells were displayed at the three dimensions. Proteins were annotated as 4 groups, including T cell signaling (blue), migration (green), vesicle transportation (red) and others (black). Z-scores of proteins enriched Intensity in different PE species were shown as three coordinates.

i-j, Colocalization analysis of PE and Reep3. Activated $CD8^+$ T cells were stained by duramycin and anti-Reep3. Representative image (**i**) and Mander's colocalization quantitation of PE granules with Reep3 (**j**) are shown. Dash line indicates the common cutoff value of 0.5. Activated $CD8^+$ T cells were generated and imaged as in panel **d**. Each dot represents a cell (n = 17).

k, Effect of Munc13-4 inhibition on secreted PE levels in CD8 ACM. OT-I T cells were pretreated with mock or Munc13-4 inhibitor Bexin-1 (Munc13-4i) for 45 minutes (n = 3). ACM was collected as **Figure 1a**, followed by PE measurement by mass spectrometry.

Data were shown as mean ± SD and were analyzed by unpaired Student's t test (**h**), two-way ANOVA (**b-c**) or one-way ANOVA (**k**). Experiments were repeated three (**d**), two (**i**) times.

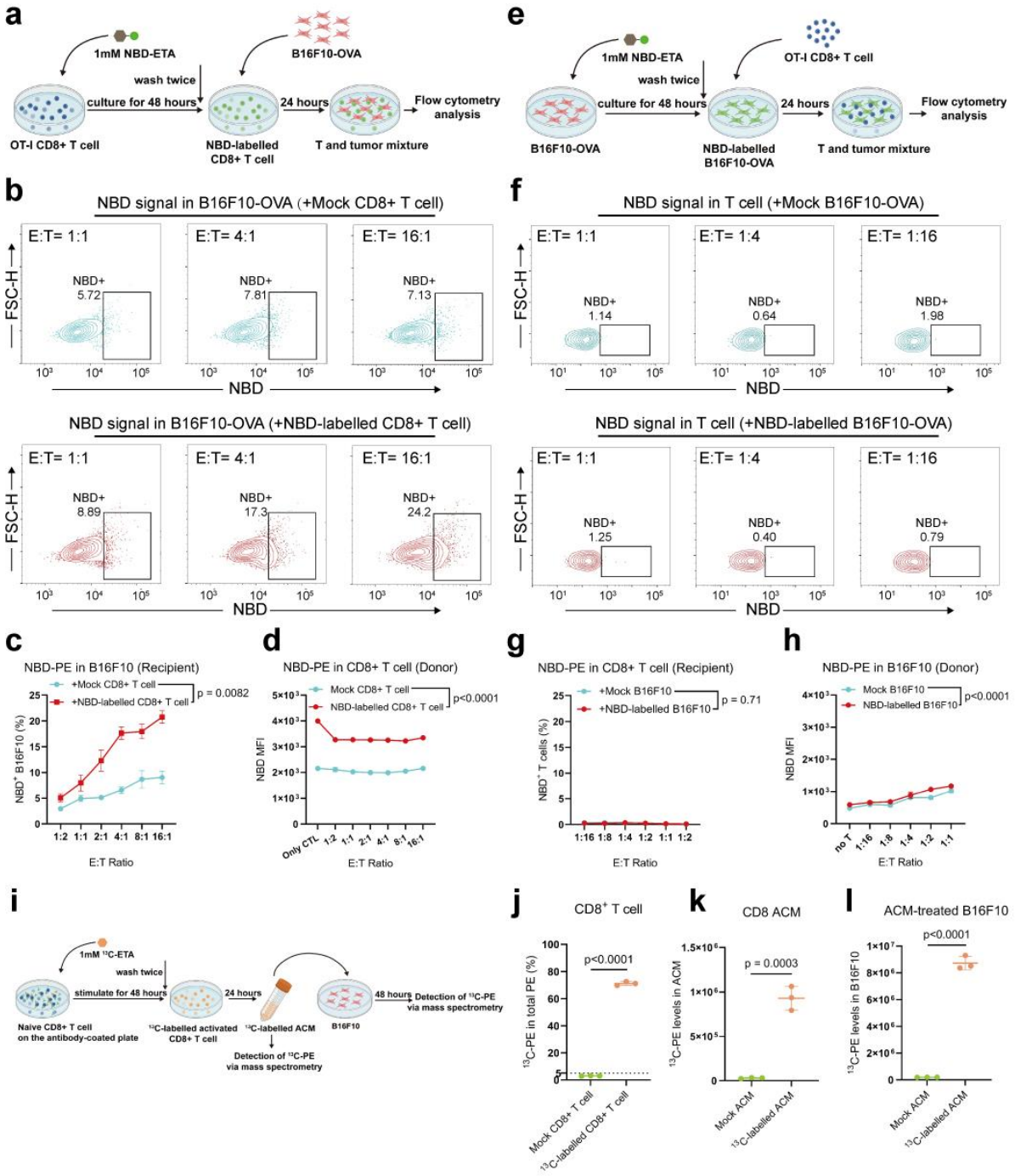


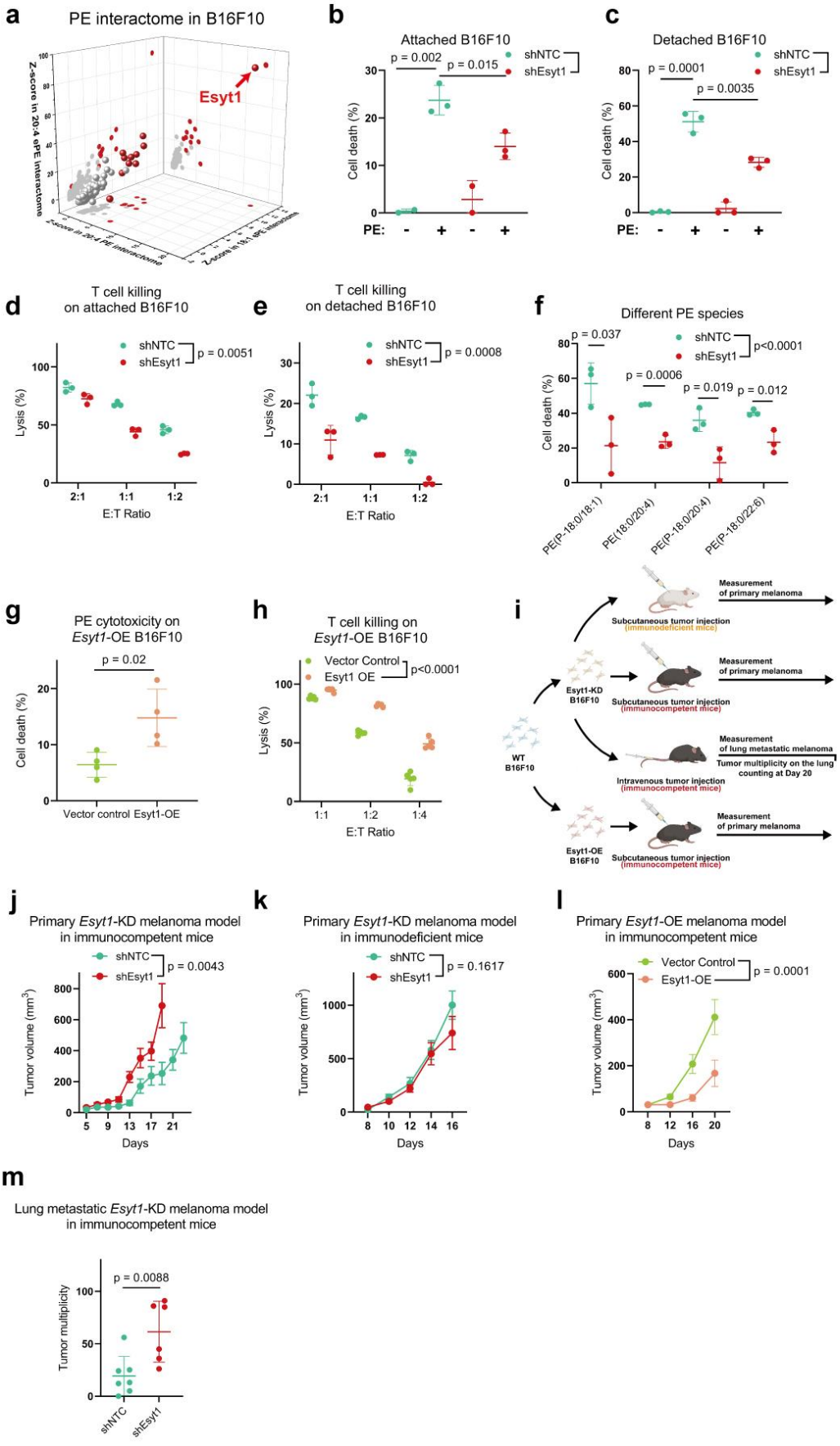
Figure 3. Intercellular transportation of CD8-derived PE lipids.

a-d, Fluorescent tracing of PE transportation from $CD8^+$ T cells to tumor cells. **a**, schematic illustration of the experimental design. OT-I $CD8^+$ T cells were generated as mentioned in Figure 1a and then pretreated with NBD-labeled ethanolamine (NBD-ETA, 1mM) or ETA (Mock, 1mM) for 48 hours to label biosynthesized PE lipids. After removal of residual NBD-ETA, $CD8^+$ T cells were co-cultured with B16F10-OVA cells at different E:T ratios for 24 hours, followed by flow cytometry analysis of NBD signals in both $CD8^+$ T cells and B16F10 cells. The population of NBD^+ B16F10-OVA cells co-cultured with mock $CD8^+$ T cells or NBD-labelled $CD8^+$ T cells was analyzed via FlowJo and shown in **b**. **c-d**, Quantification of NBD signals in the recipient B16F10-OVA cells (**c**, $n = 3$) and the donor $CD8^+$ T cells (**d**, $n = 3$) after co-culture. **e-h**, Fluorescent tracing of PE transportation from tumor cells to $CD8^+$ T cells. **e**, schematic illustration of

the experimental design. B16F10-OVA cells were pretreated with NBD-ETA (1mM) or ETA (Mock, 1mM) for 48 hours to label biosynthesized PE lipids. After removal of residual NBD-ETA, B16F10-OVA cells were co-cultured with activated $CD8^+$ T cells at different E:T ratios for 24 hours, followed by flow cytometry analysis of NBD signals in both $CD8^+$ T cells and B16F10 cells. The population of NBD^+ T cells co-cultured with mock B16F10-OVA or NBD-labelled B16F10-OVA was analyzed via FlowJo and shown in **f**. **g-h**, Quantification of NBD signals in the recipient $CD8^+$ T cells (**g**, $n = 3$) and the donor B16F10-OVA cells (**h**, $n = 3$) after co-culture.

i-l, ^{13}C isotype tracing of PE transportation from $CD8^+$ T cells to tumor cells. ^{13}C-PE was analyzed by mass spectrometry that cannot separate $CD8^+$ T cells and tumor cells like flow cytometry. An experimental approach of conditioned medium treatment was therefore utilized to trace intercellular PE transportation, as illustrated in **i**. Naïve $CD8^+$ T cells were isolated from mouse spleen, seeded on the plates coated with anti-mCD3ε (10 μg/mL) and anti-mCD28 (10 μg/mL) and stimulated for 48 hours supplemented with IL-2 (10 ng/mL) and ^{13}C-ETA (1mM) or ETA (Mock, 1mM). After removal of residual ^{13}C-ETA, activated $CD8^+$ T cells were transferred to the fresh medium with IL-2 (10 ng/mL) and cultured for 24 hours to collect ACM. B16F10 cells were treated with ACM for 48 hours. ^{13}C-PE levels in ACM and B16F10 cells were measured by mass spectrometry. **j,** ^{13}C-PE levels in the labelled $CD8^+$ T cells ($n = 3$). **k**, ^{13}C-PE level of ACM ($n = 3$). **l**, ^{13}C-PE level of ACM-treated B16F10 cells ($n = 3$).

Data were shown as mean ± SD and were analyzed by unpaired Student's t test (**j-l**), two-way ANOVA (**c-d, g-h**). Experiments were repeated three (**b-d**), two (**f-h**) times.



587

588 **Figure 4. Esyt1 in tumor cells mediated PE cytotoxicity.**

a, PE binding proteins in B16F10 cells, identified by a PE interactome assay described in Extended Data Figure 9a. The proteins interacting with 20:4 PE (PE 18:0/20:4), 18:1 ePE (PE P-18:0/18:1) and 20:4 ePE (PE P-18:0/20:4) were displayed at the three dimensions. The top hits with highest intensities were highlighted by red, in which Esyt1 ranked the first. Z-scores of proteins enriched intensity in different PE species were shown as three coordinates.

b-c, PE cytotoxicity on Esyt1-knockdown (Esyt1-KD) B16F10 cells at either attachment (**b**) or detachment (**c**) condition. To silence Esyt1, cells were transfected with lentivirus leading to stable expression of shRNA No.1 towards Esyt1 (knockdown efficiency in Extended Data Figure 11a). Cells were treated with 30 μg/mL PE (18:0/20:4) for 24 hours (n = 3). Absolute cell numbers were counted by flow cytometry.

d-e, T cell killing of Esyt1-KD B16F10-OVA cells at attachment (**e**) or detachment (**f**) condition. Cells were co-cultured with activated OT-I $CD8^+$ T cells at different E:T Ratios for 24 hours (n = 3). Activated OT-I $CD8^+$ T cells were prepared as in Figure 1a. Esyt1 in tumor cells was silenced by shRNA No.1. Tumor cell numbers were counted by flow cytometry.

f, Cytotoxicity of different PE species on Esyt1-KD B16F10 cells. Esyt1 in tumor cells was silenced by shRNA No.1. Cell death was evaluated by cell number count after cell treatment with methanol (mock), PE (P-18:0/18:1), PE (18:0/20:4), PE (P-18:0/20:4) or PE (P-18:0/22:6) for 24 hours (n = 3).

g, Effect of Esyt1 overexpression (Esyt1-OE) in tumor cells on PE cytotoxicity. Attached Esyt1-OE B16F10 cells were treated with 15 μg/mL PE (18:0/20:4) for 24 hours (n = 4).

h, Effect of Esyt1 overexpression in tumor cells on T cell killing. Attached Esyt1-OE B16F10-OVA cells were co-cultured with OT-I T cells at different E:T ratios for 24 hours (n = 4).

i-m, Schematic illustration (**i**) of preclinical models of primary (**j-l**) or lung-metastatic melanoma (**m**). **j-k**, In the primary B16F10 melanoma model, $4x10^5$ Esyt1-KD or control B16F10 cells were subcutaneously injected to either immunocompetent C57BL/6 mice (shNTC, n = 6; shEsyt1, n = 7) (**j**) or immunodeficient B-NDG mice (**k**) (shNTC, n = 11; shEsyt1, n = 11). Tumor progression was recorded every 2 days. **l**, In the primary B16F10 melanoma model, $6x10^5$ Esyt1-OE or vector control B16F10 cells were subcutaneously injected to immunocompetent C57BL/6 mice (vector control, n = 20; Esyt1-OE, n = 18). Tumor progression was recorded every 4 days. **m**, In the lung metastatic B16F10 melanoma model, 5×10^5 Esyt1-KD or wild-type B16F10 cells were intravenously injected into immune-competent C57BL/6 mice (shNTC, n=7; shEsyt1, n=6). Tumor numbers on the lungs were measured on day 20 post-injection.

Data were shown as mean ± SD (**b-h**, **m**) and mean ± SEM (**j-l**), and were analyzed by unpaired Student's t-test (**b-c, m**), two-way ANOVA (**d-f, h, j-l**) or one-way ANOVA (**f**). Experiments were repeated four (**c**), three (**d-e**), two (**b, f, h**) times.

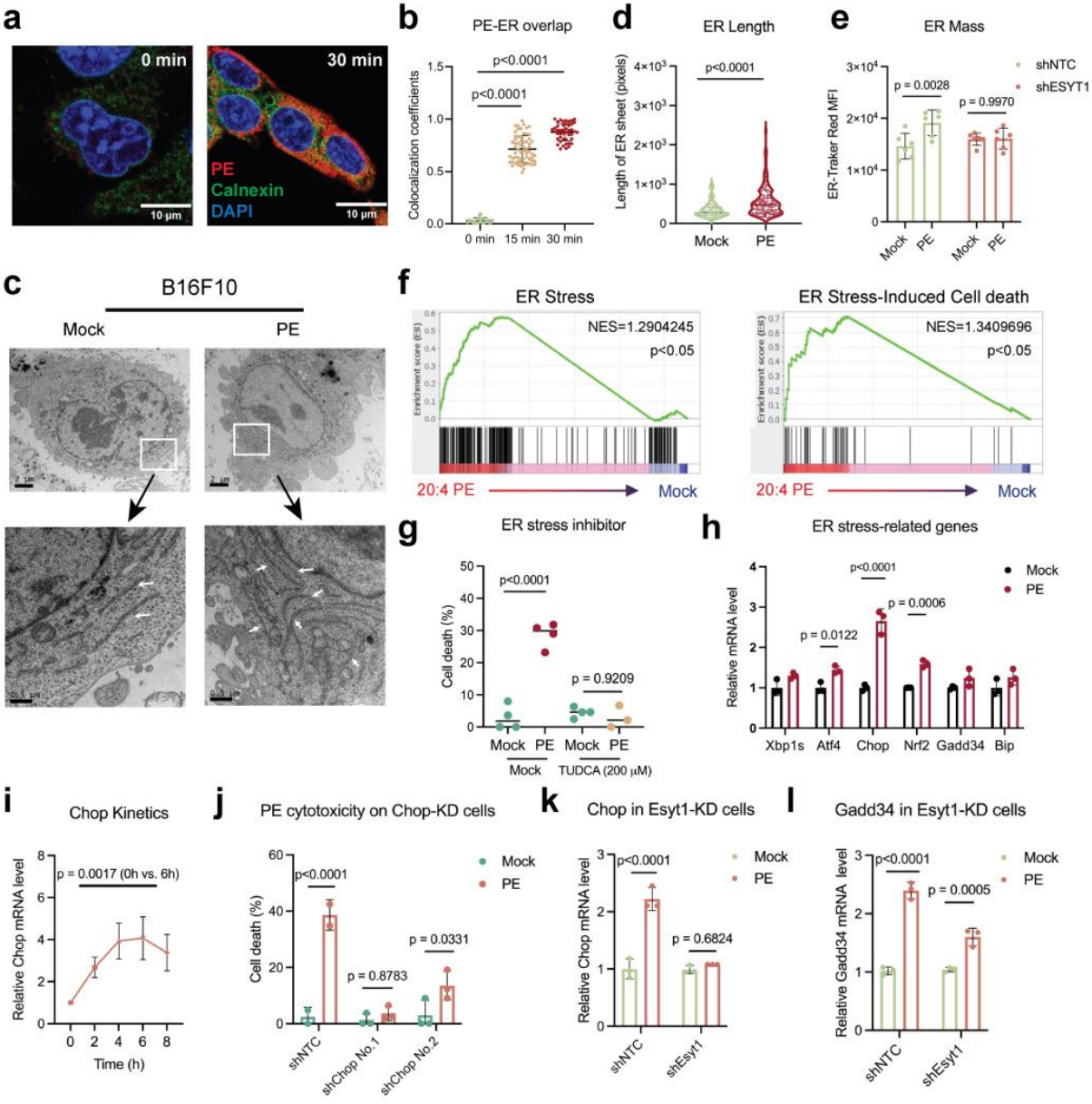


Figure 5. PE treatment of tumor cells altered ER morphology and caused ER stress.

a-b, PE levels of ER in tumor cells before and after PE treatment. B16F10 cells were seeded in the plate overnight and treated with 30 μg/mL PE (18:0/20:4) for 0-30 minutes. Cells were then fixed and stained with duramycin-cy3 for PE lipids, anti-Calnexin for ER (2A2C6, Proteintech) and DAPI for nucleus. Representative images (**a**) and Mander's colocalization quantitation of PE signals with Calnexin (**b**) are presented. Each dot represents a cell (0 min, $n = 25$; 15 min, $n = 64$; 30 min, $n = 45$).

c-d, Transmission electron microscopy (TEM) analyzing ER morphology in tumor cells before and after PE treatment. B16F10 cells were treated with 30 μg/mL PE (18:0/20:4) for 48 hours. Representative images (**c**) and quantification (**d**) of relative ER length are presented. Each dot represents one ER sheet (Mock, $n = 145$; PE, $n = 142$). Scale bar, 2 μm or 0.5 μm.

e, ER mass was indicated by ER-Tracker Red (Beyotime) staining, in non-target control or Esyt1-knockdown B16F10 cells treated with 10 μg/mL PE for 24 hours (18:0/20:4) ($n = 6$).

f, Gene set enrichment analysis (GSEA) of the ER stress and ER-induced apoptosis pathway in PE-treated versus Mock B16F10 cells. Tumor cells were treated with 30 μg/mL PE (18:0/20:4) for 24 hours, then

collected and subjected to bulk RNA sequencing. Data of other PE species were shown in Extended Data Fig 7a-b.

g, Cytotoxicity of 30 μg/mL PE (18:0/20:4) combined with 200 μM ER stress inhibitor Tauroursodeoxycholate (TUDCA) on B16F10 cells for 24 hours. Tumor cell numbers were counted by flow cytometry (n = 3-4).

h, Transcriptional changes of ER-stress-related genes following PE treatment. B16F10 cells were treated with 30 μg/mL PE (18:0/20:4) for 24 hours. Transcription levels of the indicated genes were measured by RT-qPCR and normalized to 18S rRNA (n = 3).

i, Time curve of *Chop* transcriptional levels in B16F10 cells treated with 30 μg/mL PE (18:0/20:4), measured by RT-qPCR (n = 3).

j, Cytotoxicity of 10 μg/mL PE (18:0/20:4) on Chop-knockdown (Chop-KD) B16F10 cells. Cells were treated with 10 μg/mL PE (18:0/20:4) for 24 hours. Tumor cell numbers were counted by flow cytometry (n = 2-3).

k-l, Transcriptional levels of Chop (**k**) and Gadd34 (**l**) in non-target control or Esyt1-knockdown B16F10 cells treated with 30 μg/ml PE (18:0/20:4) for 24 hours. The transcriptional levels of the indicated genes were measured by RT-qPCR and normalized to 18S rRNA (n = 3).

Data were shown as mean ± SD and were analyzed by unpaired Student's t-test (**d**), two-way ANOVA (**e, h, j-l**) or one-way ANOVA (**b, g, i**). Experiments were repeated twice (**a, e, h**).

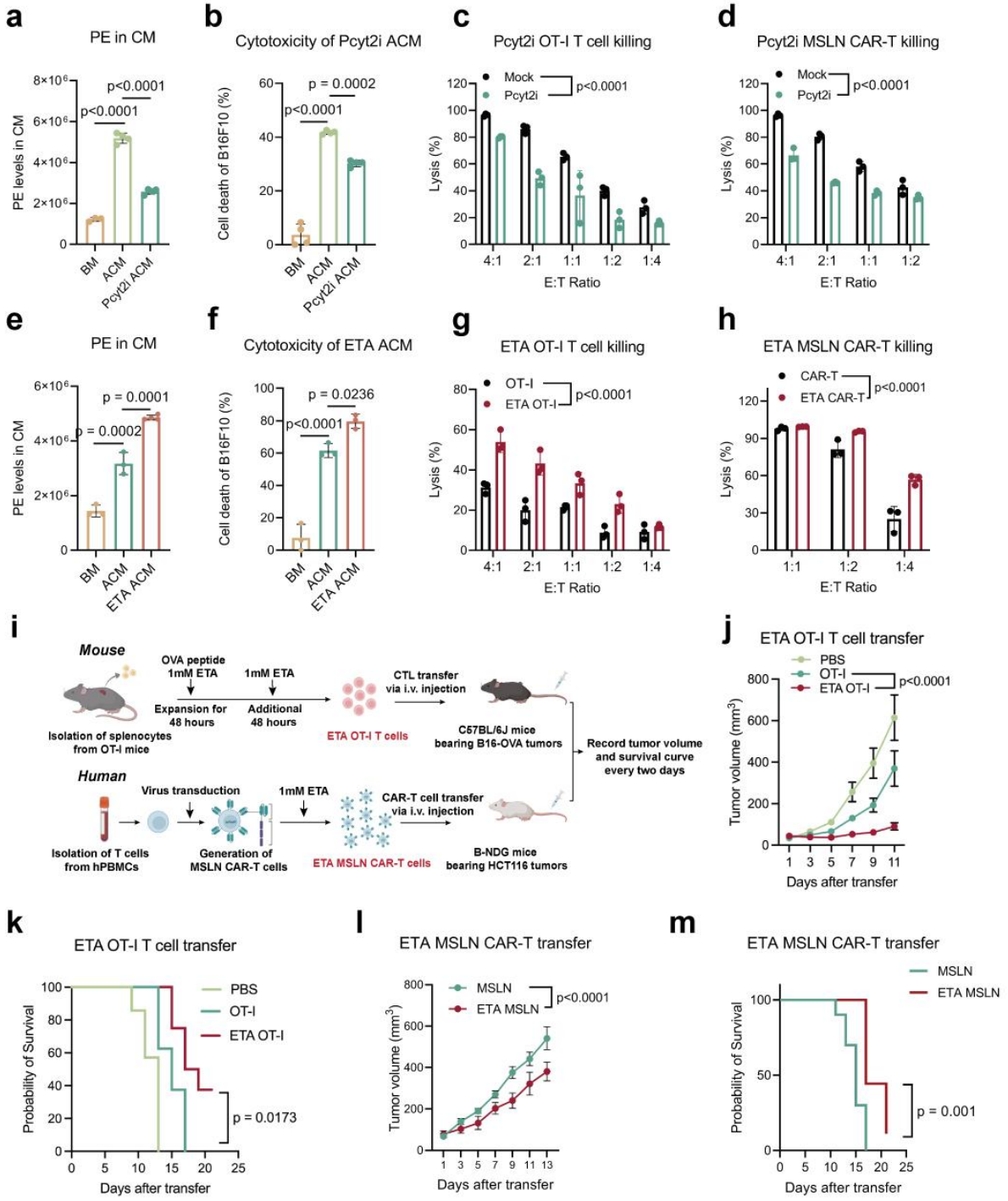


Figure 6. Manipulations of T-cell PE levels altered antitumor immunity.

a-b, PE levels and cytotoxicity of the conditioned medium of OT-I T cells pretreated with Pcyt2 inhibitor (Pcyt2i OT-I cells). Activated OT-I T cells were prepared as **Figure 1a** and then pretreated with 50 μM Meclizine for 8 hours. To generate conditioned medium, T cells were co-incubated with B16F10-OVA cells at an E:T ratio of 2:1 for 24 hours. **a.** The ACM was collected and measured by mass spectrometry for PE levels (n = 3-4). **b.** B16F10 cells were treated with ACM for 24 hours and tumor cell numbers were counted by flow cytometry (n = 4).

c, Killing function of Pcyt2i-preated OT-I T cells against B16F10-OVA cells. OT-I T cells were co-incubated with B16F10-OVA cells at different E:T Ratios for 24 hours. Tumor cell numbers were counted by flow

cytometry (n = 3).

d, Killing function of Pcyt2i-pretreated MSLN CAR-T cells against HCT116 cells. Human MSLN CAR-T cells were pretreated with 50 μM Pcyt2i for 24 hours. CAR-T cells were co-incubated with HCT116 cells at different E:T Ratios for 24 hours. Tumor cell numbers were counted by flow cytometry (n = 3).

e-f, PE levels and cytotoxicity of the conditioned medium of ethanolamine-pretreated OT-I T cells (ETA OT-I cells). For ETA OT-I T cell generation, ETA (1 mM) was added into the medium during the 48-hour activation process. ETA OT-I T cells were subsequently cultured in fresh ETA (1mM)-containing medium for 2 days. Cells were then washed twice and co-incubated with B16F10-OVA cells at an E:T ratio of 2:1 for 24 hours to acquire ACM. **e,** The ACM was collected and measured by mass spectrometry for PE levels (n = 3). **f,** B16F10 cells were treated with ACM for 24 hours and tumor cell numbers were counted by flow cytometry (n = 3).

g, Killing function of ETA OT-I T cells against B16F10-OVA cells. OT-I T cells were co-cultured with B16F10-OVA cells at different E:T Ratios for 24 hours. Tumor cell numbers were counted by flow cytometry (n = 3).

h, Killing function of ETA-pretreated MSLN CAR-T cells (ETA CAR-T) against HCT116 cells. MSLN CAR T cells were generated as described in **Method.** ETA-MSLN CAR-T cells were pretreated with 1 mM ETA and maintained in IL-2 (10 ng/mL) prior to the killing assays. CAR T cells were co-cultured with HCT116 cells at different E:T Ratios for 24 hours. Tumor cell numbers were counted by flow cytometry (n = 3).

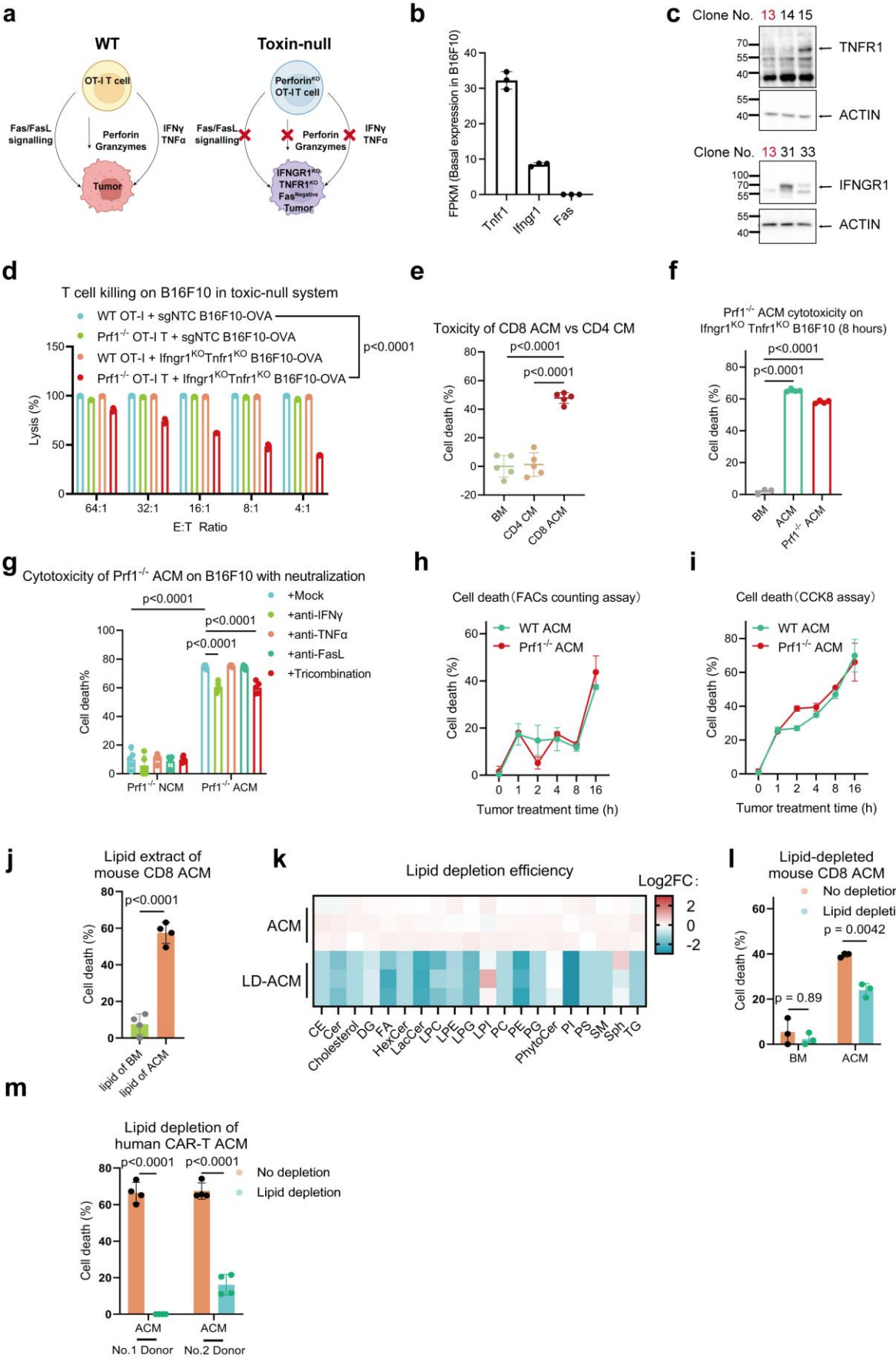
i, Schematic illustration of adoptive T cell transfer experiments. ETA or control cells were transferred into tumor-bearing recipient mice: OT-I T cells into C57BL/6 mice 5 days post-B16F10 (4×10^5 cells per mice) transplantation (n = 8, 7, 8 for PBS, OT-I, and ETA OT-I, respectively) and MSLN CAR-T cells into B-NDG mice 7 days post-HCT116 (1.5×10^6 cells per mice) transplantation (n = 10, 9 for CAR-T and ETA CAR-T, respectively). Tumor size and survival was monitored every two days.

j-k, Tumor growth **(j)** and overall survival **(k)** in B16F10 tumor-bearing mice after OT-I T cell transfer.

l-m, Tumor growth **(l)** and overall survival **(m)** in HCT116 tumor-bearing mice after CAR-T cell transfer. Mice with tumors larger than 13 mm along the longest axis were euthanized for ethical consideration.

Data were shown as mean ± SD (**a-h**) and mean ± SEM (**j-m**), and were analyzed by two-way ANOVA (**c-d, g-h, j, l**) or one-way ANOVA (**a-b, e-f**). Survival (**k, m**) was analyzed by log-rank (Mantel–Cox) test. Experiments were repeated four (**g**), three (**d, h**), two (**a**, **b-c, h. j, l**) times.

Extended Data Figures and legends



Extended Data Figure 1. CD8$^+$ T cells had lipid-dependent cytotoxic mechanism that was distinct from conventional cytotoxic pathways.

a, A toxin-null system in which the major pathways of protein-mediated cytotoxicity were deficient. *Prf1*$^{-/-}$ OT-I T cells were isolated from *Prf1*$^{-/-}$ OT-I mice and pre-activated as Figure 1a. B16F10 cells did not express Fas, as shown in panel b. *Ifngr1*^{KO} and *Tnfr1*^{KO} in B16F10-OVA cells were generated via CRISPR-Cas9 system, as shown in panel c.

b, Transcriptional levels of *Tnfr1, Ifngr1* and *Fas* in wildtype B16F10 cells, according to the bulk RNA sequencing data.

c, Immunoblotting of Ifngr1 and Tnfr1 expression in the B16F10-OVA single clones transfected with *Ifngr1*-sgRNA and *Tnfr1*-sgRNA. Anti-Ifngr1 (EPR24127-89, Abcam) and anti-Tnfr1 (H-5, Santa Cruz) were used for immunoblotting. Clone13 with double knockout of *Ifngr1* and *Tnfr1* was labelled in red.

d, Contribution of conventional cytotoxic pathways on 24-hour T cell killing. Perforin-KO in T cells and IFNGR1/TNFR1-KO in tumor cells were used to remove conventional cytotoxic pathways. T cells were co-incubated with tumor cells at different E:T ratios for 24 hours (n = 3).

e, Cytotoxicity of conditioned medium generated from OT-I CD8$^+$ T cells and OT-II CD4$^+$ T cells activated by tumor cells. To generate OT-I CD8$^+$ T cells, splenocytes from OT-I mice were firstly boosted with OVA$_{257–264}$ (N4) in the presence of IL-2 (10 ng/mL) for 48 hours to acquire pre-activated CD8$^+$ T cells. Cells were then mixed with B16F10-OVA cells at the effector cells: target cells (E:T) ratio = 2:1 in the fresh medium for 24 hours, followed by the collection of the conditioned medium. To generate OT-II CD4$^+$ T cells, splenocytes from OT-II mice were firstly isolated and boosted with OVA$_{323-339}$ in the presence of IL-2 (10 ng/mL) for 72 hours to acquire pre-activated CD4$^+$ T cells. Cells were then mixed with B16F10-OVA cells at the E:T ratio = 2:1 in the fresh medium for 24 hours, followed by the collection of the conditioned medium. Conditioned media were collected and then used to treat B16F10 cells for 24 hours (n = 5).

f, ACM cytotoxicity on tumor cells under the toxin-null condition. Wild-type OT-I T cells or *Prf1*$^{-/-}$ OT-I T cells were co-cultured with B16F10-OVA cells at an E:T ratio of 2:1 for 24 hours. ACM was collected and then used to treat *Ifngr1*^{KO}*Tnfr1*^{KO} B16F10 cells for 8 hours (n = 3).

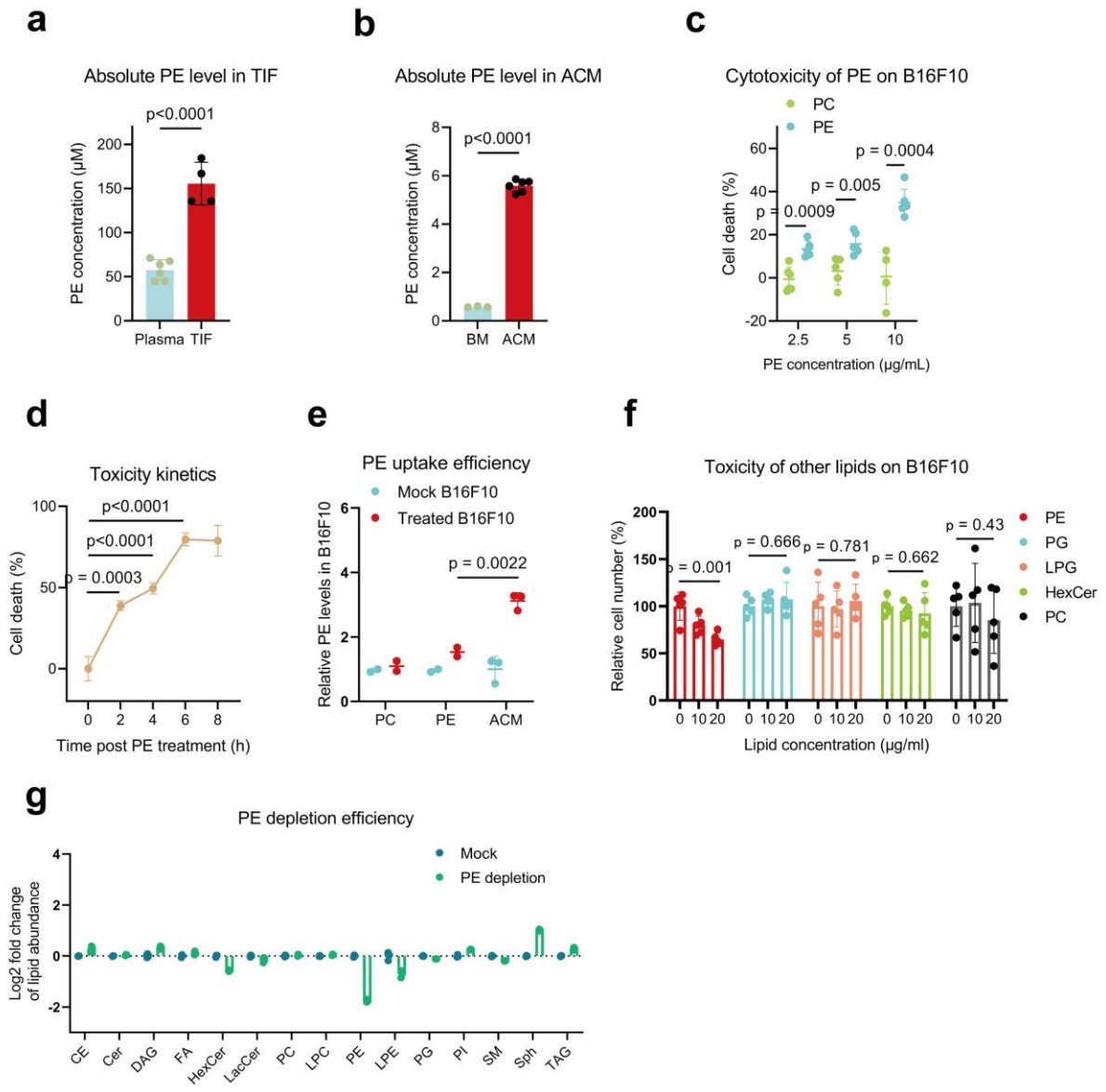
g, Blocking conventional cytotoxic pathways by neutralizing antibodies. ACM was collected from *Prf1*$^{-/-}$ OT-I T cells. Anti-IFNγ (10 μg/mL), anti-TNFα (25 μg/mL), anti-FasL (10 μg/mL), or their combination were used to block conventional cytotoxic pathways during CD8 ACM killing. B16F10 tumor cells were treated with ACM for 24 hours (n = 5).

h-i, Cytotoxic kinetics of ACM on tumor cells. Wild-type OT-I T cells or *Prf1*$^{-/-}$ OT-I T cells were activated by B16F10-OVA cells at an E:T ratio of 2:1. ACM was collected at the 16-hour timepoint. B16F10 cells were treated with ACM for different durations, followed by assessment of cell number **(h)** and cell viability **(i)** using FACS-based cell counting and the CCK8 assay (n = 2-3).

j, Cytotoxicity of lipid extracts of mouse CD8 ACM on attached B16F10 cells. Lipids were extracted from target-cell-stimulated mouse CD8 ACM using fumed silica. The control was blank medium (BM). Fumed silica (20 g/L) was added into ACM or BM, followed by overnight mixture and subsequent centrifugation. Lipids were then stripped from fumed silica with methyl-tert-butyl ether (MTBE) and methanol (MTBE: methanol: fumed silica= 5: 1: 2 (v: v: v)). The organic phase was collected, dried using a vacuum concentrator and reconstituted with methanol. Lipid extracts were diluted to the original volume of condition medium. B16F10 cells were treated with lipid extracts for 24 hours (n = 4).

k, Efficiency of lipid depletion on ACM. Lipids were removed from target-cell-stimulated mouse CD8 ACM using the fumed silica protocol same as panel **j**. The control was blank medium (BM). Fumed silica (20 g/L) was added into conditioned medium followed by mixing overnight and centrifugated to collect lipid-depleted

742 medium (n = 3).
743 **l**, Cytotoxicity of lipid-depleted ACM of mouse $CD8^+$ T cells on attached B16F10 cells. Lipid-depleted ACM
744 were generated as panel **k**. B16F10 cells were treated for 24 hours (n = 4).
745 **m**, Cytotoxicity of lipid-depleted ACM of human CD19.28Z CAR-T on attached huh7 cells. Lipids were
746 removed from target-cell-stimulated CAR-T ACM using the same fumed silica protocol. Huh7 cells were
747 treated for 24 hours (n = 4). CAR-T cells from two donors were used.
748 Data were shown as mean ± SD, and were analyzed by unpaired Student's t-test (**j**), two-way ANOVA (**d, g**)
749 or one-way ANOVA (**e-f, l-m**). Experiments were repeated four (**l**), three (**m**), two (**d, g**) times.
750



751

752 **Extended Data Figure 2. Cytotoxic PE lipids were enriched in physiological conditions**

753 **a-b**, Absolute concentration of PE lipids in tumor interstitial fluid (TIF) versus plasma **(a)** and CD8 ACM
754 versus blank medium **(b)**. For TIF isolation, $4x10^5$ B16F10 cells were subcutaneously injected to C57BL/6
755 mice. Tumors were harvested, chopped, and centrifuged in the columns with 20 μm filters at 100 g for 15
756 minutes. As control, plasma samples were collected from C57BL/6 mice in the same batch. Each dot
757 represents an individual mouse sample. To generate ACM, T cells were co-incubated with B16F10-OVA
758 cells at an E:T ratio of 2:1 for 24 hours. Blank medium (BM) was used as a control. Samples were collected
759 and subjected to lipidomics (plasma, $n = 6$; TIF, $n = 4$; BM, $n = 3$; ACM, $n = 6$).

760 **c,** Cytotoxicity of PE and PC on attached B16F10 melanoma cells at low concentrations of 2.5-10 μg/mL.
761 B16F10 cells were treated for 24 hours ($n = 4$-5).

762 **d,** Kinetics of cytotoxicity induced by PE treatment in tumor cells. B16F10 cells were treated by 30 μg/mL
763 PE (18:0/20:4) for different durations. Cell death was evaluated by cell number count ($n = 2$-3).

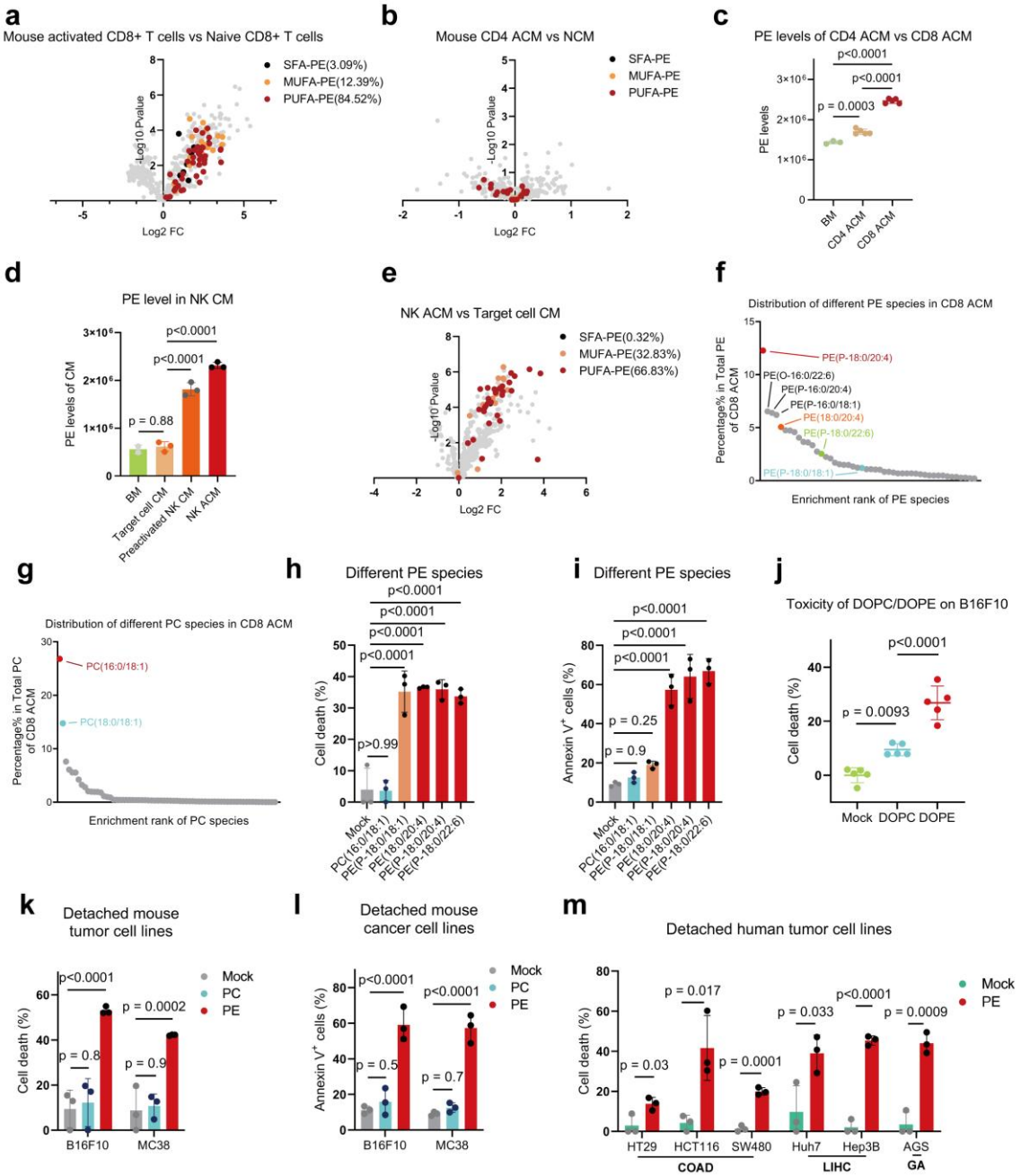
764 **e,** Increase of PE levels in tumor cells after the treatment of CD8 ACM or blank medium supplied with
765 solublized PE. Blank medium supplied with solublized PC was used as a control. B16F10 cells were treated
766 with CD8 ACM, 30 μg/mL PE (18:0/20:4), or 30 μg/mL PC (16:0/18:1) for 48 hours, followed by lipidomic

analysis of PE levels (n = 2-3).

f, Cytotoxicity of different ACM lipids on B16F10 cells. Cells were treated with PE (18:0/20:4), PG (18:1/18:1), Lyso PG (18:1), HexCer, and PC (18:0/18:1) for 24 hours at concentrations of 10 μg/mL and 20 μg/mL (n = 5).

g, Lipid profiles in the PE-depleted ACM shown in Figure 1c (n = 3). CE, cholesteryl ester; DAG, Diacylglycerol; FA, fatty acid; HexCer, Hexosylceramide; LacCer, Lactosylceramide; PC, phosphatidylcholine; LPC, lyso-phosphatidylcholine; PE, phosphatidylethanolamine; LPE, lyso-phosphatidylethanolamine; PG, phosphatidylglycerol; PI, phosphatidylinositol; SM, sphingomyelin; Sph, sphingosine; TAG, Triacylglycerol.

Data were shown as mean ± SD, and were analyzed by unpaired Student's t-test (**a-b**), two-way ANOVA (**c, e-f**) or one-way ANOVA (**d**). Experiments were repeated three (**d**), two (**f**) times.



Extended Data Figure 3. Cytotoxic functions of PE lipids.

a, Cellular lipidome of antibody-stimulated mouse CD8$^+$ T cells (n = 3). Non-activated CD8$^+$ T cells were isolated from spleen and cultured in the fresh medium with IL-7 for 48 hours. PE lipids with different saturation levels were labelled.

b, Secreted lipidome of the ACM of antibody-stimulated mouse CD4$^+$ T cells (CD4 ACM) (n = 3). Non-activated T cell conditioned medium (NCM) collected from naïve CD4$^+$ T cells cultured with IL-7 (10 ng/mL) for 48 hours.

c, PE levels of the conditioned medium generated from OT-I CD8$^+$ T cells and OT-II CD4$^+$ T cells activated by tumor cells. Preparation of conditioned media was mentioned in **Extended Data Figure 1e**. Medium samples were then analyzed via mass spectrometry (n = 3-5).

d, Secreted PE lipids from human NK cells. Human NK cells were cultured in fresh medium with 500 IU/mL IL-2 and 100 IU/mL IL-15 for 3 weeks for pre-activation. The conditioned medium of these cells was

denoted as Preactivated NK CM. Next, preactivated NK cells were mixed with γ-irradiated feeder cells at an E:T ratio of 2:1 and co-cultured for 24 hours to further activate NK cells. The conditioned medium of these cells was denoted as NK ACM. Blank medium (BM) and conditioned medium from γ-irradiated feeder cells cultured for 24 hours (Target cell CM) were served as controls. PE levels were quantitated by mass spectrometry (n = 3).

e, Secreted lipidome of NK ACM versus Target cell CM.

f-g, Abundance ranking of natural PE **(e)** and PC **(f)** species in CD8 ACM. The abundance of each PE or PC species was determined based on its proportion within the total PE or PC lipid pool. The PE species used in cellular experiments are labeled in color. PC (16:0/18:1) was identified as the most abundant PC species and was used as a negative control in multiple experiments. Detailed data are provided in Supplementary Table 4.

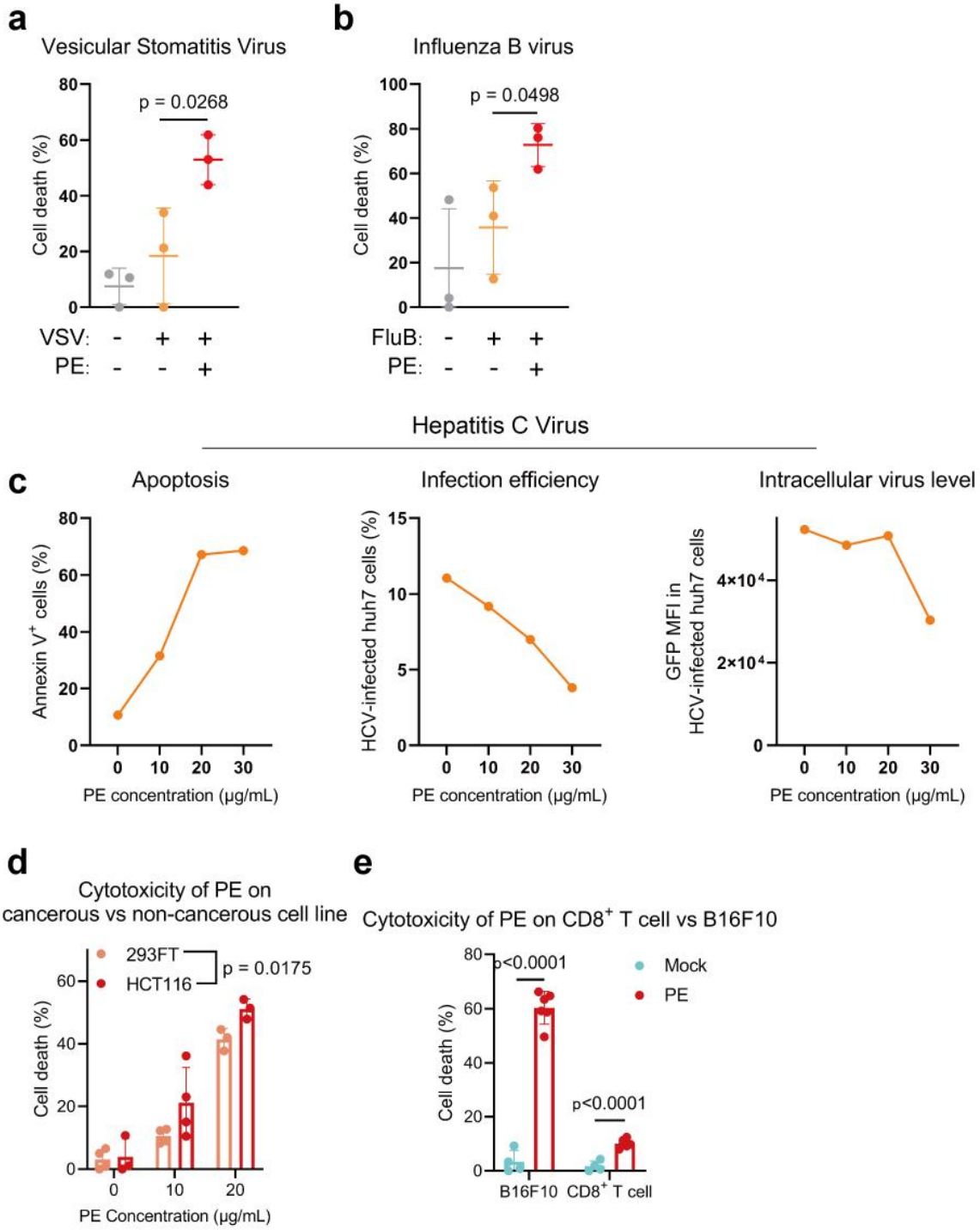
h-i, Cytotoxicity of PE lipids with either polyunsaturated or monounsaturated sidechains on MC38 cells. MC38 cells were treated with methanol (Mock), 30 μg/mL PC (16:0/18:1), PE (P-18:0/18:1), PE (18:0/20:4), PE (P-18:0/20:4) or PE (P-18:0/22:6) for 24 hours. P- represents ether bond. Cell death was evaluated by cell number count (**g,** n = 3) and Annexin V staining (**h,** n = 3).

j, Cytotoxicity of DOPC (18:1/18:1) and DOPE (18:1/18:1) on B16F10 cells. Cells treated with 30 μg/mL DOPC or DOPE for 24 hours (n = 5).

k-l, Cytotoxicity of PE on detached B16F10 and MC38 tumor cells. Cells were treated with methanol (Mock), 30 μg/mL PC (16:0/18:1) or PE (18:0/20:4) for 24 hours. Cell death was evaluated by cell number count (**j,** n = 3) and Annexin V staining (**k,** n = 3).

m, PE cytotoxicity on different species of human cancer cell lines under the detachment condition. Cell death was evaluated by cell number count via flow cytometry (n = 3). COAD, Colorectal cancer; LIHC, Liver Hepatocellular Carcinoma; GA, gastric adenocarcinoma.

Data were all shown as mean ± SD, and were analyzed by two-way ANOVA (**k-m**) or one-way ANOVA (**c-d, h-j**). Experiments were repeated two (**a-b, h-i, k-l**) times.



Extended Data Figure 4. PE cytotoxicity on virus-infected and non-cancerous cells.

a, Cytotoxicity of PE on Vesicular Stomatitis Virus (VSV)-infected huh7 cells. VSV-infected huh7 cells were treated with 30 μg/mL PE (18:0/20:4) and residual cell numbers were counted via flow cytometry to measure cell death (n = 3).

b, Cytotoxicity of PE on Influenza B Virus (FluB)-infected A549 cells. FluB-infected A549 cells were treated with 30 μg/mL PE (18:0/20:4) and residual cell numbers were counted via flow cytometry to measure cell death (n = 3).

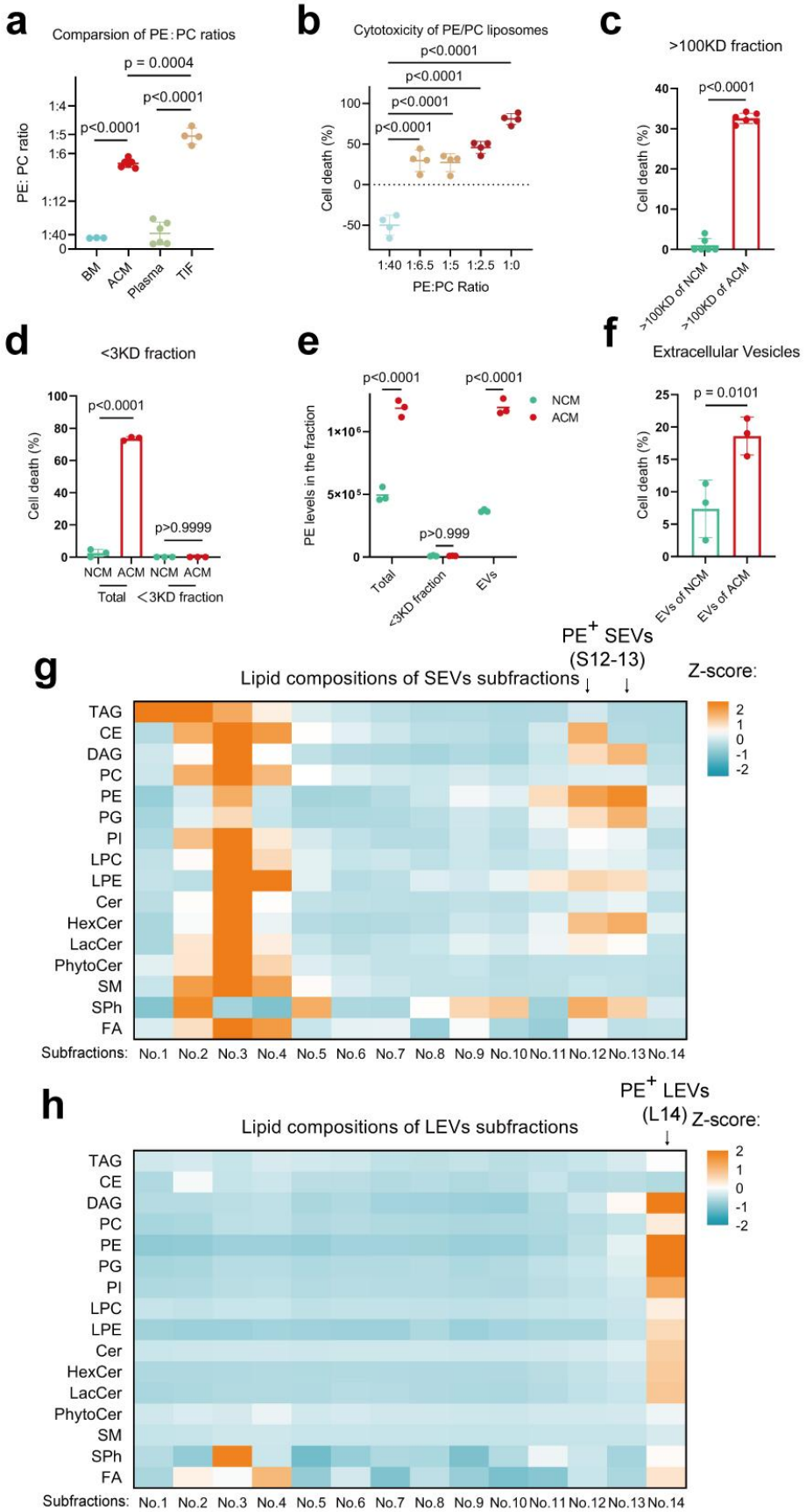
c, Cytotoxicity of PE on Hepatitis C Virus (HCV)-infected human huh7 cells, the efficiency of HCV infection and intracellular virus level of infected cells. Apoptosis was evaluated by Annexin V staining after HCV-

infected huh7 cell treatment with Mock or PE (18:0/20:4) for 48 hours, the level of intracellular virus was indicated as the GFP level of infected cells.

d, Cytotoxicity of PE on non-cancerous human 293FT and cancerous human HCT116 cells. Both 293FT cells and HCT116 cells were treated with PE (18:0/20:4) at various concentrations for 24 hours (n = 3-4).

e, Cytotoxicity of PE on mouse $CD8^+$ T cells and B16F10 tumor cells. OT-I T cells were prepared as **Figure 1a**. Cells were treated with methanol (Mock) and 30 μg/mL PE (18:0/20:4) for 24 hours (n = 5-6).

Data were shown as mean ± SD, and were analyzed by unpaired Student's t-test (**a-b**), two-way ANOVA (**d-e**). Experiments were repeated two (**e**) times.



Extended Data Figure 5. Characterization of PE$^+$ extracellular vesicles (PE$^+$ EVs) in CD8 ACM.

a, PE:PC ratios in blank medium (BM), CD8 ACM, murine plasma, and TIF. Samples were prepared as **Extended Data Figure 2a-b** and quantified by lipidomic analysis (BM, $n = 3$; ACM, $n = 6$; plasma, $n = 6$; TIF, $n = 4$).

b, Cytotoxicity of liposomes with distinct PE:PC ratios on tumor cells. B16F10 cells were treated with liposomes for 24 hours, with the PE (P-18:0/20:4) concentration fixed to 6 μM across all groups ($n = 5$).

c, Cytotoxicity of the >100KD fraction of the conditioned medium. The conditioned medium was ultrafiltered via varying ultrafilters. Concentrates were diluted with blank medium to the original volume, and B16F10 cells were treated with diluted concentrates for 24 hours. Blank medium was served as control. Cell death was evaluated by cell number count via CCK-8 kit ($n = 6$).

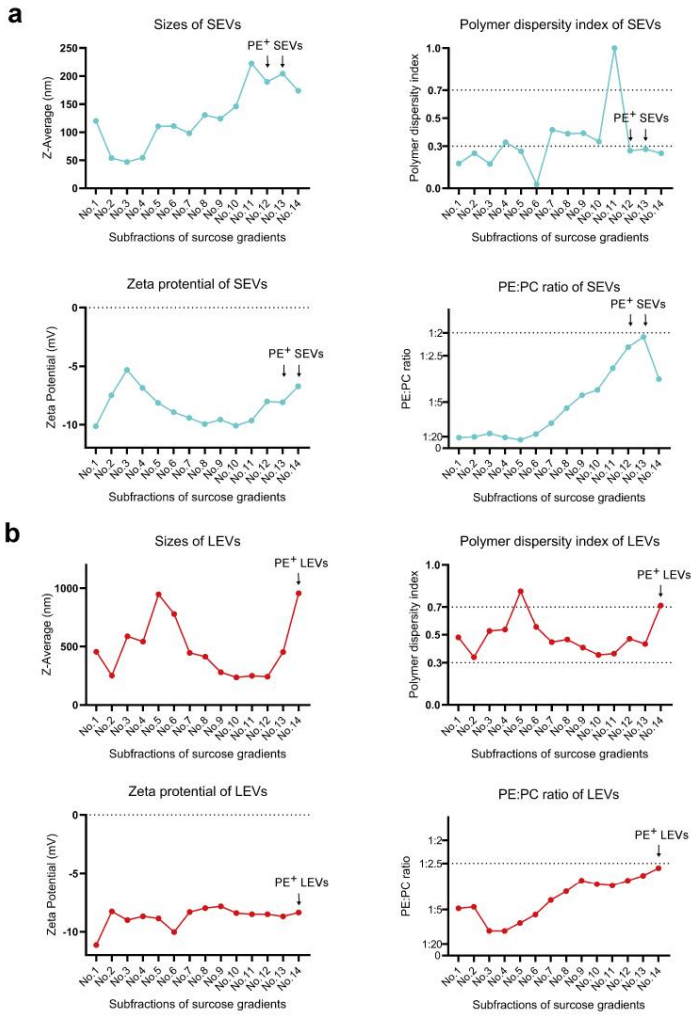
d, Cytotoxicity of <3KD fraction of the conditioned medium. To generate the particle-free medium, the conditioned medium was centrifuged in the 3KD ultrafilter tube at 6000 g and the <3KD soluble fraction was collected. was collected. B16F10 cells were treated with the <3kD soluble fraction for 24 hours. Blank medium was served as control. Cell death was evaluated via CCK-8 kit ($n = 3$).

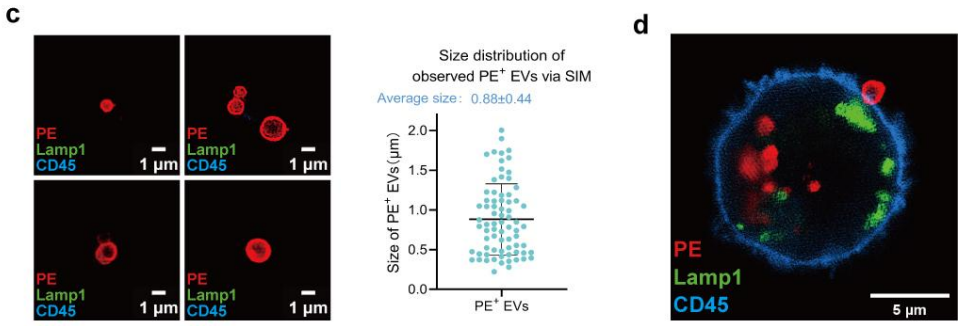
e, PE levels of different fractions of mouse CD8 ACM. The conditioned medium was centrifuged in the 3KD ultrafilter tube at 6000 g and the <3KD soluble fraction was collected in the bottom. Extracellular vesicles were isolated through the total extracellular vesicle isolation kit for medium (Invitrogen). The preparation of ACM and NCM was mentioned in **Figure 1a**. PE levels were measured by mass spectrometry ($n = 3$).

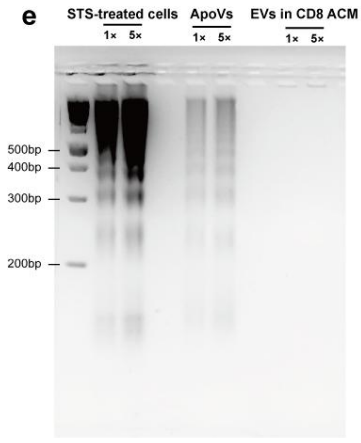
f, Cytotoxicity of the extracellular vesicles (EVs) isolated from the conditioned medium. EVs were isolated as in panel **e** and dissolved in H_2O. EVs were diluted with blank medium (BM) to the original volume and B16F10 cells were then treated with EVs-containing medium for 24 hours. Blank medium was served as control. Cell death was evaluated via flow cytometry ($n = 3$).

g-h, Lipid compositions of small (**e**) and large (**f**) EV subfractions from CD8 ACM. $CD8^+$ T cell cultures were centrifuged at 500×g for 10 minutes to remove cells and debris. Supernatant was collected and centrifuged at 3000×g for 30 minutes. The resulting supernatant (small EVs, SEVs) and pellet (large EVs, LEVs) were collected separately, and pellet was resuspended in PBS. Both SEVs and LEVs were mixed with 5× concentration buffer (40% (w/v) PEG8000, 375 mM NaCl) and incubated at 4°C overnight. Mixtures were centrifuged at 3000×g for 30 minutes to precipitate particles. The precipitated SEVs and LEVs were separately resuspended in sucrose buffer (5% (w/v) sucrose, 20 mM HEPES) and layered onto 5–50% (w/v) continuous sucrose gradients (generated by BioComp gradient maker). After centrifuging at 200,000×g for 16 hours, SEVs or LEVs were fractionated into 14 subfractions from light to heavy density (BioComp fraction collector). All subfractions were subsequently subjected to lipidomic analysis.

Data were shown as mean ± SD, and were analyzed by unpaired Student's t-test (**c, f**), two-way ANOVA (**e**) or one-way ANOVA (**a-b, d**).


a
Sizes of SEVs
PE+ SEVs
Z-Average (nm)
Subfractions of surcose gradients
Polymer dispersity index of SEVs
Polymer dispersity index
Zeta protential of SEVs
Zeta Potential (mV)
PE:PC ratio of SEVs
PE:PC ratio
b
Sizes of LEVs
PE+ LEVs
Polymer dispersity index of LEVs
Zeta protential of LEVs
PE:PC ratio of LEVs
No.1 No.2 No.3 No.4 No.5 No.6 No.7 No.8 No.9 No.10 No.11 No.12 No.13 No.14


c
PE
Lamp1
CD45
1 μm
Size distribution of
observed PE+ EVs via SIM
Average size: 0.88±0.44
Size of PE+ EVs (μm)
PE+ EVs
d
5 μm


e
STS-treated cells
ApoVs
EVs in CD8 ACM
1× 5×
500bp
400bp
300bp
200bp

Extended Data Figure 6. Physicochemical properties of PE^+ EVs in CD8 ACM.

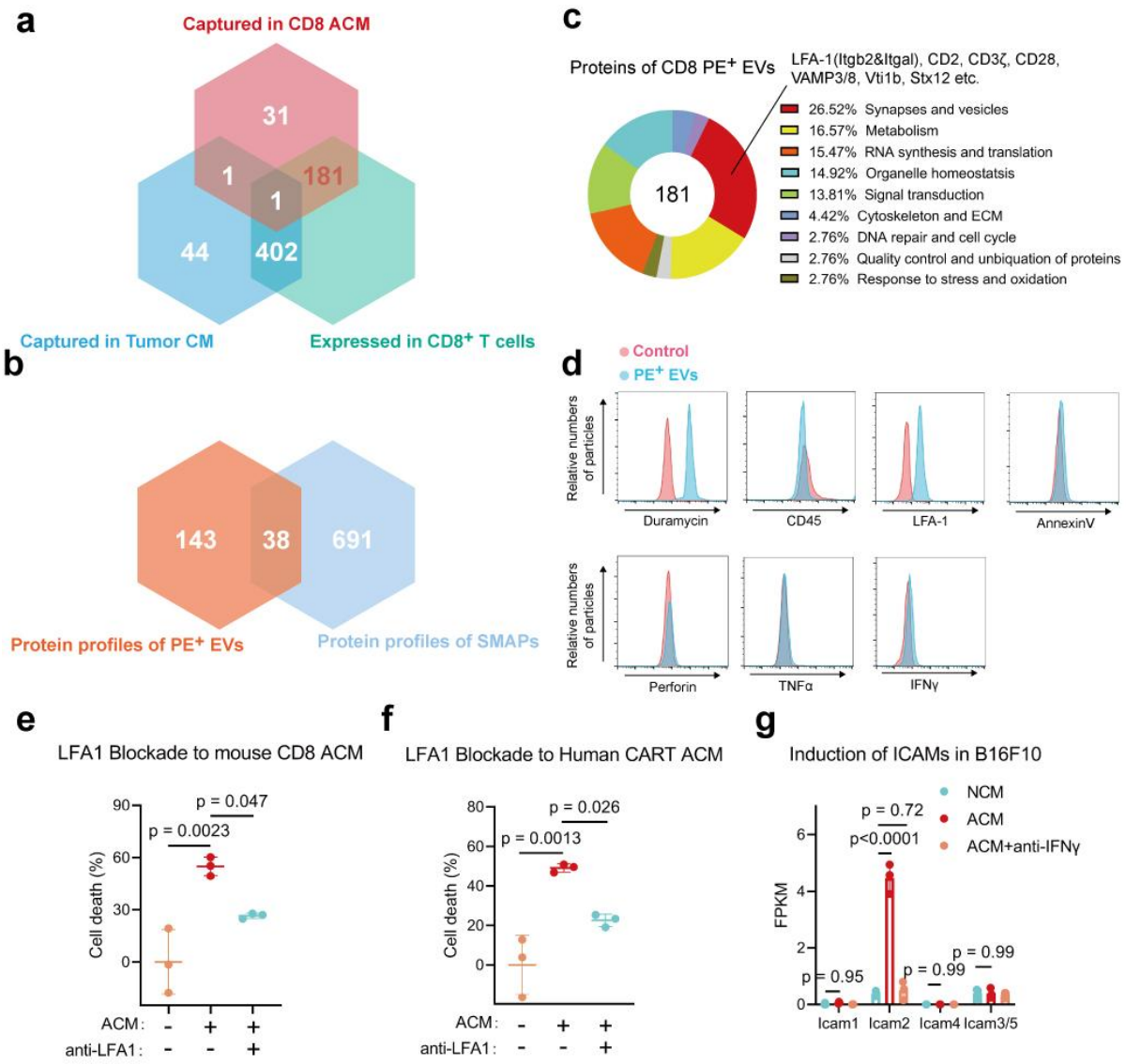
a-b, Average size, polymer dispersity index, PE:PC ratios and zeta potential of SEV (**a**) or LEV (**b**) subfractions**.** The average size, polymer dispersity index and zeta potential were measured by Zetasizer Pro. The EV subfractions were prepared as **Extended Data Figure 5g-h.**

c, PE^+ EVs imaged by High Intelligent and Sensitive Structured Illumination Microscopy (HIS-SIM). Live pre-activated $CD8^+$ T cells were seeded on the poly-L-serine-coated plates for 4 hours in fresh medium containing IL-2, then fixed and stained with duramycin (red), anti-Lamp1 (green), and anti-CD45 (blue). Size distribution and the mean diameter of observed PE^+ EVs were indicated (n = 74). No Lamp1 and CD45 were detected on PE^+ EVs. Scale Bar, 1 μm.

d, Confocal imaging of PE^+ signals in activated $CD8^+$ T cells. Splenocytes isolated from OT-I mice were stimulated by OVA peptides for 2 days to pre-activate $CD8^+$ T cells. Afterward, live $CD8^+$ T cells were seeded on poly-L-serine plate for staining and imaging in the fresh medium containing IL2. Scale bar = 5 μm.

e, DNA fragmentation assay of apoptotic cells, apoptotic bodies, and EVs isolated from antibody-stimulated CD8 ACM. To generate a positive control, $CD8^+$ T cells were treated with 200 nM staurosporine (STS) for 8 hours to induce apoptosis. Supernatant from STS-treated T cells was collected and centrifuged at 3000×g for 30 minutes to harvest apoptotic bodies. EVs were isolated from ACM of anti-CD3/CD28-activated $CD8^+$ T cells via a standard kit. DNA was extracted and analyzed by electrophoresis. Two different amounts (1× and 5×) of each DNA sample were loaded.

Data were shown as mean ± SD (**c**), Experiments were repeated two (**c-e**) times.



Extended Data Figure 7. Protein profiles of PE$^+$ EVs derived from CD8$^+$ T cells.

a, Proteome comparison between PE-containing EVs in CD8 ACM and tumor CM captured by duramycin (Details in Method). In the protein list of the CD8 sample, the overlapped proteins between CD8 and tumor samples were removed. Moreover, the proteins that are not expressed by CD8$^+$ T cells, likely contributed by the medium, were also removed. The remaining 181 proteins, highlighted by red color, were defined as specific proteins of CD8 PE$^+$ EVs.

b, Comparison of proteins in CD8 PE$^+$ EVs and supramolecular attacking particles (SMAPs)[39].

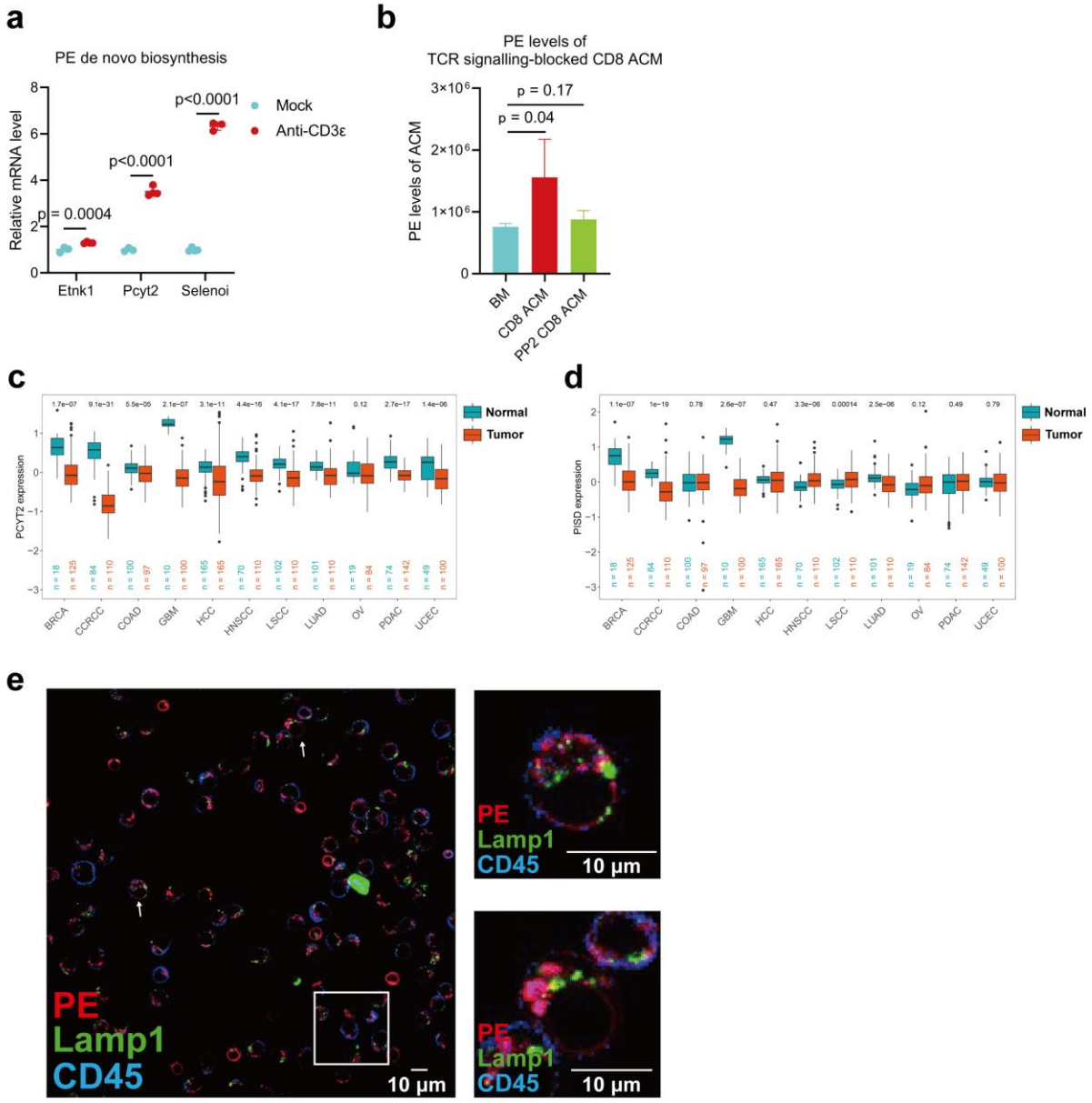
c, Functional annotation of the 181 proteins of CD8 PE$^+$ EVs.

d, FACS analysis of surface markers or conventional cytotoxic effectors on CD8 PE$^+$ EVs.

e-f, Effect of LFA-1 blockade on the cytotoxicity of mouse CD8 ACM (**e**) or human CAR-T ACM (**f**). B16F10 cells (**e**) or HCT116 cells (**f**) were treated with mouse CD8 ACM or human CAR-T ACM in the presence of mock or anti-LFA1 (1:50) for 24 hours ($n = 3$).

g, Effect of IFNγ blockade on ICAM expression in B16F10 cells induced by mouse CD8 ACM. B16F10 cells were treated with mouse CD8 ACM for 48 hours, with or without IFNγ blockade antibody (1:50). Data are from bulk RNA sequencing.

Data were all shown as mean ± SD, and were analyzed by two-way ANOVA (**g**) or one-way ANOVA (**e-f**).



912

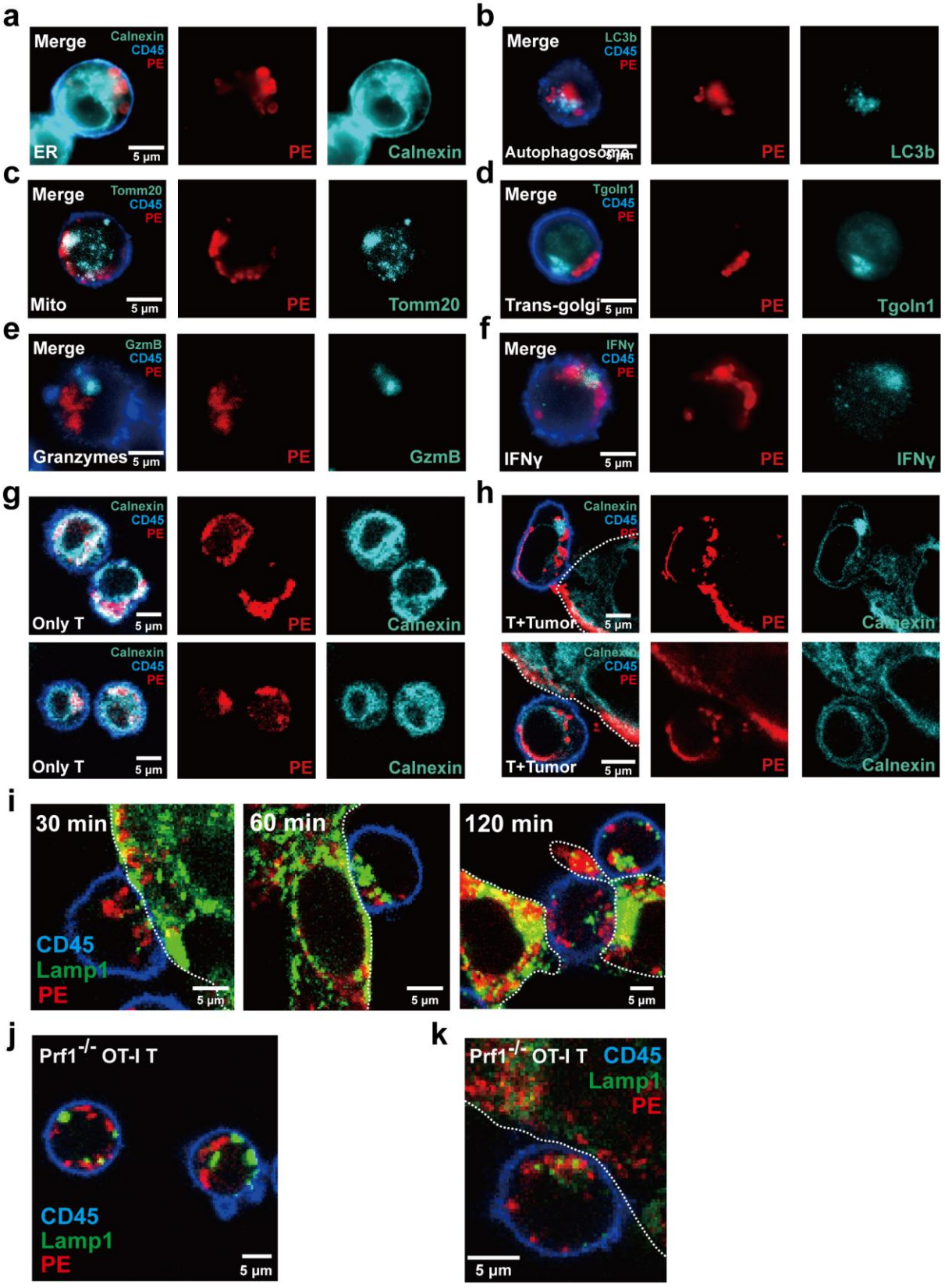
913 **Extended Data Figure 8. PE production in T cells and tumor cells.**

914 **a,** Transcriptional changes of PE *de novo* biosynthesis genes following anti-CD3 stimulation. Naïve $CD8^+$
915 T cells isolated from mouse spleens were treated with mock or anti-CD3ε (10 μg/mL) for 48 hours.
916 Transcription levels of the indicated genes were measured by RT-qPCR and normalized to 18S rRNA (*n* =
917 3).

918 **b**, PE levels in CD8 ACM generated from PP2-treated T cells (PP2 CD8 ACM). OT-I T cells and B16F10-
919 OVA cells were cocultured at an E:T ratio of 2:1 in the presence of mock or 10 μM PP2 for 24 hours.
920 Conditioned media were then collected and subjected to lipidomic analysis (*n* = 2-4).

921 **c-d,** Protein levels of PCYT2 **(c)**, the rate-limiting of PE *de novo* biosynthesis, and PISD **(d)**, the key enzyme
922 in the PE salvage pathway, in tumor and peritumoral tissues. All data was acquired from the National Cancer
923 Institute (NIH)'s Clinical Proteomic Tumor Analysis Consortium (CPTAC) Database. BRCA, breast cancer;
924 CCRCC, clear cell renal cell carcinoma; COAD, colorectal cancer; GBM, glioblastoma; HCC, hepatocellular
925 carcinoma; HNSCC, head and neck squamous cell carcinoma; LSCC, laryngeal squamous cell carcinoma;
926 LUAD, lung adenocarcinoma; OV, ovary cancer; PDAC, pancreatic adenocarcinoma; UCEC, uterine corpus

endometrial carcinoma. P-value of each cohort was at the top and numbers of patients was at the bottom. **e**, Representative confocal images showing Lamp1 and PE lipid localization in activated $CD8^+$ T cells. The region used in **Figure 2d** is highlighted by a while box. White arrows indicate representative cells with PE signals localized at both PM and intracellular vesicles, and they are enlarged on the right. Scale bar, 10 μm. Data were shown as mean ± SD (**a, b**), and were analyzed by unpaired Student's t-test (**a, b**). Experiments were repeated two (**a**) times.



Extended Data Figure 9. Localization of PE$^+$ intracellular vesicles in CD8$^+$ T cells.

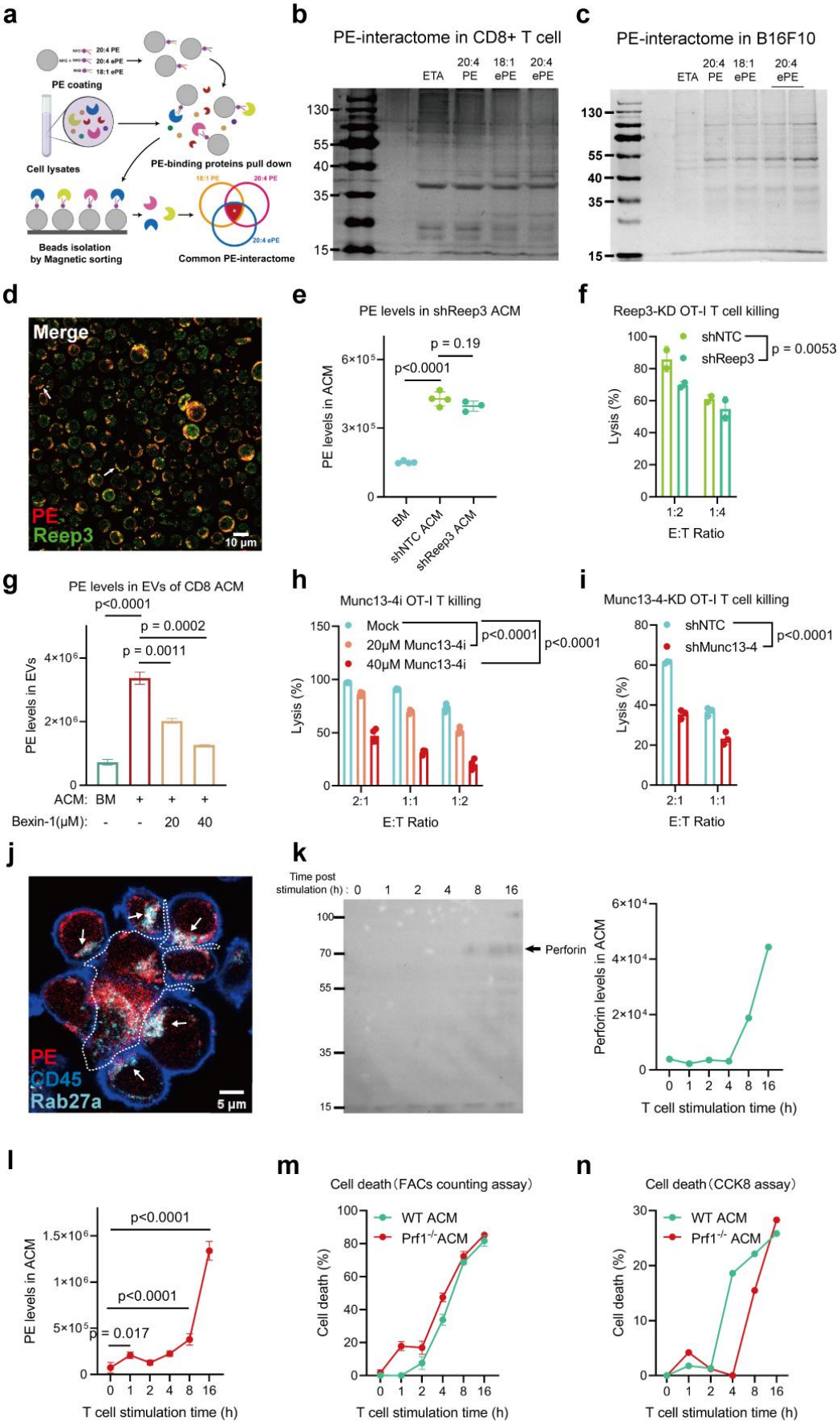
a-f, Colocalization of PE$^+$ intracellular vesicles with organelles (**a-d**) and cytotoxic proteins (**e-f**) in activated CD8$^+$ T cells, imaged by HIS-SIM. Cells were stained with ER marker calnexin (**a**), autophagosome marker LC3b (**b**), mitochondrial marker Tomm20 (**c**), trans-Golgi marker Tgoln1 (**d**) and anti-IFNγ (**f**). In **e**,

Granzyme B-mCherry fusion proteins were expressed in CTLL-2 cytotoxic T cell lines to trace Granzyme B localization. All cells were stained with duramycin (red, indicates PE^+ intracellular vesicles) and CD45 (blue, indicates T cell membrane). Scare Bar, 5 μm.

g-h, Colocalization of PE^+ intracellular vesicles with ER marker calnexin in activated $CD8^+$ T cells under T cell-only condition (**g**) or T cell-tumor conjugation condition (**h**), imaged by confocal microscopy. Cells in **h** were conjugated for 2 hours. Dash lines mark the boundary of tumor cells. Scare Bar, 5 μm.

i, Spatial distribution of PE^+ intracellular vesicles and $Lamp1^+$ granules in $CD8^+$ T cells conjugated with tumor cells, imaged by confocal microscopy. B16F10-OVA cells were seeded on poly-L-serine-coated plates overnight. Activated $CD8^+$ T cells were added and co-incubated with tumor cells for 30 minutes (left), 60 minutes (middle), and 120 minutes (right), then fixed and stained with duramycin (indicates PE^+ vesicles), anti-Lamp1 (indicates cytotoxic granules), and anti-CD45 (indicates T cell membrane). Dash lines mark the boundary of tumor cells. Scare Bar, 5 μm.

j-k, Spatial distribution of PE^+ intracellular vesicles and $Lamp1^+$ granules in activated *Prf1*$^{-/-}$ $CD8^+$ T cells without tumor conjugation (**j**) or with tumor conjugation (**k**). Dash lines mark the boundary of tumor cells. Scare Bar, 5 μm.



Extended Data Figure 10. PE secretion from CD8⁺ T cells was mediated by Munc13-4.

a-c, A newly designed PE-interactome assay. (**a**) Schematic illustration. Briefly, the exposed primary amine group in the PE headgroup was immobilized on NHS-functionalized magnetic beads, through the NHS-amine covalent bond. Three types of PE lipids, 20:4 PE (PE 18:0/20:4), 18:1 ePE (PE P-18:0/18:1) and 20:4 ePE (PE P-18:0/20:4) were used to generate individual type of PE-coated beads. Ethanolamine (ETA)-coated bead was also generated as a control. PE-coated or ETA-coated magnetic beads were then co-incubated with lysates of activated $CD8^+$ T cell lysates or B16F10 cell lysates overnight to capture PE-binding proteins on the beads. Following magnetic sorting and protein elution, mass spectrometry was performed to identify PE-binding proteins. Only the hits shared by all three PE lipids were selected as common PE-binding proteins. Moreover, the experiment was repeated to validate the protein hits. **b-c**, Silver staining of the proteins pulled down by different types of PE-coated beads in $CD8^+$ T cells (**b**) or B16F10 cells (**c**).

d, Representative confocal images showing the localization of Reep3 and PE lipids in activated $CD8^+$ T cells. The cells shown in **Figure 2i** were indicated by white arrows.

e, Effect of Reep3 knockdown on secreted PE levels in CD8 ACM. Control (shNTC) or Reep3-knockdown (shReep3) OT-I T cells were activated, and ACM was collected as **Figure 1a**, followed by PE measurement by mass spectrometry (n = 3-4).

f, Effect of Reep3 knockdown on T cell killing. Reep3-KD OT-I T cells were co-incubated with B16F10-OVA cells at different E:T ratios for 24 hours (n = 2).

g, Effect of Munc13-4 inhibition on secreted PE levels in EVs of CD8 ACM. OT-I T cells were pretreated with mock or Munc13-4 inhibitor Bexin-1 (Munc13-4i) for 45 minutes. ACM was collected as **Figure 1a** and EVs were isolated through the total extracellular vesicle isolation kit for medium (Invitrogen). PE levels of EVs were measured by mass spectrometry (n = 2).

h, Effect of Munc13-4 inhibition on T cell killing. OT-I T cells were pretreated with Munc13-4 inhibitor (Munc13-4i) Bexin-1 or solvent control for 45 min, then co-incubated with B16F10-OVA cells at different E:T ratios for 24 hours (n = 3).

i, Effect of Munc13-4 knockdown on T cell killing. Munc13-4-KD OT-I T cells were co-incubated with B16F10-OVA cells at different E:T ratios for 24 hours (n = 3).

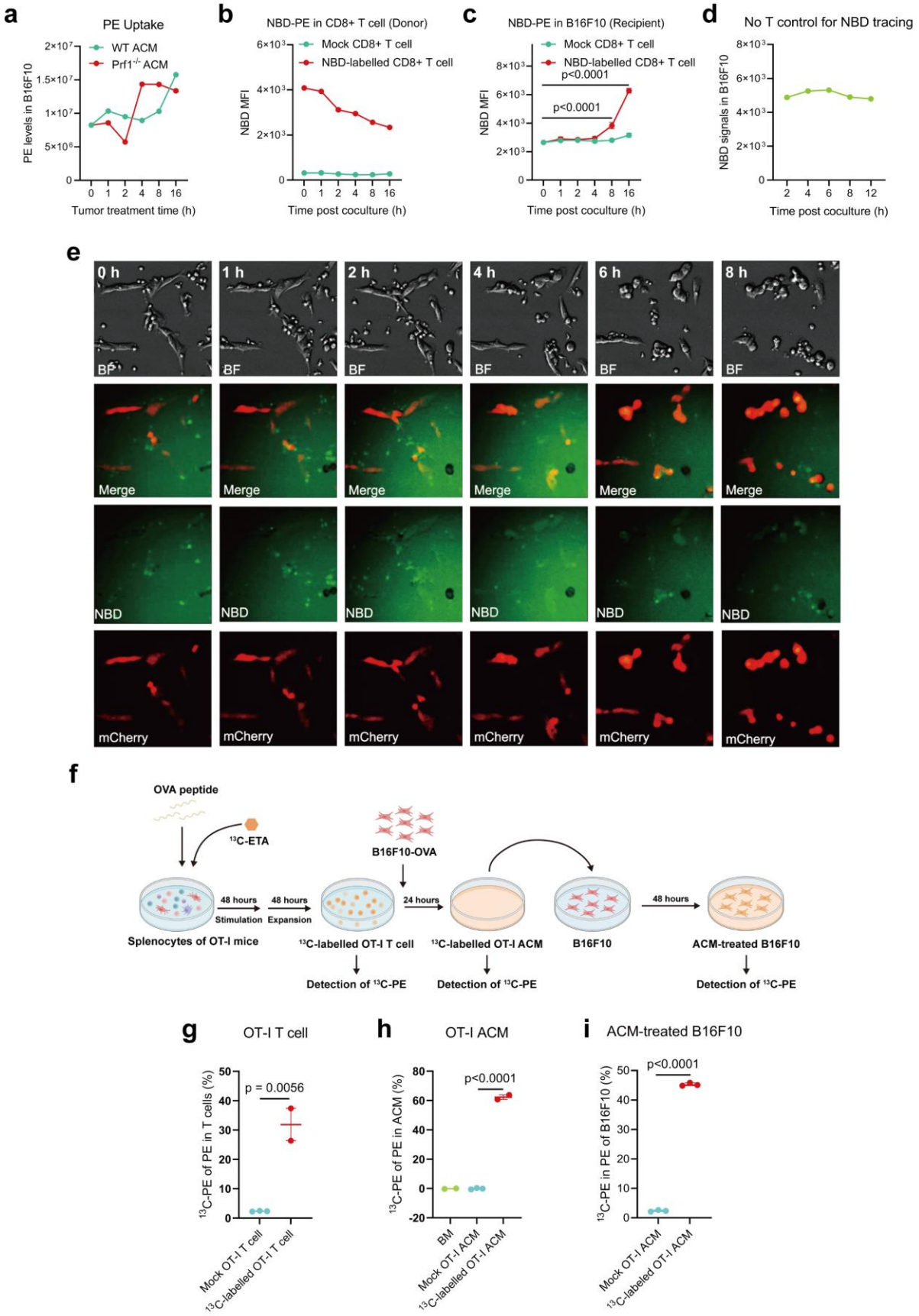
j, Colocalization of PE lipids and Rab27a at the T cell-tumor contact sites, imaged by confocal microscopy. B16F10-OVA cells were seeded on poly-L-serine-coated plates overnight. Activated $CD8^+$ T cells were added and co-incubated with tumor cells for 2 hours, then fixed and stained with duramycin (imaging PE lipids), anti-Rab27a, and anti-CD45. White arrows indicate the colocalization of PE and Rab27a at the T cell-tumor contact sites. The dash line indicates tumor cell shape.

k, Secretion kinetics of perforin by $CD8^+$ T cells, measured by immunoblotting. OT-I T cells were co-cultured with B16F10-OVA cells at an E:T ratio of 2:1, and CD8 ACM was collected at different time points (0, 1, 2, 4, 8, 16 hours). Perforin levels were semi-quantitated by gray value analysis using ImageJ and normalized to the blank zone.

l, Secretion kinetics of PE lipids by $CD8^+$ T cells, measured by lipid mass spectrometry. OT-I T cell stimulation and CD8 ACM collection were the same as panel **j**. PE levels were normalized to blank medium (n = 4).

m-n, Cytotoxicity of ACM collected at different T-cell stimulation timepoints. Wild-type OT-I T cells or *Prf1*$^{-/-}$ OT-I T cells were co-cultured with B16F10-OVA cells at an E:T ratio of 2:1. CD8 ACM were collected at different stimulation timepoints, and then used to treat B16F10 cells for 16 hours. Tumor cell number (**l**) and cell viability (**m**) were assessed by flow cytometry and CCK-8, respectively.

Data were all shown as mean ± SD, and were analyzed by two-way ANOVA (**f, h-i**) or one-way ANOVA (**e, g, l**). Experiments were repeated two (**f, h-i**) times.



Extended Data Figure 11. Temporal Kinetics of PE transportation from T cells to tumor cells.

a, Kinetics of PE uptake from ACM by B16F10 cells. The experimental conditions were the same as

Extended Data Figure 1h-i. After 16-hour co-culture of WT or *Prf1*$^{-/-}$ OT-I T cells with target cells, ACM was collected and then used to treat B16F10 cells for different durations. PE levels were measured by mass spectrometry.

b-c, Time-course of PE transfer from CD8^{+} T cells to tumor cells. OT-I T cells were pretreated with NBD-ETA (1 mM) or mock (1 mM ETA) for 48 hours to label biosynthesized PE. After NBD-ETA removal, T cells were co-cultured with B16F10-OVA cells at E:T = 8:1 for 0-16 hours. NBD signals in T cells (**b**) and B16F10 cells (**c**) were analyzed by flow cytometry (n = 2–3).

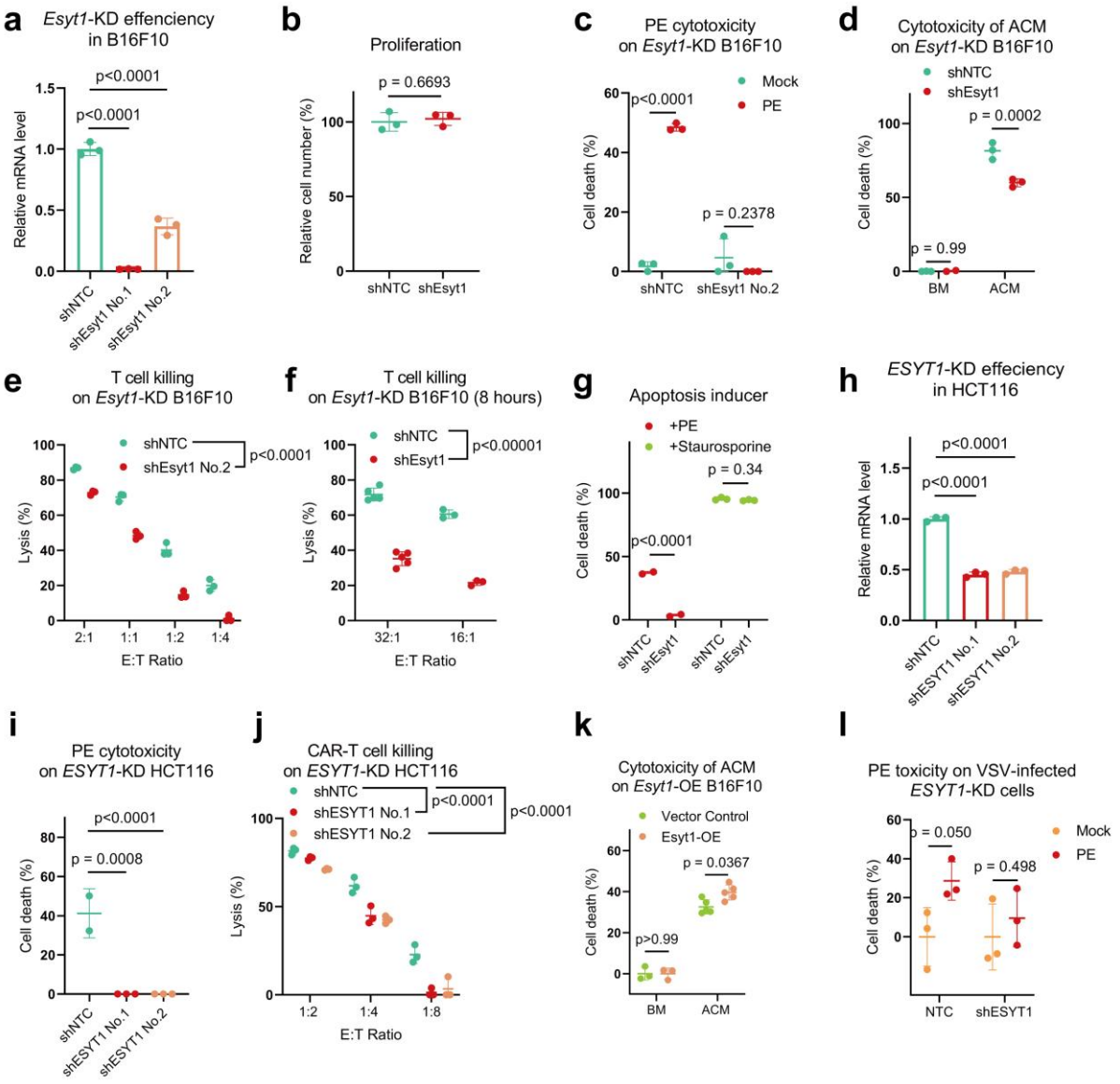
d, Basal fluorescence levels in NBD-unlabeled B16F10 cells cultured for different durations, measured by flow cytometry.

e, Live-cell imaging of PE transfer from CD8^{+} T cells to tumor cells. The experiment was the same as in panel **b-c**, and cells were imaged by Zeiss Celldiscoverer 7 microscope **(Supplementary Movie 1)**.

f, ^{13}C-isotope tracing of intercellular PE transfer from CD8^{+} T cells to tumor cells. Splenocytes from OT-I mice were stimulated with OVA peptide (10 nM), IL-2 (10 ng/mL), and ^{13}C-ETA (1 mM) or mock for 48 hours. Next, OVA peptide was removed, and cells were cultured in the medium with IL-2 and ^{13}C-ETA for additional 48 hours. After removal of ^{13}C-ETA, T cells were further stimulated by B16F10-OVA cells at an E:T ratio of 2:1 for 24 hours, followed by ACM collection. B16F10 cells were treated with ACM for 48 hours. ^{13}C-PE levels were measured by mass spectrometry.

g-i, ^{13}C-PE levels in stimulated CD8^{+} T cells (**g**), ACM (**h**) and tumor cells (**i**). Stimulated OT-I T cells (as in **f**; n = 2–3) were labeled with ^{13}C-ETA. Levels and fractions of both ^{13}C-PE signals in labelled T cells, ACM (as in **f,** n = 2-3) and ACM-treated B16F10 cells (as in **f**, n = 3) were assessed by mass spectrometry.

Data were shown as mean ± SD, and were analyzed by unpaired Student's t-test (**g, i**), two-way ANOVA (**c**) or one-way ANOVA (**h**). Experiments were repeated three (**b-c**) or two (**a**) times.



Extended Data Figure 12. Manipulation of Esyt1 levels in mouse and human cells affected PE cytotoxicity.

a, Relative mRNA levels of Esyt1 in the B16F10 cells with Esyt1 knockdown (Esyt1-KD). To silence Esyt1, cells were transfected with lentivirus leading to stable expression of shRNA No.1 or No.2 towards Esyt1. Transcription levels of ESYT1 were normalized to 18S rRNA (n = 3). Targeted sequences of shRNAs were in **Method**.

b, Proliferation of Esyt1-KD B16F10 cells. Esyt1-KD B16F10 cells were generated with shRNA No.1. Control and knockdown tumor cells were seeded in the plates with the same density, and tumor cell numbers were counted using flow cytometry after 24 hours (n = 3).

c, Cytotoxicity of PE on attached Esyt1-KD B16F10 cells generated with shRNA No.2. Cells were treated with 30 μg/mL PE (18:0/20:4) for 24 hours (n = 3).

d, Effect of Esyt1 knockdown in tumor cells on CD8 ACM cytotoxicity. Esyt1-KD B16F10 cells were generated by shRNA No.1, and treated with conditioned media for 24 hours (n = 3).

e, T cell killing of attached Esyt1-KD B16F10-OVA cells generated with shRNA No.2. Activated $CD8^+$ T cells were co-cultured with control or Esyt1-KD B16F10-OVA cells at different E:T Ratios for 24 hours (n

= 3).

f, Effect of Esyt1 knockdown in tumor cells on 8-hour T cell killing. Esyt1-KD B16F10-OVA cells generated by shRNA No.1. Esyt1-KD B16F10-OVA cells were co-cultured with T cells at varying E:T ratios for 8 hours (*n* = 3).

g, Apoptosis induction of attached Esyt1-KD B16F10 cells. Cells were treated with 200 nM Staurosporine for 8 hours or with 30 μg/mL PE (18:0/20:4) for 24 hours (*n* = 2-3).

h, Relative mRNA levels of Esyt1 in the HCT116 with ESYT1 knockdown. Transcription levels of ESYT1 were normalized to 18S rRNA (*n* = 3).

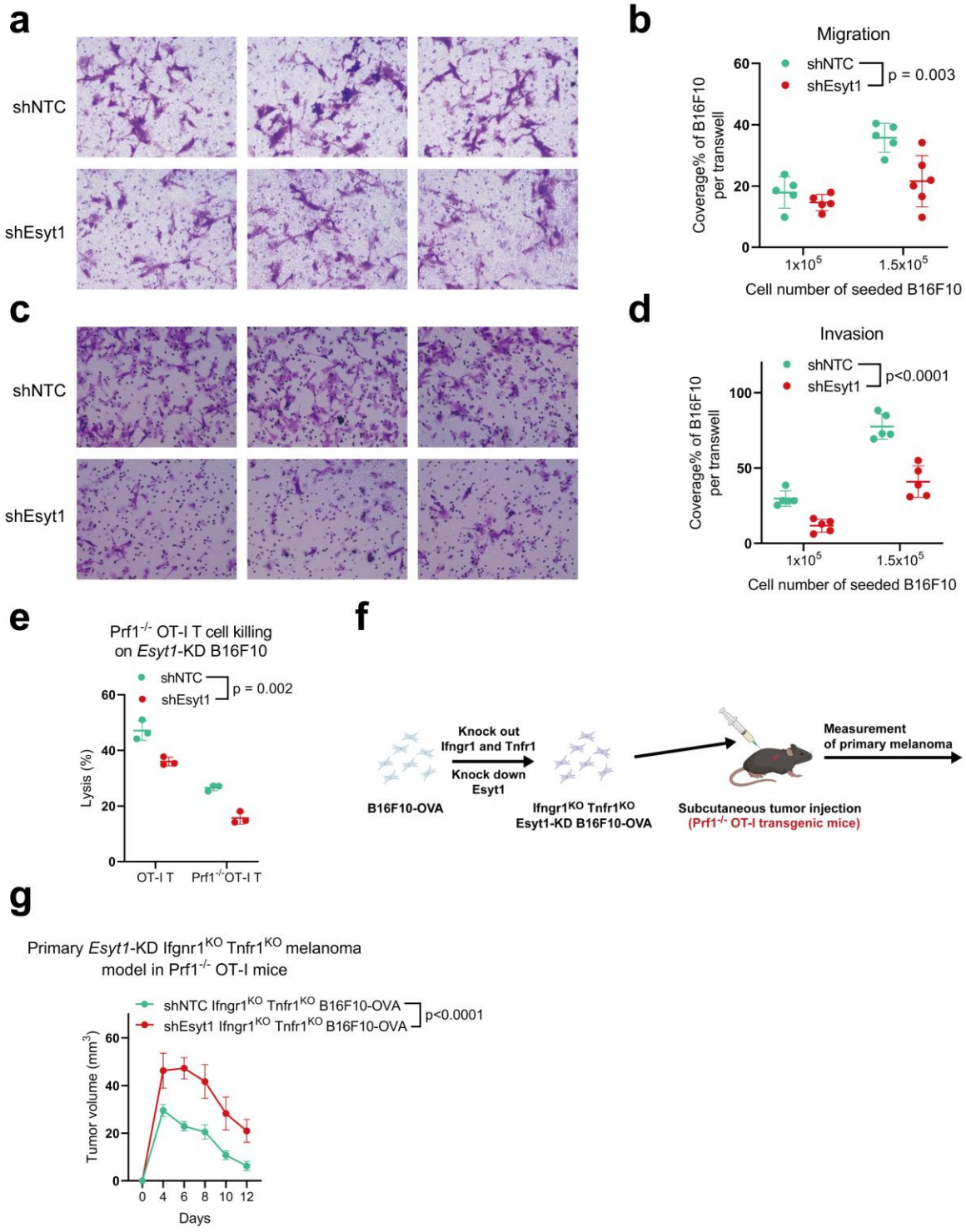
i, Cytotoxicity of PE on ESYT1-KD HCT116 cells. Human HCT116 cells were treated with 20 μg/mL PE (18:0/20:4) for 48 hours (*n* = 3).

j, CAR-T killing of attached ESYT1-KD HCT116 cells. Human MSLN.28Z CAR T cells were co-cultured with control or ESYT1-KD HCT116 cells at different E:T Ratios for 24 hours (*n* = 3).

k, Effect of Esyt1 overexpression in tumor cells on CD8 ACM cytotoxicity. Attached Esyt1-OE B16F10 cells were treated with conditioned media for 24 hours (*n* = 3).

l, Cytotoxicity of PE on VSV-infected ESYT1-KD Huh7 cells. Huh7 cells were transduced with non-target shRNA or ESYT1 shRNA No. 1. Cells were infected with VSV virus for 6 hours, followed by 30 μg/mL PE (18:0/20:4) treatment for 24 hours (*n* = 3).

Data were shown as mean ± SD, and were analyzed by unpaired Student's t-test (**b, l**), two-way ANOVA (**c-g, j-k**) or one-way ANOVA (**a, h-i**).



Extended Data Figure 13. Esyt1 deficiency in tumor reduced intrinsic migration and invasion, while promoted resistance to T cell killing.

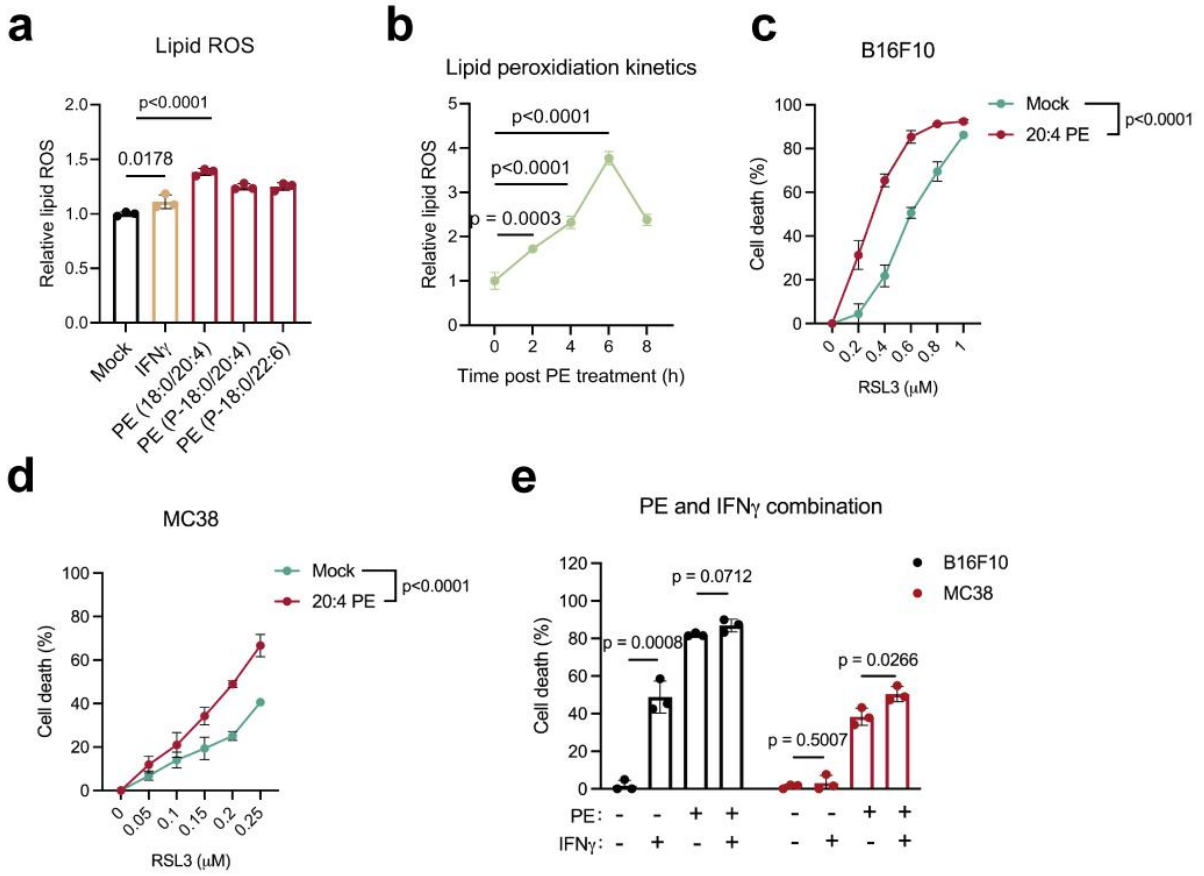
a-d, Migration **(a-b)** and invasion **(c-d)** capacity of Esyt1 knockdown (Esyt1-KD) B16F10 cells. **a-b,** Representative images **(a**, 1×10^5 group**)** of migrated Esyt1-KD B16F10 cells through uncoated transwell membranes after 48-hour incubation. Cells were stained with crystal violet and visualized under a microscope. Quantification of migrated cells are shown in **b**. Each dot represents one field of view (n = 5). **c-d,** Representative images (**c**, 1×10^5 group) of invaded Esyt1-KD B16F10 cells through matrigel-coated (invasion) transwell membranes after 48-hour incubation. Cells were stained with crystal violet and

visualized under a microscope. Quantification of invaded cells are shown in **d**. Each dot represents one field of view (n = 5). Quantification of coverage was performed by ImageJ.

e, Killing function of wildtype OT-I T cells and *Prf1*$^{-/-}$ OT-I T cells against Esyt1-KD B16F10 cells. B16F10-OVA cells were seeded overnight, then co-cultured with T cells at an E:T ratio of 2:1 for 24 hours (n = 3).

f-g, *In vivo* effect of Esyt1 knockdown in tumor cells under the toxin-null condition. (**f**) Schematic of a primary melanoma model using the toxin-null system. 3.5×10^6 *Ifngr1*^{KO}*Tnfr1*^{KO} B16F10-OVA cells (Esyt1-KD or non-targeting control) were subcutaneously injected into *Prf1*$^{-/-}$ OT-I transgenic mice (shNTC, n = 8; shEsyt1, n = 7). (**g**) Tumor progression was monitored every 2 days.

Data were shown as mean ± SD (**b, d, e**) and mean ± SEM (**g**), and were analyzed by two-way ANOVA.



Extended Data Figure 14. PE lipids navigated ferroptosis in tumor cells.

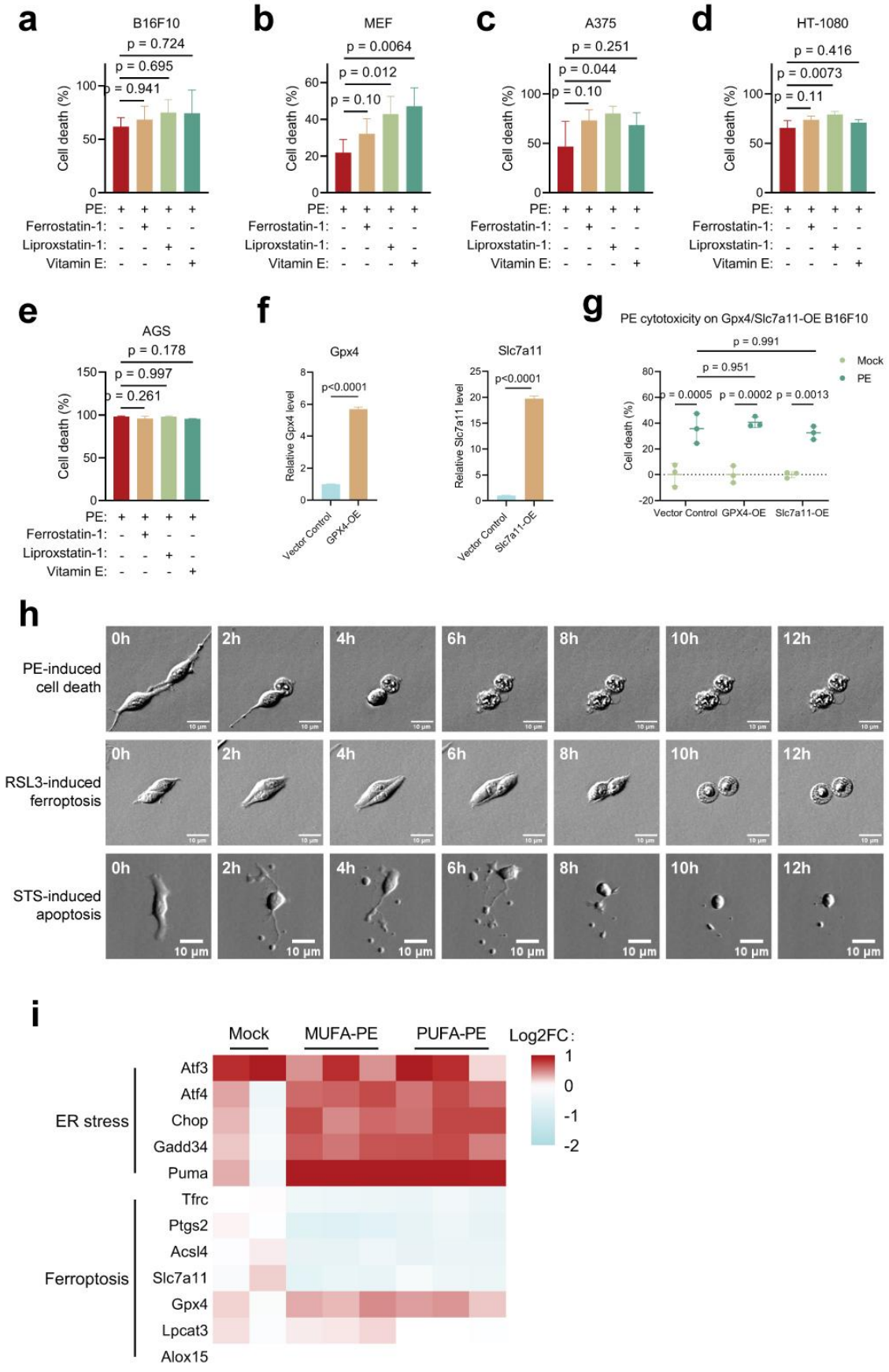
a, Lipid ROS levels in B16F10 cells with PE treatment. Cells were treated with 30 μg/mL PE (18:0/20:4), PE (P-18:0/20:4) or PE (P-18:0/22:6) for 24 hours, then stained by BODIPY 581/591 C11 and detected by flow cytometry. As control, recombinant IFNγ (10 ng/mL) was used to treat B16F10 cells for 24 hours (n = 3).

b, Kinetics of lipid peroxidation induced by PE treatment in tumor cells. B16F10 cells were treated by 30 μg/mL PE (18:0/20:4) for different durations. Lipid ROS levels were measured by BODIPY 581/591 C11 staining (n = 2-3).

c-d, Ferroptosis induction by RSL3 titration in B16F10 cells (**a**) and MC38 cells (**b**) pretreated with PE carrying polyunsaturated fatty acid. Cells were pre-treated with 30 μg/mL PE (18:0/20:4) for 48 hours and then the medium was changed to fresh medium with RSL3 for 24 hours. (n = 3).

e, Combined treatment of IFNγ with PE to B16F10 and MC38 cells. B16F10 cells were treated with 10 ng/mL IFNγ and 30 μg/mL PE (18:0/20:4) for 24 hours. MC38 cells were treated with 50 ng/mL IFNγ and 30 μg/mL PE (18:0/20:4) for 24 hours. Tumor cell numbers were counted by flow cytometry (n = 3).

Data were shown as mean ± SD, and were analyzed by unpaired Student's t-test (**e**), two-way ANOVA (**c-d**) or one-way ANOVA (**a-b**). Experiments were repeated two (**a, c**) times.



Extended Data Figure 15. PE treatment did not induce canonical ferroptosis.

a-e, Effects of ferroptosis inhibitors on PE killing of ferroptosis-sensitive cells. B16F10 (a), mouse embryo fibroblast (b), A375 (c), HT-1080 (d), and AGS (e) were treated with the ferroptosis inhibitor ferrostatin-1, Liproxstatin-1, or Vitamin E. Cells were treated with 30 μg/mL PE (18:0/20:4) for 24 hours in the presence of 10 μM ferrostatin-1, 20 nM Liproxstatin-1, or 10 μM Vitamin E. Cell death was evaluated by flow cytometry (n = 3).

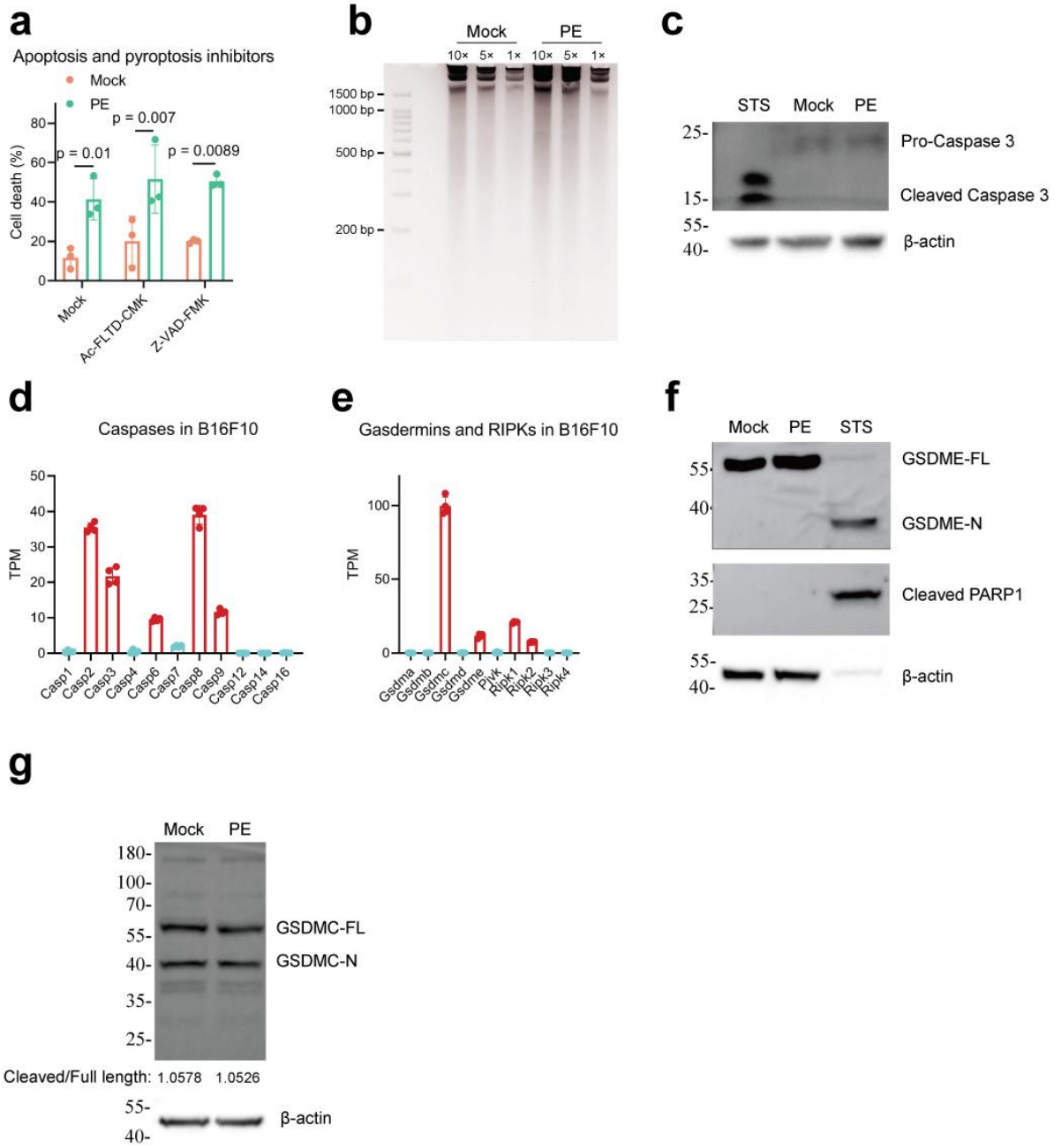
f, Overexpression efficiency of Gpx4 and Slc7a11 in B16F10 cells (Gpx4-OE or Slc7a11-OE). Transcription levels of Gpx4 and Slc7a11 were normalized to 18S rRNA (n = 5-6).

g, Effect of Gpx4 or Slc7a11 overexpression on PE killing of tumor cells. Attached control, Gpx4-OE or Slc7a11-OE B16F10 cells were treated with 6 μM PE (18:0/20:4) for 24 hours (n = 3).

h, Live-cell imaging of the morphological changes in tumor cells treated with PE, RSL3, or staurosporine (STS). B16F10 cells were treated with 30 μg/mL PE (18:0/20:4), 100 nM RSL3, or 100nM STS and imaged by Zeiss Celldiscoverer 7 microscope.

i, Transcriptional levels of death-associated genes in B16F10 cells treated with mock, PE (P-18:0/18:1) (MUFA-PE), or PE (18:0/20:4) (PUFA-PE). Cells were treated with 30 μg/mL PE lipids for 24 hours. Cells were then collected and subjected to bulk RNA sequencing.

Data were shown as mean ± SD, and were analyzed by unpaired Student's t-test (**f**), two-way ANOVA (**g**) or one-way ANOVA (**a-e**). Experiments were repeated two (**a, g**) times.



Extended Data Figure 16. PE treatment did not induce canonical apoptosis and pyroptosis.

a, Effects of pyroptosis inhibitor (Ac-FLTD-CMK) or pan caspase inhibitor (Z-VAD-FMK) on PE cytotoxicity. B16F10 cells were pre-treated with 50 μM Ac-FLTD-CMK and Z-VAD-FMK for 1 hour followed by co-treatment with inhibitors and 30 μg/mL PE (18:0/20:4) for 24 hours (n = 3).

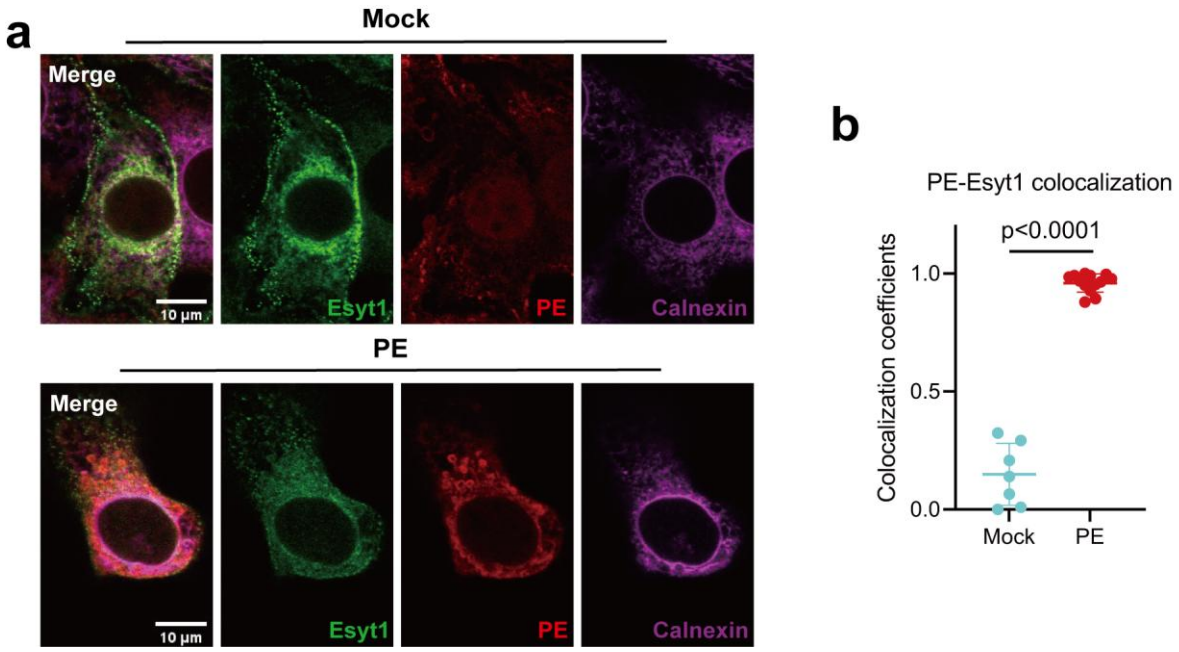
b, DNA fragmentation assay of PE-treated B16F10 cells. Cells were treated with mock or 30 μg/mL PE (18:0/20:4) for 24 hours. Three amounts of each DNA sample (1×, 5× and 10×) were loaded for analysis.

c, Immunoblotting of caspase 3 in B16F10 cells treated with 30 μg/mL PE (18:0/20:4) or 200 nM staurosporine (STS) for 24 hours. STS-treated cells were served as a positive control for caspase 3 cleavage.

d-e, Transcriptional levels of Caspases (**i**), Gasdermins and receptor-interacting serine/threonine-protein kinases (**j**) family genes in B16F10 cells. Data from bulk RNA sequencing (**d-e**, n = 4).

f, Immunoblotting of GSDME and PARP1 in B16F10 cells treated with 30 μg/mL PE (18:0/20:4) or 200 nM STS for 24 hours.

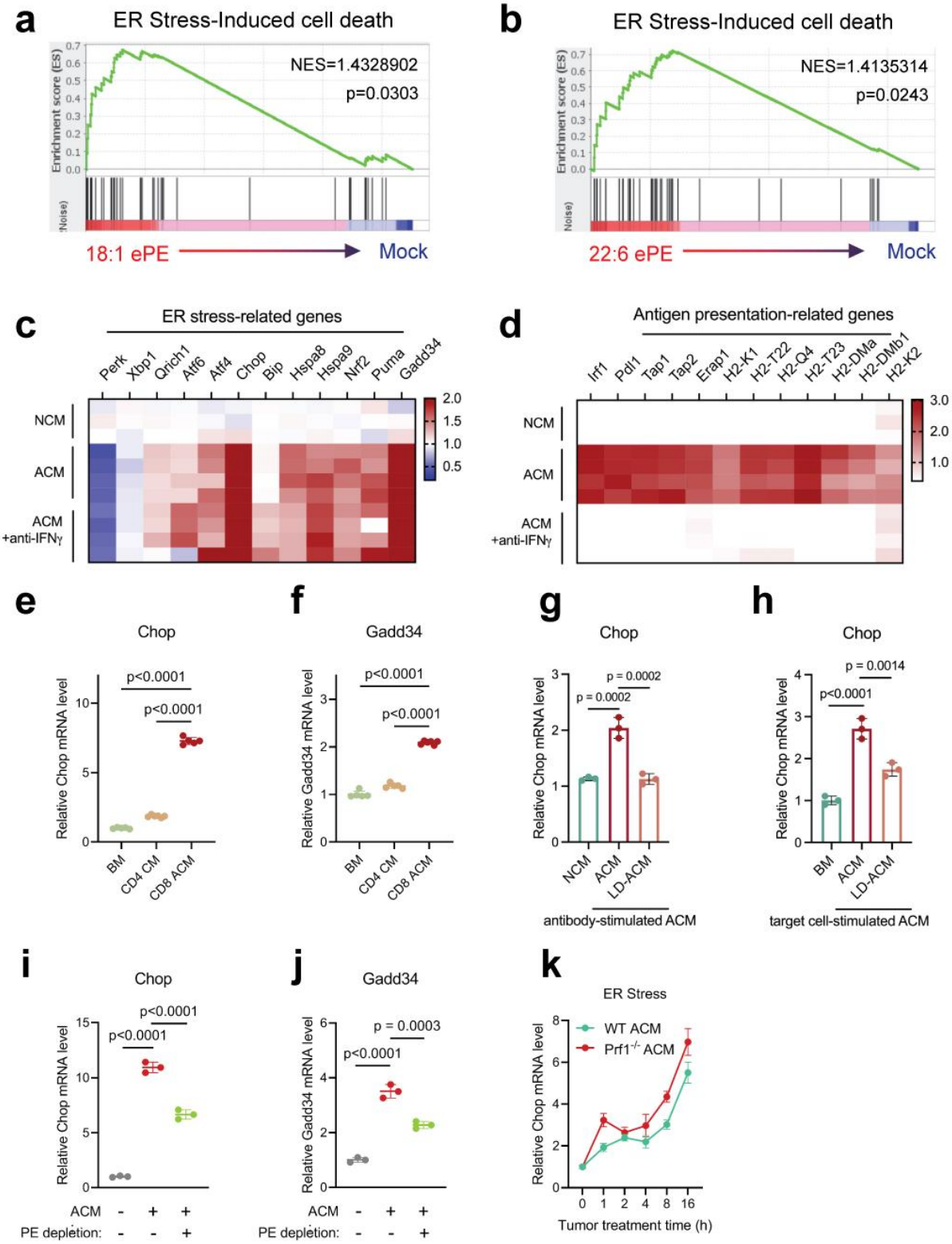
g, Immunoblotting of GSDMC in B16F10 cells treated with 30 μg/mL PE (18:0/20:4) for 24 hours. B16F10 cells overexpressing flag-tagged GSDMC were used to study GSDMC cleavage. The ratio of N-terminal cleaved GSDMC (GSDMC-N)/ full-length GSDMC (GSDMC-FL) was quantitated by ImagJ.
Data were shown as mean ± SD, and were analyzed by two-way ANOVA (**a**).



Extended Data Figure 17. Localization of exogenous PE in tumor cells.

a-b, Colocalization of PE and Esyt1 before and after PE treatment. B16F10 cells expressing N-terminal GFP-tagged Esyt1 (Esyt1-GFP) were seeded overnight and treated with 30 μg/mL PE (18:0/20:4) for 1 hour. Cells were fixed and stained with duramycin-Cy3 (red) for PE lipids and anti-Calnexin (magenta) for ER. (**a**) Representative confocal images; (**b**) Mander's colocalization quantitation of PE signals with Esyt1. Scale bars: 10 μm. Each dot represents an individual cell (Mock: $n = 7$; PE: $n = 13$).

Data were shown as mean ± SD, and were analyzed by unpaired Student's t-test (**b**).



Extended Data Figure 18. PE-caused ER stress was mediated by Chop.

a-b, Gene set enrichment analysis (GSEA) of the ER-induced apoptosis pathway in PE-treated versus Mock B16F10 cells. Cells were treated with 30 μg/mL PE (P-18:0/18:1) (**a**, 18:1 ePE) or 30 μg/mL PE (**b**, P-18:0/22:6) (22:6 ePE) for 24 hours. Cells were then collected and subjected to bulk RNA sequencing. **c-d**, Heatmap illustrating the transcription levels of genes related to ER stress (**c**) or IFNγ response (antigen presentation) (**d**) in B16F10 cells treated with conditioned medium of naïve $CD8^+$ T cell (NCM), activated

CD8$^+$ T cell (ACM), or ACM combined with anti-IFNγ for 48 hours. To neutralize IFNγ, 10 μg/mL anti-IFNγ (clone: XMG1.2, BioXcell) was added into the conditioned medium. The transcriptional levels of the indicated genes were from bulk RNA sequencing. Preparation of NCM and ACM were mentioned in **Figure 1d**.

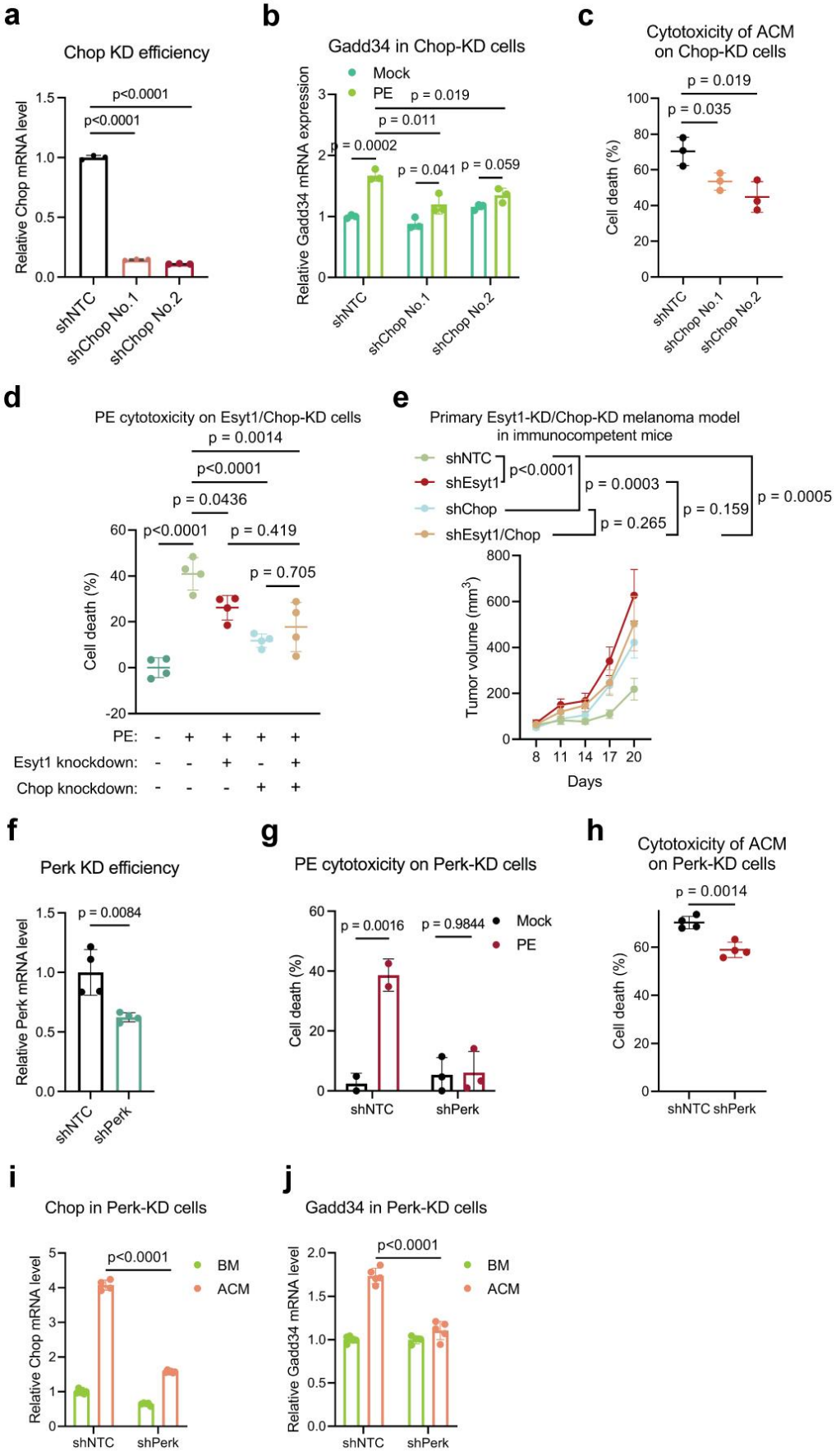
e-f, Relative mRNA levels of Chop (**e**) and Gadd34 (**f**) in B16F10 cells treated with the conditioned medium from activated OT-I CD8$^+$ T cells and OT-II CD4$^+$ T cells. Preparation of conditioned media was mentioned in **Extended Data Figure 1e**. Cells were treated with the conditioned medium for 24 hours. The transcription level of Chop and Gadd34 was measured by RT-qPCR (n = 5).

g-h, Relative mRNA levels of Chop in B16F10 cells treated with the conditioned medium from antibody-stimulated CD8$^+$ T cells (**g**) and target-cell-stimulated CD8$^+$ T cells (**h**). Generation of the conditioned medium was mentioned in **Figure 1a**. To generate the lipid-depleted conditioned medium from antibody-stimulated CD8$^+$ T cells and target-cell-stimulated CD8$^+$ T cells (LD-ACM), the collected medium was incubated with fumed silica (20 g/L) for 12-16 hours at 4°C, then the lipid-depleted medium was collected after the removal of fumed silica via centrifugation. Cells were treated with the conditioned medium for 24 hours. The transcription level of Chop was measured by RT-qPCR (n = 3).

i-j, Effects of PE depletion on ACM-induced upregulation of Chop (**i**) and Gadd34 (**j**) in tumor cells. PE depletion in ACM was performed as described in **Figure 1c**. B16F10 cells were treated with ACM for 24 hours. Transcriptional levels of the indicated genes were quantified by RT-qPCR and normalized to 18S rRNA (n = 3).

k, Kinetics of ACM-induced ER stress. The experimental conditions were the same as **Extended Data Figure 1h-i**. After 16-hour co-culture of WT or *Prf1*$^{-/-}$ OT-I T cells with target cells, ACM was collected and then used to treat B16F10 cells for different durations. Chop mRNA levels were measured by RT-qPCR and normalized to 18S rRNA.

Data were shown as mean ± SD, and were analyzed by one-way ANOVA (**e-j**).



Extended Data Figure 19. The connection between Esyt1, Perk, and Chop in response to PE killing.

a, Relative mRNA levels of Chop in the B16F10 cells with Chop knockdown (Chop-KD) (n = 3).

b, Effect of Chop knockdown on PE-induced Gadd34 upregulation in tumor cells. B16F10 cells were treated with 30 μg/mL PE (18:0/20:4) for 24 hours, and Gadd34 transcription levels were measured by RT-qPCR (n = 3).

c, Effect of Chop knockdown in tumor cells on CD8 ACM cytotoxicity. Chop-KD B16F10 cells were treated with CD8 ACM for 24 hours (n = 3).

d, Effect of single or dual knockdown Esyt1 and Chop in tumor cells on PE cytotoxicity. B16F10 cells were treated with 30 μg/ml PE (18:0/20:4) for 24 hours (n = 4).

e, Tumor progression of B16F10 cells with single or dual knockdown of Esyt1 and Chop. $8x10^5$ Esyt1-KD, Chop-KD or Esyt1/Chop-dual KD B16F10 cells were subcutaneously injected into immunocompetent C57BL/6 mice (n = 10 per group). Tumor progression was recorded every 3 days.

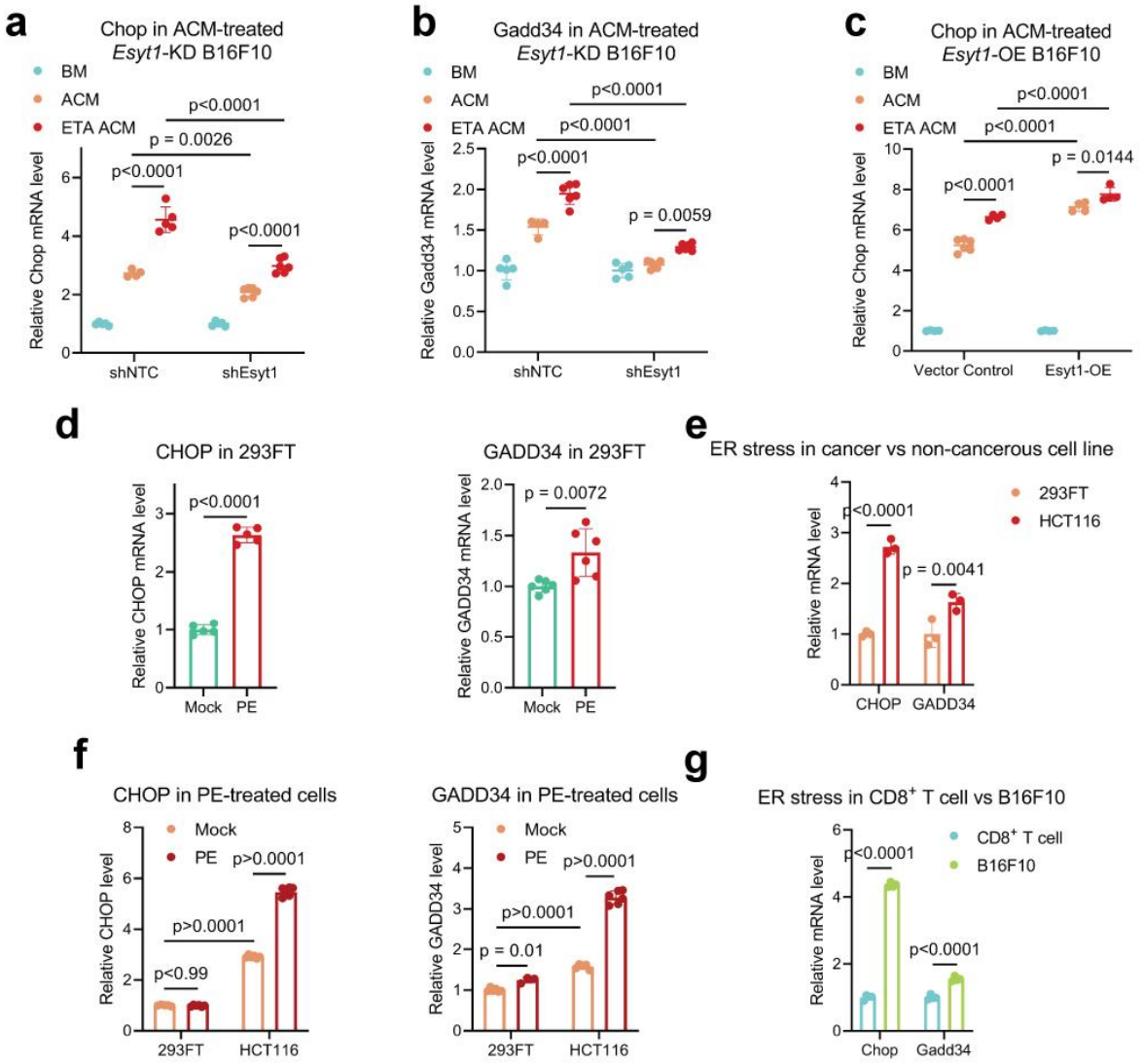
f. Relative mRNA levels of Perk in B16F10 cells with Perk knockdown (Perk-KD) (n = 4).

g, Cytotoxicity of 10 μg/mL PE (18:0/20:4) on Perk-knockdown (Perk-KD) B16F10 cells. Cells were treated with 10 μg/mL PE (18:0/20:4) for 24 hours. Tumor cell numbers were quantified using flow cytometry (n = 2-3).

h, Effect of Perk knockdown in tumor cells on CD8 ACM cytotoxicity. Perk-KD B16F10 cells were treated with CD8 ACM for 24 hours (n = 4).

i-j. Effects of Perk knockdown on ACM-induced upregulation of Chop (**i**) and Gadd34 (**j**) in tumor cells. B16F10 cells were treated with conditioned media for 24 hours. Transcription levels of indicated genes were measured by RT-qPCR and normalized to 18S rRNA (n = 4-5).

Data were shown as mean ± SD (**a-d, f-j**) and mean ± SEM (**e**), and were analyzed by unpaired Student's t-test (**b-c, f, h**), two-way ANOVA (**d-e, g, i-j**) or one-way ANOVA (**a**). Experiments were repeated two (**c**) times.



Extended Data Figure 20. The Esyt1-Perk-Chop axis mediated PE-induced ER stress.

a-c, Effects of Esyt1 knockdown (**a-b**) or overexpression (**c**) on ACM-induced tumor ER stress. ETA-treated OT-I T cells (ETA OT-I T cells) were generated as **Figure 6e**. CD8 ACM were generated from mock OT-I T cells or ETA OT-I T cells (ETA ACM). B16F10 cells were treated with ACM for 24 hours, and the transcriptional expression of Chop (**a, c**) and Gadd34 (**b**) was assessed by RT-qPCR (n = 4-6).

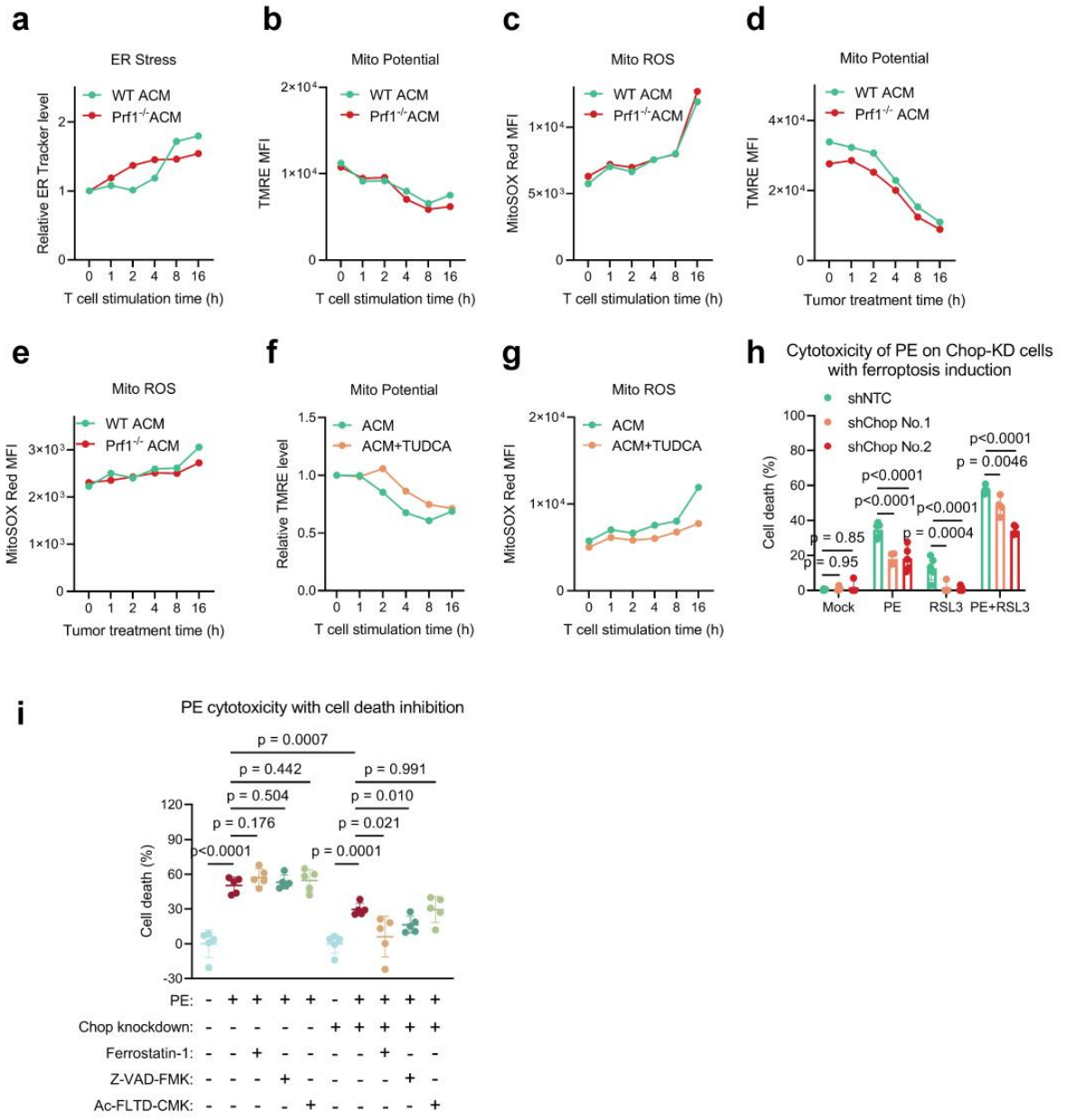
d, Transcriptional levels of CHOP and GADD34 in non-cancerous human 293FT cells treated with 30 μg/mL PE (18:0/20:4) for 24 hours. The transcriptional expression of indicated genes was assessed by RT-qPCR (n = 5-6).

e, Transcriptional expression of ER stress-related genes in non-cancerous human 293FT versus cancerous human HCT116 cells. Data were analyzed by RT-qPCR (n = 3).

f. Transcriptional expression of CHOP and GADD34 in non-cancerous human 293FT cells and HCT116 tumor cells. Cells were treated with 30 μg/mL PE (18:0/20:4) for 2 hours. The transcriptional expression of indicated genes was assessed by RT-qPCR (n = 3-6).

g, Transcriptional expression of ER stress-related genes in mouse $CD8^+$ T cells versus mouse B16F10 tumor cells. OT-I T cells were prepared as **Figure 1a**. Data were analyzed by bulk RNA sequencing (n = 3).

Data were shown as mean ± SD, and were analyzed by unpaired Student's t-test (**d**), two-way ANOVA (**a-c, e-g**).



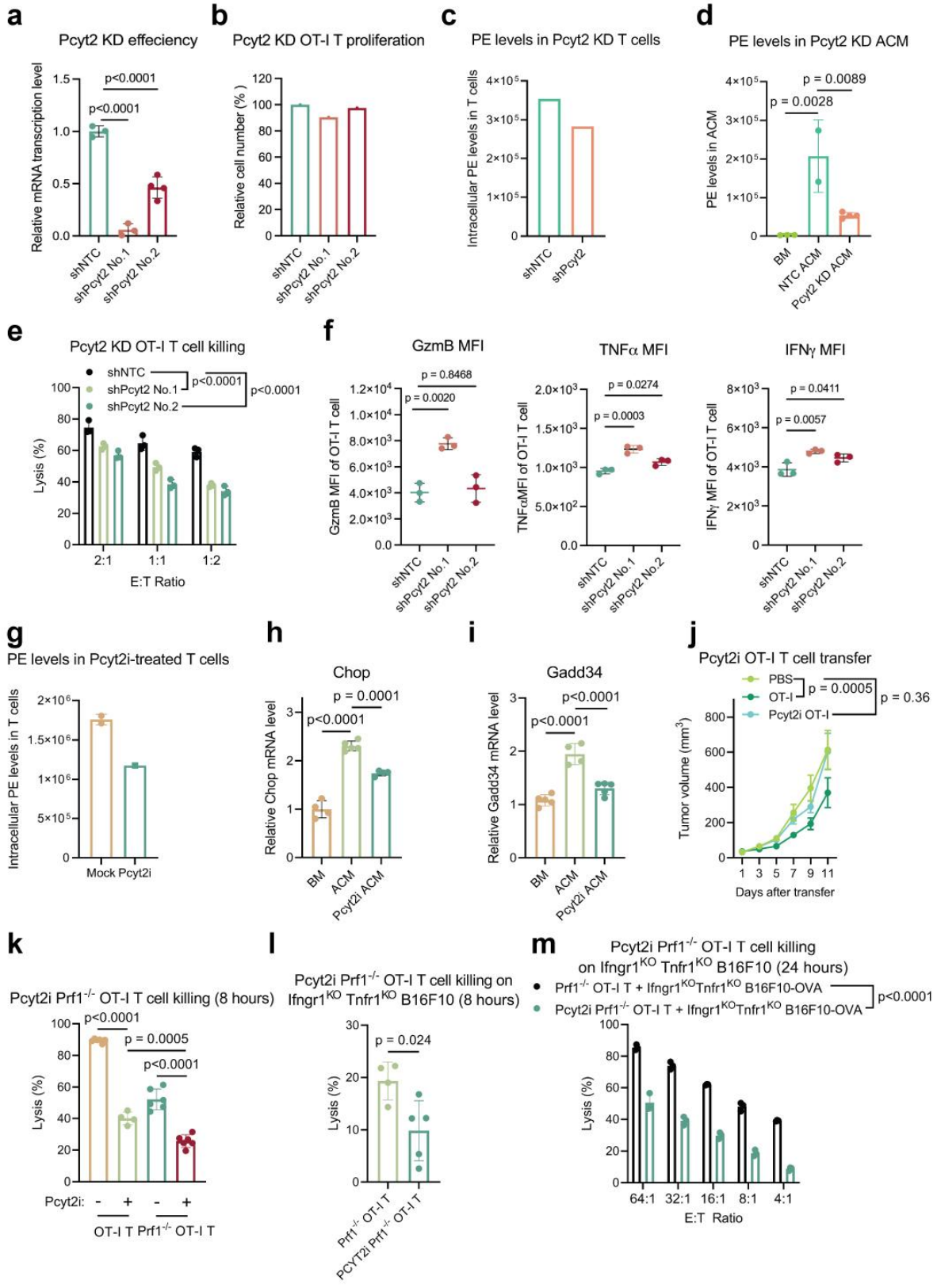
Extended Data Figure 21. ER stress was intercoupled with mitochondria dysfunction and ferroptosis. **a,** ER stress induced by ACM collected at different T-cell stimulation timepoints. CD8 ACM were collected from different time points as **Extended Data Figure 10m-n**. ER tracker was stained to represents ER stress. **b-c,** Mitochondrial dysfunction induced by ACM collected at different T-cell stimulation timepoints, represented by mitochondrial membrane potential (**c**) and mitochondrial ROS (**c**). CD8 ACM were collected from different time points as **Extended Data Figure 10m-n.** TMRE and MitoSOX Red were stained to represents mitochondrial membrane potential and mitochondrial ROS stress, respectively. **d-e,** Kinetics of ACM-induced mitochondrial dysfunction. The experimental conditions were the same as **Extended Data Figure 1h-i**. After 16-hour co-culture of WT or *Prf1*$^{-/-}$ OT-I T cells with target cells, ACM was collected and then used to treat B16F10 cells for different durations. Mitochondrial membrane potential (**d**) and mitochondrial ROS (**e**) were measured by TMRE and MitoSOX Red, respectively. **f-g,** Effect of ER stress inhibition on mitochondrial dysfunction induced by ACM. The experimental conditions and ACM controls were the same as **Extended Data Figure 21b-c**. ER stress was inhibited by

200 μM TUDCA.

h, Cytotoxicity of PE on Chop-KD B16F10 cells with or without ferroptosis induction. Cells were treated with 30 μg/mL PE (18:0/20:4), 50 nM RSL3, or their combination for 24 hours (n = 3-5).

i, Effects of cell death inhibitor targeting ferroptosis, apoptosis, or pyroptosis on PE-mediated killing of WT or Chop-KD B16F10 cells. Cells were pre-treated with cell death inhibitor to block specific pathway (10 μM Ferrostatin-1 for ferroptosis, 50 μM Z-VAD-FMK for apoptosis, or 50 μM Ac-FLTD-CMK for pyroptosis) for 1 hour. Subsequently, cells were treated with 30 μg/mL PE (18:0/20:4) for 24 hours in the continuous presence of the corresponding cell death inhibitor (n = 5).

Data were shown as mean ± SD, and were analyzed by one-way ANOVA(**i**) two-way ANOVA (**h**). Experiments were repeated two (**h**) times.



Extended Data Figure 22. Pcyt2 inhibition in CD8$^+$ T cells impaired PE-mediated cytotoxicity.

a, Relative mRNA levels of *Pcyt2* in the mouse OT-I T cells with Pcyt2 knockdown (Pcyt2-KD). Generation of Pcyt2-KD CD8$^+$ T cells and two shRNA sequences were mentioned in **Method** (n = 3-4).

b, Proliferation of Pcyt2-KD OT-I T cells. Control or Pcyt2-KD OT-I T cells were seeded in the flask at the

same density for 2 days, and then cell numbers were measured via flow cytometry.

c-d, Relative intracellular PE levels (**c**) and secreted PE levels (**d**) of Pcyt2-KD OT-I T cells. shPcyt2 No.1 was used to generate Pcyt2-KD $CD8^+$ T cells. To generate CD8 ACM, knockdown cells were seeded on plates coated with anti-CD3/CD28 (10 μg/mL) and stimulated for 24 hours. Cells and conditioned media were collected and measured by mass spectrometry for PE levels.

e, Killing function of Pcyt2-KD OT-I T cells against B16F10-OVA cells. T cells were co-incubated with B16F10-OVA cells at different E:T Ratios for 24 hours (n = 3).

f, Production of Granzyme B, TNFα, and IFNγ of Pcyt2-KD OT-I T cells, after stimulation with B16F10-OVA cells at the E:T ratio = 2: 1 for 24 hours (n = 3).

g, Relative intracellular PE levels of meclizine (Pcyt2i)-treated OT-I T cells. Pcyt2 inhibitor (meclizine, 50 μM) was used to pretreat the cells for 8 hours, followed by lipidomic analysis.

h-i, Effects of Pcyt2 inhibition on ACM-induced upregulation of Chop (**h**) and Gadd34 (**i**). ACM generated from Pcyt2i-pretreated T cells (Pcyt2i ACM) were generated as **Figure 6a**. B16F10 cells were treated with conditioned media for 24 hours. Transcription levels of indicated genes were measured by RT-qPCR and normalized to 18S rRNA (n = 4-5).

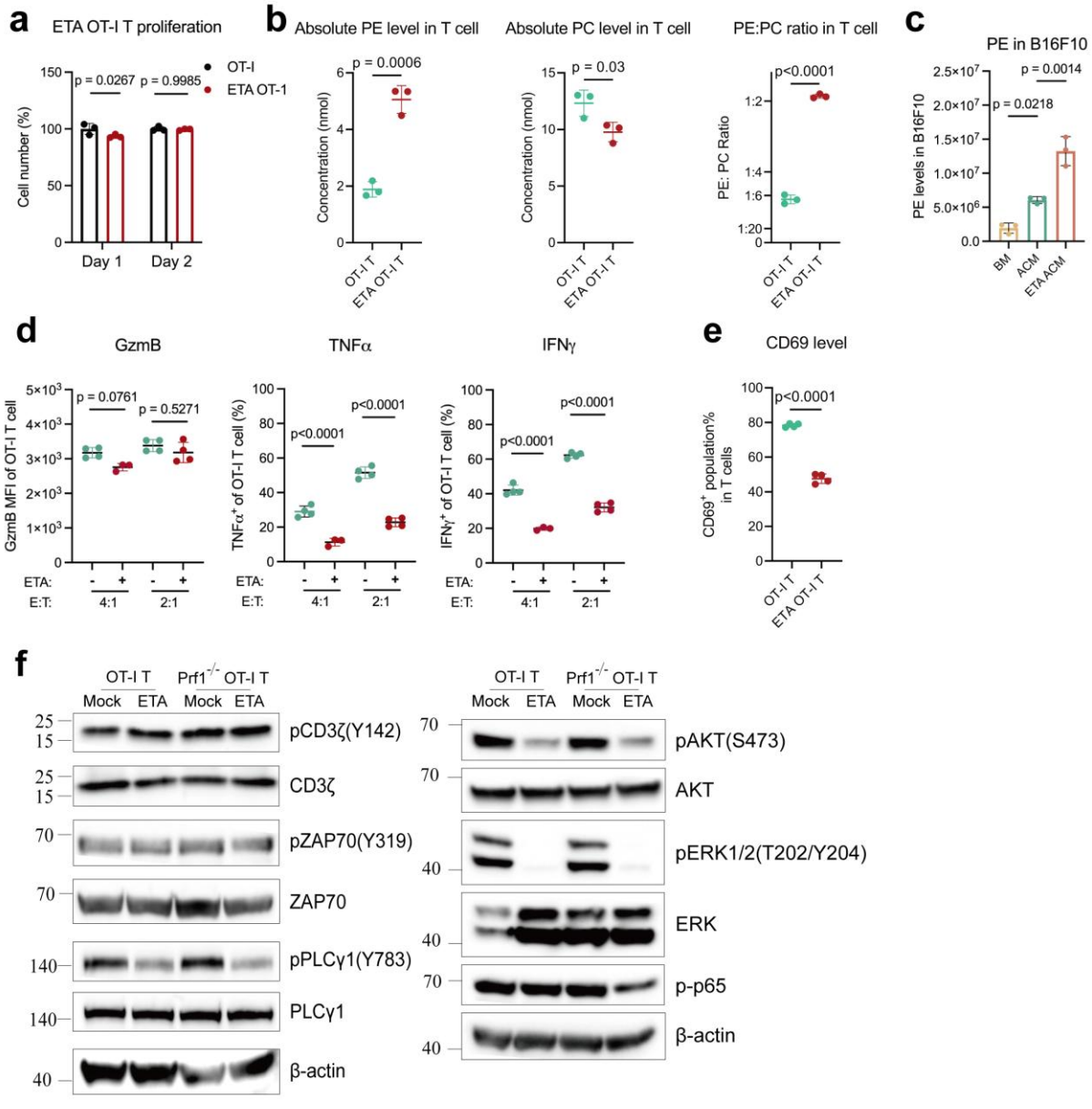
j, Adoptive transfer of Pcyt2i-pretreated OT-I T cells (Pcyt2i OT-I T) in a B16F10 melanoma model. Pcyt2i-OT-I T cells were generated as **Figure 6a**. Pcyt2i OT-I T or control OT-I T cells were transferred into tumor-bearing recipient mice 5 days post-B16F10 (4×10^5 cells per mouse) transplantation (n = 8, 7, 7 for PBS, OT-I, and Pcyt2i OT-I, respectively). This experiment shares the same controls (PBS and OT-I groups) with **Figure 6j**.

k, Effect of PE biosynthesis inhibition on 8-hour T cell killing under the wildtype or perforin-deficient condition. Pcyt2i WT OT-I T cells and Pcyt2i *Prf1*$^{-/-}$ OT-I T cells were generated as **Figure 6a**. T cells pretreated by mock or meclizine were co-cultured with B16F10-OVA cells at E:T = 16:1 for 8 hours (n = 4-6).

l, Effect of PE biosynthesis inhibition on 8-hour T cell killing under the toxin-null condition. Pcyt2i WT OT-I T cells and Pcyt2i *Prf1*$^{-/-}$ OT-I T cells were generated as **Figure 6a-b**. T cells were co-cultured with *Ifngr1*^{KO}*Tnfr1*^{KO} B16F10 cells at E:T = 32:1 for 8 hours (n = 4-5).

m, Killing of Pcyt2i *Prf1*$^{-/-}$ OT-I T cells against *Ifngr1*^{KO} *Tnfr1*^{KO} B16F10-OVA cells. T cells were co-incubated with tumor cells at varying E:T ratios for 24 hours (n = 3).

Data were shown as mean ± SD (**a, d-g, h-i, k-m**) and mean ± SEM (**j**), and were analyzed by unpaired Student's t-test (**l**), two-way ANOVA (**e, j, m**) or one-way ANOVA (**a, d, f, h-i, k**).



Extended Data Figure 23. ETA treatment promoted PE biosynthesis while dampened TCR signaling.

a, Proliferation of ETA-pretreated OT-I T cells (ETA OT-I T). Cells were cultured in mock or ETA-containing fresh medium for 2 days, and cell numbers were quantified by flow cytometry (n = 3).

b, Intracellular PE and PC levels of OT-I T cells and ETA OT-I T cells. Absolute lipid levels were quantified by lipidomic analysis and the PE:PC ratios were calculated accordingly (n = 3).

c, PE levels in B16F10 cells treated with ACM from ETA OT-I T cells (ETA ACM). ETA ACM was prepared as described in **Figure 6e**. B16F10 cells were treated with conditioned media for 48 hours, followed by collection and measurement of residual B16F10 cells by mass spectrometry (n = 3).

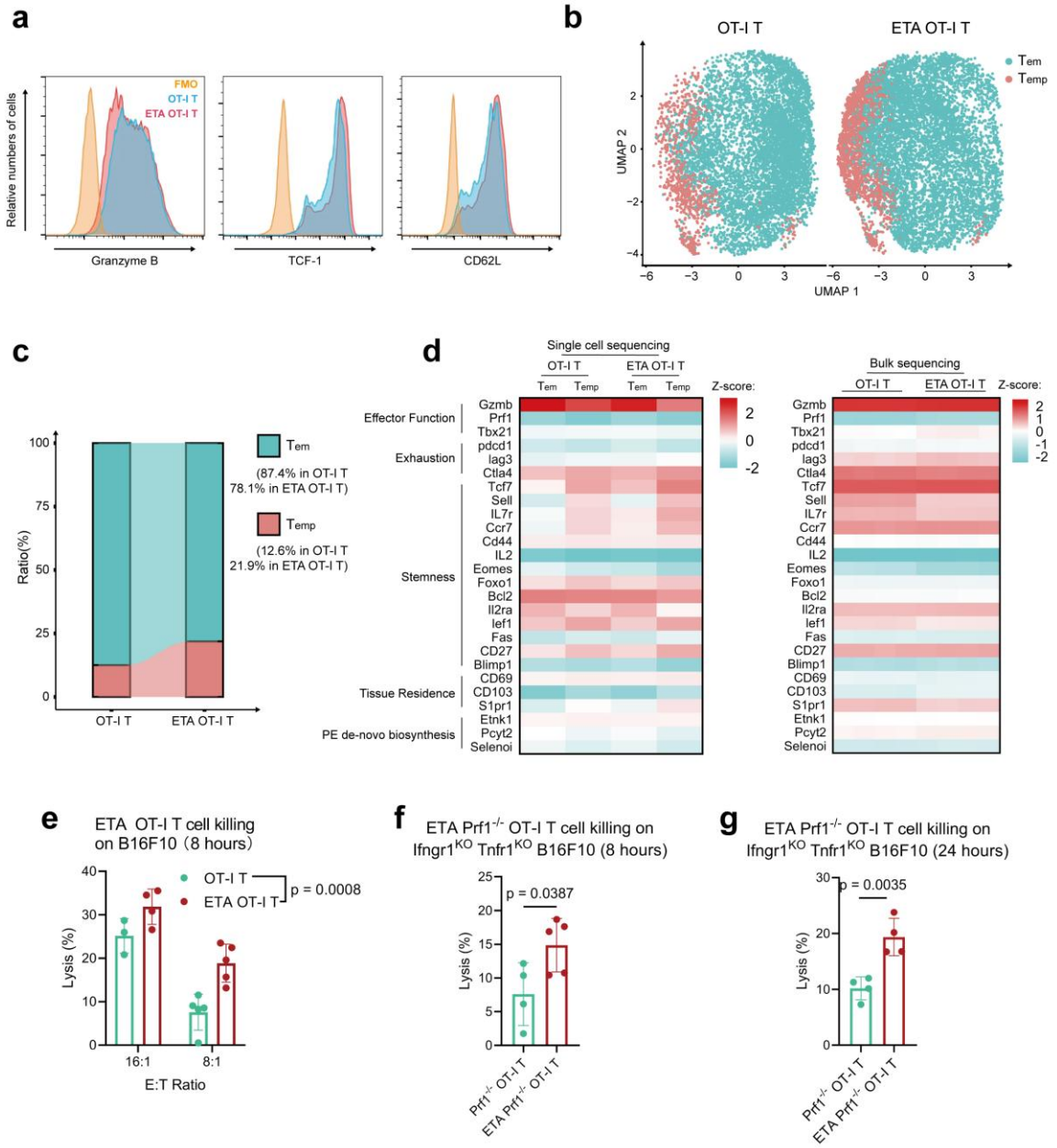
d, Production of Granzyme B, TNF-α, and IFN-γ by ETA OT-I T cells after stimulation with B16F10-OVA cells at an E:T ratio of 4:1 or 2:1 for 24 hours (n = 3-4).

e, Percentage of $CD69^+$ cells in ETA OT-I T cells (n = 4). ETA OT-I T cells were prepared as described in **Figure 6e**.

f, Immunoblotting of proximal and distal TCR signaling in wild-type or *Prf1*$^{-/-}$ OT-I T cells pretreated with ETA. Signals for total and phosphorylated CD3ζ, ZAP70, PLCγ1, AKT, ERK, and P65 were detected. β-

Actin served as a loading control.

Data were shown as mean ± SD, and were analyzed by unpaired Student's t-test (**b, e**), two-way ANOVA (**a**) or one-way ANOVA (**c, d**). Experiments were repeated four (**a**) times.



Extended Data Figure 24. ETA markedly promoted effector function and mildly promoted stemness of CD8$^+$ T cells.

a, Flow cytometry analysis of Granzyme B, TCF1, and CD62L levels in OT-I T cells and ETA OT-I T cells. For ETA-pretreated OT-I T cells (ETA OT-I T cells) generation, ETA (1 mM) was added into the medium during the 48-hour activation process. ETA OT-I T cells were subsequently cultured in fresh ETA (1mM)-containing medium for 2 days.

b-c, UMAP visualization (**b**) of single-cell transcriptomes showing effector memory precursor with greater stemness (T_{emp}) and effector memory with stronger effector function (T_{em}) clusters in OT-I T cells and ETA OT-I T cells. Percentages of the two clusters are shown in **c**.

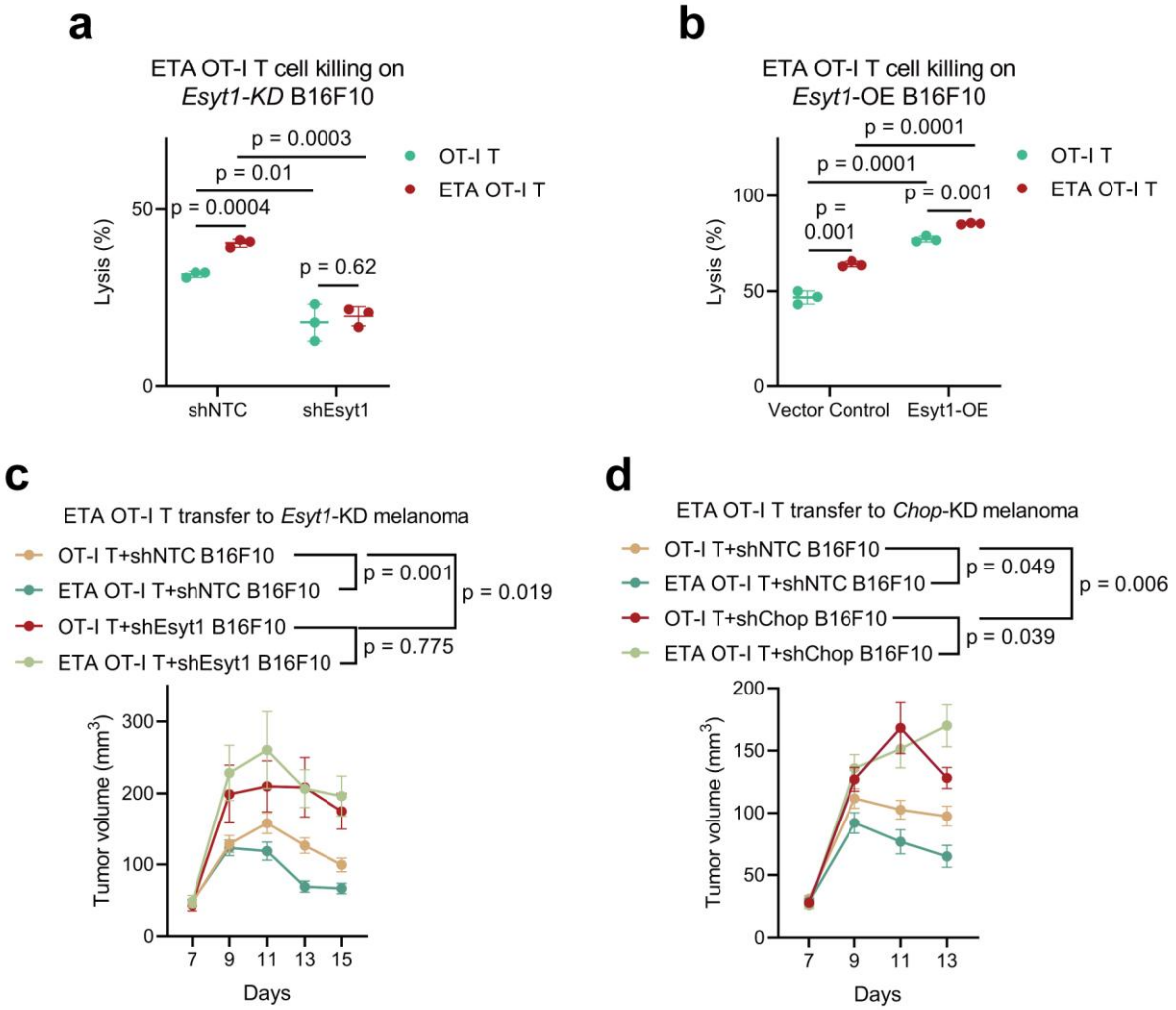
d, Transcriptional comparison of functional genes between OT-I T cells and ETA OT-I T cells measured by single-cell RNA sequencing (left) or bulk RNA sequencing (right).

e, Effect of PE biosynthesis enhancement on 8-hour T cell killing under the wildtype condition. B16F10 cells were co-cultured with ETA OT-I T cells at indicated E:T ratios for 8 hours (n = 3-5).

f, Effect of PE biosynthesis enhancement on 8-hour T cell killing under the toxin-null condition. ETA *Prf1*$^{-/-}$ OT-I T cells were generated as in **panel a**. T cells were co-cultured with *Ifngr1*^{KO}*Tnfr1*^{KO} B16F10 cells at E:T = 32:1 for 8 hours (n = 4-5).

g, Effect of PE biosynthesis enhancement on 24-hour T-cell killing under the toxin-null condition. ETA *Prf1*$^{-/-}$ OT-I T cells were generated as in **panel a**. *Prf1*$^{-/-}$ OT-I T cells and ETA *Prf1*$^{-/-}$ OT-I T cells were co-cultured with *Ifngr1*^{KO}*Tnfr1*^{KO} B16F10 cells at E:T = 8:1 for 24 hours (n = 4-5).

Data were shown as mean ± SD, and were analyzed by unpaired Student's t-test (**f-g**), two-way ANOVA (**e**).



Extended Data Figure 25. Gain of antitumor function via ETA pretreatment could be rescued by Esyt1 or Chop ablation.

a-b, Effect of Esyt1 knockdown (**a**) or overexpression (**b**) in tumor cells on the enhanced cytotoxicity by ETA supplementation. Attached Esyt1-KD or Esyt1-OE B16F10-OVA cells were co-cultured with OT-I or ETA OT-I T cells for 24 hours (n = 3).

c, Effects of Esyt1 knockdown in tumor cells and ETA pretreatment of T cells on antitumor responses in a tumor model of adoptive T-cell transfer therapy. Immunodeficient B-NDG mice were subcutaneously transplanted with 8×10^5 control or Esyt1-KD B16F10-OVA tumor cells. After 7 days, 4×10^6 control or ETA-pretreated OT-I T cells were transferred into tumor-bearing mice (n = 9 for each shNTC group, and n = 8 for each shEsyt1 group). Tumor progression was recorded every 2 days. ETA-pretreated OT-I T cells were generated as **Figure 6e**.

d, Effects of Chop knockdown in tumor cells and ETA pretreatment of T cells on antitumor responses in a tumor model of adoptive T-cell transfer therapy. Immunodeficient B-NDG mice were subcutaneously transplanted with 4×10^5 control or Chop-KD B16F10-OVA tumor cells. After 7 days, 4×10^6 control or ETA-pretreated OT-I T cells were transferred into tumor-bearing mice (n = 9 for each shNTC group, and n = 12 for each shChop group). Tumor progression was recorded every 2 days. ETA-pretreated OT-I T cells were generated as **Figure 6e**.

Data were shown as mean ± SD (**a-b**) and mean ± SEM (**c-d**), and were analyzed by two-way ANOVA (**a-d**).

EXPERIMENTAL MODEL AND STUDY PARTICIPANT DETAILS

Cell Lines

HEK-293FT, B16F10, MC38, huh7, HCT116, and CTLL-2 cell lines were obtained from the American Type Culture Collection (ATCC). SW480, HT-29, Hep3B, AGS and A549 were purchased from Cell Bank of Chinese Academy of Sciences (Shanghai, China). The B16F10-OVA and MC38-OVA cell line were established via lentivirus transduction using a pHAGE-fEF1a-OVA-IRES-mCherry construct. All cell lines were proven mycoplasma free. All mentioned cell lines were maintained in complete Dulbecco's Modified Eagle Medium (DMEM) supplemented with 10% fetal bovine serum (FBS) and antibiotics (100 U/mL penicillin and 100 μg/mL streptomycin, GIBCO). All cell lines were cultured at 37℃ in an atmosphere of 5% CO_2.

Mice

C57BL/6J CD45.2 wild type mice were obtained from LingChang (Shanghai, China). OT-I TCR transgenic mice (RRID: IMSR_JAX:003831) were sourced from the Jackson Laboratory. NOD.CB17-Prkdc^{scid}Il2rg^{tm1}/Bcgen (B-NDG, Cat#110586) mice were from Biocytogen (Beijing, China). Perforin knockout mice were provided by Dr. Yong Zhao (Institute of Zoology, Chinese Academy of Sciences, Beijing, China). All mice were maintained in specific pathogen-free facilities. Mice were allocated to experimental groups with comparable average tumor size. The animal experiments were performed in a double-blinded manner. All animal experiments were approved by the Institutional Animal Care and Use Committee (IACUC) and complied with all relevant ethical regulations.

Plasmids and reagents

All shRNA constructs were cloned into pLKO.1B vector with *BFP* gene, which was used as a sorting marker. The shRNA sequences were as follows: mouse *Esyt1*, 5′-TCACCGCAGAGACGCTTTATA-3′ and 5′-GTCAGCTATGTAGGTGATGTA-3′; mouse *Chop*, 5′-GATTCCAGTCAGAGTTCTATG-3′ and 5′-GAAACGAAGAGGAAGAATCAA-3′; mouse *Perk*, 5′-GTGACCCATCTGCACTAATTT-3′; mouse *Pcyt2*, 5′-TAATGCACCATGTCATAGCAG-3′ and 5′-AAACTGTCAGCATATTCCCGG-3′; mouse *Munc13-4,* 5′-*CCAGAAACTCATTGGCGTCAA*-3′*; mouse Reep3,* 5′-*GAAATCTGTCAAGACCATCAA*-3′*;* human *ESYT1*, 5′-CTCGTGTTGCCCAACCGATTA-3′ and 5′-GTTCGACAAGGATCCAGATAA-3′). sgRNAs for *Ifngr1* and *Tnfr1* knockout were inserted into a lenti-CRISPRv.2 vector with a *GFP* gene as a sorting marker. The sgRNA sequences were as follows: mouse *Ifngr1*, 5′- ACTTGGCGACTAGTCTGCGG-3′; mouse *Tnfr1*, 5′-AGTAAGATGATCGGACCAGG-3′. The Esyt1-overexrepssion construct was cloned into Phage vector, in which Esyt1 was fused with a 3xGGGGS linker and a GFP tag at its N-terminus. GFP-overexpressing constructs was served as vector control. The Gsdmc-overexpression construct was cloned into Phage vector, in which Gsdmc was fused with a 3×flag tag at its N-terminus. GzmB-mCherry-overexpression construct was cloned into Phage vector, in which Granzyme B was fused with a GSGGSG linker and a mCherry tag at the C-terminus. Packaging plasmids for lentiviruses psPAX2 and pMD.2G were purchased from Addgene. All constructs were confirmed by sequencing.

PE lipids, including PE (18:0/20:4) (Cat# PHOZ-150), PE (P-18:0/18:1) (Cat# PHOZ-007), PE (P-18:0/20:4) (Cat# PHOZ-008), and PE (P-18:0/22:6) (Cat# PHOZ-009), were purchased from Creative Enzyme. PC (16:0/18:1) (Cat# 850457P), PC (18:1/18:1) (Cat# 850375P) and PE (18:1/18:1) (Cat# 850725P) were purchased from Avanti. 18:1 Lyso-PG (Cat# HY-145505), PC (18:0/18:1) (Cat# HY-W440982), and HexCer (HY-165035) were purchased from MedChemExpress.

Reagents for flow cytometry, imaging, neutralization and western blot were sourced as follows: anti-murine-TNFα-PE (Clone: MP6-XT22), anti-murine-Granzyme B-FITC (Clone: NGZB), anti-murine IFNγ-APC (Clone: XMG 1.2), anti-murine CD18-FITC (Cat# 11-0181-82), anti-murine CD18 (Cat# 16-0181-81), AnnexinV-PE (Cat# 640908), anti-Perforin-PE (Cat# 12-9392-80), anti-TNFα-APC (Cat# 17-7321-82), anti-IFNγ-FITC (Cat# 11-7311-82) were purchased from eBioscience; murine IFNγ neutralizing antibody (Clone: XMG1.2, Cat# BE0055), murine TNFα neutralizing antibody (Clone: XT3.11, Cat# BE0058) , murine FasL neutralizing antibody (Clone: MFL3, Cat# BE0319) were purchased from BioXCell; anti-mCD3ε (Clone: 145-2C11), anti-mCD28 (Clone: 37.51), biotinylated anti-mCD3ε (Clone: 145-2C11), biotinylated anti-mCD28 (Clone: 37.51), anti-murine LAMP1-Alexa Fluor 488 (Cat# 121608), anti-murine TCR β chain-BV421 (Cat# 109230), anti-murine CD45-BV421 (Cat# 103133), and Brefeldin A Solution (Cat# 420601), were purchased from Biolegends; anti-Reep3 (Cat# PA5-20884) was purchased from Invitrogen; anti-IFNGR1 (Cat# EPR24127-89), anti-Munc13-4-Alexa Fluor 647 (Cat# ab320369), anti-Trans-Golgi network integral membrane protein 1 (Clone: EPR24831-36), anti-CD3 zeta (Phospho Y142) (Cat#68234), anti-ZAP70 (Cat#32410), and anti-ERK1 (pT202/pY204)/ERK2 (pT185/pY187) (Cat#32538) were purchased from Abcam; anti-TNFR1 (Clone: H-5) and anti-CD3 zeta (Cat#1239) were purchased from Santa Cruz Biotechnology; anti-Calnexin (Clone: 2A2C6) was purchased from Proteintech; anti-Rab27A (Clone: P2G19) and anti-GSDME (Clone: G9F19) were purchased from Selleck; anti-LC3B (Cat# #2775), anti-Tomm20 (Cat# 42406), anti-Cleaved Caspase-3 (Asp175) (Clone: 5A1E), anti-Phospho-Zap-70 (Try319)/Syk (Try352) (Cat# 2701), anti-Phospho-PLCγ1 (Try783) (Cat# 2821), anti-PLCγ1 (Cat# 5690), anti-Phospho-Akt (Ser473) (Cat# 4060), anti-Akt (Cat# 4691), anti-Erk1/2 (Cat# 4695), and anti-Phospho-NF-κB p65 (Ser536) were from Cell Signaling Technology; recombinant murine ICAM-1 protein with His-tag (Cat# 50440-M08H) was purchased from Sinobiological. Anti-human CD18 (Clone: TS1-18) was purified.

Reagents for biochemical and cellular assays were sourced as follows: 18:1 Biotinyl PE (Cat# HY-W800796), Fructose-6-phosphate (Cat# HY-113407A), 5'-Methylthioadenosine (HY-16938), NBD-F (Cat# HY-D0785), RSL3 (Cat# HY-100218A), Ferrostatin-1 (Cat# HY-100579), Ac-YVAD-CMK (Cat# HY-16990), Z-VAD(OMe)-FMK (Cat# HY-16658), PP2 (Cat# HY-13805), Tauroursodeoxycholate (Cat# HY-19696B), and meclizine dihydrochloride (Cat# HY-B0349) were purchased from MedChemExpress; Bexin-1 (Cat# DC42587) was purchased from DC Chemicals Limited; Duramycin-LC-biotin (Cat# D-1003) and Duramycin-Cy3-Conjugate (Cat# D-1006) were purchased from Molecular Targeting Technologies; centrifugal columns with 20 μm nylon filter (Cat# FCL122) was purchased from Beyotime; Pierce™ NHS-Activated Magnetic Beads (Cat# 88826), Pierce™ Streptavidin Magnetic Beads (Cat# 88817) and Exosome isolation kit (Cat# 4478359) was purchased from Thermo Fisher; BeyoMag™ Streptavidin Magnetic nanobeads (Cat# P2151) was purchased from Beyotimes; 3KD (Cat# UFC200324) and 100KD (Cat# UFC210024) Ultrafilters were purchased from Merck. Methyl tert-butyl ether (Cat# 650560), fumed silica (Cat# S5130), ethanolamine (Cat# 411000), C^{13}-ethanolamine (Cat# 606316), and N-Acetyl-L-cysteine (Cat# A9165) were purchased from Sigma. Culture media X-VIVO 15 Medium with L-glutamine, gentamicin, and phenol red (Cat# 04-418Q) was purchased from Lonza. Cytokine and growth factors, such as murine IFNγ (Cat# 315-05), IL-2 (Cat# 200-02), murine IL-7 (Cat# 217-17), murine IL-15 (Cat# 210-15), human IL-7 (Cat# 200-07), and human IL-15 (Cat# 200-15) was purchased from PeproTech.

METHOD DETAILS

Conditioned medium

Conditioned medium collection

Mouse T cells

For antibody stimulation, naïve mouse T cells were isolated from the spleens of OT-I mice using the naïve $CD4^+$ or $CD8^+$ T-cell negative selection kit (StemCell Technologies). The isolated naïve T cells ($3x10^5$ cells/well) were seeded onto 48-well plates pre-coated with 10 μg/mL anti-mCD3ε/anti-mCD28 antibodies for indicated time. Cells were cultured in complete RPMI-1640 medium (10% FBS, antibiotics, 50 μM β-mercaptoethanol (β-ME)) containing 10 ng/mL IL-2. As control, isolated naïve T cells were cultured in complete RPMI-1640 medium supplemented with 10 ng/mL IL-7. After 48 hours of stimulation, the antibody-activated T cell-conditioned medium was collected and centrifuged at 2000 g to remove T cells and cell debris.

For target cell stimulation, splenocytes from OT-I mice were harvested and cultured in completed RPMI-1640 medium containing 10 ng/mL IL-2 and 10 nM OVA peptide (257-264, SIINFEKL) for 2 days. The activated T cells were transferred to fresh medium without OVA peptide and maintained in the presence of 10 ng/mL IL-2. To generate conditioned medium, activated $CD8^+$ T cells were co-cultured with B16F10-OVA tumor cells at the effector cells: target cells (E:T) ratio of 2:1 in fresh medium. As control, B16F10-OVA cells were cultured in complete RPMI-1640 medium supplemented with 10 ng/mL IL-2. After 24 hours, the target cell-activated T cell-conditioned medium and tumor-conditioned medium were collected and centrifuged at 2000 g to remove T cells and cell debris.

Human CAR-T cells

Human CD19.28Z CAR-T cells were generated and cultured in X-vivo 15 Serum-free Hematopoietic Cell medium supplemented with 5% human serum, 10 mM N-Acetyl-L-cysteine, and 10 ng/mL IL-2 (the preparation of CAR-T cells is detailed below). To generate conditioned medium, CD19.28Z CAR-T cells were co-cultured with Raji cells at the E:T ratio of 2:1 in fresh medium. As control, CD19.28Z CAR-T cells were cultured in X-vivo 15 Serum-free Hematopoietic Cell medium supplemented with 5% human serum, 10 mM N-Acetyl-L-cysteine, 10 ng/mL IL-7, and 10 ng/mL IL-15. After 48 hours, the conditioned medium was collected and centrifuged at 2000 g to remove CAR-T cells and cell debris.

Human NK cells

Human NK cells were cultured in fresh medium with 500 IU/mL IL-2 and 100 IU/mL IL-15 for 3 weeks for pre-activation (Preactivated NK CM). Next, preactivated NK cells were mixed with γ-irradiated feeder cells at an E:T ratio of 2:1 and co-cultured for 24 hours to further activate NK cells (NK ACM). Blank medium (BM) and conditioned medium from γ-irradiated feeder cells cultured for 24 hours (Target cell CM) were served as controls.

Lipid depletion and lipid extract

To prepare lipid-depleted conditioned medium, fumed silica (20 g/L) was mixed with the medium and incubated at 4°C for 16 hours. After incubation, the mixture was centrifuged at 3000 g and the supernatant was filtered by 0.22 μm filter to remove the lipid-loaded fumed silica. Lipid-depleted conditioned medium was used for further analysis.

Lipids loaded onto the fumed silica were extracted using a mixture of methyl tert-butyl ether (MTBE) and methanol (MTBE: methanol: fumed silica=5:1:2, v: v: v). The mixture was vortexed for 1 minute and subject to sonication for 15 minutes to ensure complete mixing. The sample was then centrifuged at 3000g for 15 minutes at 4°C to achieve phase separation. The upper organic phase was collected, dried using a vacuum

concentrator, and reconstituted in methanol for further analysis.

PE depletion

Conditioned medium was concentrated by 3KD ultrafiltration. Duramycin-LC-biotin was added to the concentrate at a final concentration of 100 μM and incubated at 4℃ for 16 hours to capture PE. The concentrate was subsequently mixed with streptavidin magnetic beads and incubated at 4℃ overnight to allow complete capture of the PE-duramycin-biotin complex. After the streptavidin magnetic beads were removed, the PE-depleted conditioned medium concentrate was collected for further analysis.

Identification of PE+ extracellular vesicles (PE^+ EVs)

Fractionation and physicochemical characterization of PE^+ EVs from CD8 ACM

$CD8^+$ T cell cultures were centrifuged at 500×g for 10 minutes to remove cells and debris. Supernatant was collected and centrifuged at 3000×g for 30 minutes. The resulting supernatant (small EVs, SEVs) and pellet (large EVs, LEVs) were collected separately, and pellet was resuspended in PBS. Both SEVs and LEVs were mixed with 5× concentration buffer (40% (w/v) PEG8000, 375 mM NaCl) and incubated at 4°C overnight. Mixtures were centrifuged at 3000×g for 30 minutes to precipitate particles. The precipitated SEVs and LEVs were separately resuspended in sucrose buffer (5% (w/v) sucrose, 20 mM HEPES) and layered onto 5–50% (w/v) continuous sucrose gradients (generated by BioComp gradient maker). After centrifuging at 200,000×g for 16 hours, SEVs or LEVs were fractionated into 14 subfractions from light to heavy density (BioComp fraction collector).

For lipidomic profiling, all subfractions were subjected to lipid analysis. For physicochemical characterization, average particle size, polydispersity index, and zeta-potential of each fraction were measured by Zetasizer Pro.

Protein profiling and FACS analysis of PE^+ EVs captured by duramycin

CD8 or tumor conditioned medium was concentrated by 3KD ultrafiltration. Duramycin-LC-biotin was added at a final concentration of 10 μM and incubated at 4℃ for 16 hours to capture PE^+ EVs. Subsequently, streptavidin magnetic nanobeads were added and incubated at 4℃ for 6-8 hours to capture the PE^+ EVs/duramycin-biotin complex. Nanobeads were then magnetically isolated, gently washed by PBS once, and incubated with Elution buffer (0.2 M Glycine, 0.1% NP40, pH 2.2) for 2 hours. The eluents were collected and used for protein mass spectrometry.

For the FACS analysis, Duramycin-LC-biotin was added to the CM concentrate at a final concentration of 20 μM and incubated at room temperature for 60 minutes. Subsequently, streptavidin magnetic nanobeads were added and incubated at room temperature for 60 minutes to capture of the PE^+ EVs/duramycin-biotin complex. Nanobeads were then magnetically isolated, incubated with Fixation Buffer (Invitrogen) immediately for 30 minutes at room temperature. Fixed beads were further permeabilized and stained by Duramycin-cy3 (5 μM), anti-CD45-BV421 (0.12 μg/mL), anti-CD18-FITC (2.5 μg/mL), AnnexinV-PE (50 ng/mL), anti-Perforin-PE (1 μg/mL), anti-TNFα-APC (1 μg/mL), anti-IFNγ-FITC (2.5 μg/mL). Specially, before the Annexin-V staining, concentration of Ca^{2+} in the staining buffer was adjusted by the Binding Buffer (Invitrogen). Stained beads were further detected by flow cytometry.

Mass spectrometry

Lipid extraction

The biological samples were extracted with a modified MTBE protocol[104]. Briefly, the biological samples

were firstly diluted to 400 μL with water. Then, 960 μL of the extraction solvent (MTBE: MeOH =5:1, v: v) was added. The sample was vortexed for 60 s, followed by the 10 min of sonication in a water bath (4°C). The solution was centrifuged at 3000 rpm for 15 minutes at 4 °C. The upper organic layer (500 μL) was collected into a new Eppendorf tube. Then, 500 μL of MTBE was added to the left layer for further extraction. The solution was vortexed, sonicated, and centrifuged again as the previous description. Then, the upper organic layer was collected. The re-extraction process was repeated three times in total to ensure the high extraction efficient and recovery rate. Finally, the pooled organic layer was evaporated with a vacuum concentrator (Catalog No.7310038, LABCONCO). The dry extract was reconstituted using 100 μL of DCM: MeOH (1:1, v: v) before LC-MS analysis.

For quantitative analysis of cells and condition media, the samples were mixed with water. Then, for cell samples, 960 μL of extraction solvent (MTBE:MeOH = 5:1, v/v) containing 100 ng d_7-PC (15:0/18:1) and 20 ng d_7-PE (15:0/18:1) was added. For cell media, 960 μL of extraction solvent (MTBE:MeOH = 5:1, v/v) containing 50 ng d_7-PC (15:0/18:1) and 5 ng d_7-PE (15:0/18:1) was added. The subsequent procedure was the same as described above. The deuterium labeled lipids were used for quantification of corresponding lipid classes.

LC-MS analysis and data processing

The LC–MS/MS analyses were performed using an HPLC system (1290 series, Agilent Technologies) coupled to a quadrupole time-of-flight mass spectrometer (TripleTOF 6600, AB Sciex). A Phenomenex Kinetex C18 column (particle size, 1.7 μm; 100 mm (length) × 2.1 mm (i.d.)) was used for LC separation66. The mass spectrometry parameters were applied as described in our previously published work65. Briefly, ion source gas 1 (GS1), 60 psi; ion source gas 2 (GS2), 60 psi; curtain gas (CUR), 30 psi; temperature, 600 °C; ionspray voltage floating (ISVF), 5000 V or -4500 V in positive or negative modes, respectively; declustering potential (DP), 100 V. Data-dependent acquisition (DDA) method was used for MS/MS acquisition. Each acquisition cycle consists of one rapid TOF MS survey scan (200 ms) followed by the consecutive acquisition of 11 product ion scans (50 ms each). For TOF MS survey scan, the mass range is from 200 to 2000 Da, and collision energy (CE) is set as 10 V. For product ion scan, the mass ranges are from 100 to 2000 Da, and collision energy (CE) is set as 45±25 V.

The raw data files (.wiff format) were converted to files in mzXML format using the “msconvert” program from ProteoWizard (version 3.0.6148). Then, the mzxML files were grouped for peak detection and alignment using the R package “xcms” (version 1.46.0). Detailed parameters followed our previous publication65. The generated MS1 peak table and MS2 files were uploaded to Lipid4DAnalyzer (http://lipid4danalyzer.zhulab.cn/) for lipid annotation with a previously reported combined strategy with the integration of library-based match and fragmentation rule-based refinement[105,106].

PE-binding proteins

To prepare PE-loaded magnetic beads, 1mM PE standards were dissolved in methanol: DMF mixture (1:4, v: v) and incubated with NHS-functionalized magnetic beads (Thermo Scientific) at a concentration of 10 μg beads per mL of standards for 70 minutes. The supernatant containing unbound PE was removed, and 1M ethanolamine in DMF was added to the beads, followed by incubation for 2 h to block any remaining reactive NHS groups. Then magnetic beads were then collected by centrifugation and washed three times with a methanol: DMF mixture (1: 1, v: v).

For protein extraction, 1×10^8 B16F10 or activated OT-I T cells were washed twice with PBS and lysed with Lysis Buffer (10 mM HEPES-NaOH, pH 7.9; 10 mM KCl; 2% NP40; 0.1 mM EDTA; 1 mM DTT; 0.5 mM

PMSF). Supernatants of cell lysates were collected via high-speed centrifugation at 4℃. The collected supernatants were dialyzed overnight with KCl binding buffer (20 mM HEPES, pH 7.9; 100 mM KCl; 1 mM $MgCl_2$; 0.2 mM $CaCl_2$; 0.2 mM EDTA; 0.1 mM DTT; 0.1% NP-40; 10% (v/v) glycerol; and 1x protease inhibitor cocktail (Selleck)) to dilute the concentration of detergents. PE-loaded beads were washed with KCI binding buffer and incubated with dialyzed supernatants for 24 hours at 4℃. Beads were then collected by magnetic sorting, washed three times with KCl binding buffer, and incubated with Elution buffer (0.2 M Glycine, 0.1% NP40, pH 2.2). Supernatants were collected and used for mass spectrometry.

Cellular and biochemical experiments

PE/CD8 ACM cytotoxicity

Liposome preparation

PE (P-18:0/20:4) and PC (16:0/18:1) were mixed at the indicated molar ratio, and the solvent was evaporated by centrifuging vacuum. The lipid film was resuspended in Milli-Q water to a final concentration of 1 mg/mL, followed by sonication for ~2 min, cooling to room temperature, a second round of sonication for ~2 min, and re-cooling.

Detection methods

To detect cell number, cells were harvested by trypsinization and counted by flow cytometry.

To detect phosphatidylserine (PS) exposure on the cell surface, cells were harvested by trypsinization and washed with Annexin-V binding buffer (Invitrogen). Annexin-V-FITC or Annexin-V-APC (1:100) (Cat# BMS500FI or Cat# 88-8007-74, Invitrogen) was added and incubated for 30 minutes at room temperature to label externalized PS. Labeled cells were then washed twice with Annexin-V binding buffer twice and analyzed by flow cytometry.

To detect cell viability, Cell Counting Kit-8 (Cat# HY-K0301, MedChemExpress) was used according to the manufacturer's instructions. Absorbance at 450 nm was measured using a Tecan microplate reader.

To detect lipid ROS production, BODIPY™ 581/591 C11 (Cat# D3861, Invitrogen) was used according to the manufacturer's instructions. The signals from both non-oxidized C11 (PE channel) and oxidized C11 (FITC channel) were measured by flow cytometry. The MFI ratio of oxidized C11 to MFI of non-oxidized C11 was calculated for each sample. The data were normalized to control samples as shown by relative lipid ROS.

To detect ER mass, ER-Tracker Red (Cat# C1041L, Beyotime) was used according to the manufacturer's instructions.

To detect DNA fragmentation, both apoptotic cells and apoptotic vesicles (apoVs) were prepared as positive controls. $CD8^+$ T cells were treated with 200 nM staurosporine for 8 hours to induce apoptosis. Supernatant from STS-treated T cells was collected and centrifuged at 3000×g for 30 minutes to harvest apoVs. DNA was extracted from positive controls or samples and analyzed by electrophoresis.

Attached cell treatment

For attached conditions, tumor cells (1-2×10^3 cells/well) were seeded in 96-well flat plate and incubated overnight before treatment with various reagents at the indicated dose and durations.

Detached cell treatment

For detached conditions, tumor cells (3×10^3 cells/well) were seeded in ultra-low attachment 96-well plate

(Cat# CLS3474 and CLS7007, Corning) and co-treated with various reagents at the indicated dose and durations. Spheroid formation was imaged using the Operetta high-content imaging system (Perkin Eimer).

Kinetics assays

For cytotoxicity kinetics of PE, tumor cells were exposed to 30 μg/mL PE (18:0/20:4) for 0-16 hours, and cell numbers were assessed at the indicated time points.

For CD8 ACM, two complementary designs were employed to assess the secretion and cytotoxicity kinetics.

(1) Secretion kinetics (varying T-cell stimulation time): CD8 ACM was collected after different durations of T-cell stimulation, while the tumor treatment time was held constant. This experiment aimed to determine when T cells can secrete sufficient cytotoxic molecules to induce target cell death. Detailly, preactivated OT-I T cells were mixed with B16F10-OVA cells at the E:T Ratio of 2:1, and CD8 ACM was collected after 0-16 hours of T-cell stimulation. Then collected conditioned media were used to treated tumor cells for 16 hours.
(2) Cytotoxicity kinetics (varying tumor treatment time): CD8 ACM was collected after a fixed T-cell stimulation period, while the tumor treatment duration was varied. This experiment aimed to determine how long of ACM exposure is sufficient to trigger stress and death in target cells. Detailly, preactivated OT-I T cells were mixed with B16F10-OVA cells at the E:T Ratio of 2:1 and CD8 ACM were collected after 16-hour stimulation. Then collected conditioned media were used to treated tumor cells for 0-16 hours.

Transwell migration and invasion assays

Cell migration and invasion were evaluated using 24-well Transwell inserts with 8-μm pores (Corning, Cat# 3422). For invasion assays, the upper surface of inserts was coated with 70 μL Matrigel (BD Biosciences, Cat# 356234) diluted (1:8) in ice-cold serum-free DMEM and allowed to solidify at 37°C for 4 hours; uncoated inserts were used for migration assays. Cells were serum-starved for 24 hours prior to assay, harvested, and resuspended in serum-free medium. Control or Esyt1-knockdown B16F10 cells in 100 μL serum-free medium were added to the upper chamber. The lower chamber was filled with 500 μL medium containing 10% FBS as chemoattractant. Plates were incubated at 37℃ with 5% CO_2 for 48 hours. After incubation, non-migrated cells on the upper membrane were removed with a cotton swab. Membranes were fixed in 4% paraformaldehyde, and cells were stained with 0.1% crystal violet and visualized under a microscope. Quantification of coverage was performed by ImageJ.

Tracing of intercellular PE transportation

NBD-ETA labeling

Ethanolamine (ETA) was reacted with NBD-F at 60°C for 4 hours in a methanol/acetonitrile/borate buffer mixture (1: 1: 1, v: v: v) to synthesis NBD-ETA. The NBD-ETA product was purified using a high-performance liquid chromatography (HPLC) system, lyophilized, and reconstituted in methanol. 1 mM NBD-ETA was then added to the culture medium during preparation of activated $CD8^+$ T cells. Labeled activated $CD8^+$ T cells were washed twice with fresh medium to remove residual NBD-ETA, then co-cultured with B16F10-OVA cells in 96-well plates for 24 hours. The cell mixtures were subsequently digested, washed with PBS, and analyzed by flow cytometry to validate NBD fluorescence. For time-course analysis, NBD-labeled activated $CD8^+$ T cells were cocultured with B16F10-OVA cells in 96-well plates at the E:T ratio of 8:1 and NBD signals of T cells and tumor cells were measured by FACS after 0-16 hours. For live imaging, NBD-labeled activated $CD8^+$ T cells were cocultured with B16F10-OVA cells in 96-well

plates at the E:T ratio of 8:1 and immediately imaged at 4x objective by ZEISS Celldiscoverer 7 for 8 hours. The imaging software automatically applied intensity compensation to correct for signal loss.

^{13}C-ETA isotype labeling

Naïve T cells were isolated from murine spleen, seeded on plates coated with 10 μg/mL anti-mCD3ε/anti-mCD28, and stimulated for 48 hours with 10 ng/mL IL-2 and 1mM ^{13}C-ETA. Labeled activated CD8$^+$ T cells were washed twice, transferred to fresh medium containing 10 ng/mL IL-2, and cultured for an additional 24 hours. Conditioned media were collected and analyzed by mass spectrometry to assess ^{13}C-PE level. To trace PE transfer, B16F10 cells (2×10^5 cells/well) were seeded in 48-well plates overnight and treated with conditioned medium from labeled T cells for 48 hours. Cells were collected by trypsinization, washed twice with PBS and analyzed by mass spectrometry.

Manipulations of PE levels in mouse OT-I CD8$^+$ T cells

Pcyt2 inhibitor (Pcyt2i) meclizine pretreatment

OVA-peptide activated CD8$^+$ T cells (1×10^6 cells/mL) were pre-treated with 50 μM Meclizine for 8 hours in complete RPMI-1640 medium supplemented with 10 ng/mL IL-2. After treatment, cells were washed twice with fresh medium and used for subsequent experiments.

Pcyt2, Munc13-4, or Reep3 knockdown

For *Pcyt2, Munc13-4, or Reep3* knockdown, peripheral CD8$^+$ T cells were isolated from the spleens of OT-1 mice by Total CD8$^+$ T cell isolation kit (STEM CELL Technologies). The cells were cultured with IL-7 (10 ng/mL) and IL-15 (10 ng/mL) in complete RPMI medium for two to three days. CD8$^+$ T cells (2×10^6 cells/well) were transfected with concentrated lentivirus (concentrated with PEG8000 and pelleted by centrifugation) supplemented with polybrene (8 μg/mL) in 24-well plates pre-coated with RetroNectin (1 mg/mL, T100B, Takara). The plates were centrifuged at 2000 g for 60 minutes at 30°C. After centrifugation, the lentiviral supernatant was discarded, and cells were cultured in complete RPMI medium with IL-7 (10 ng/mL) and IL-15 (10 ng/mL) for three days. Infection efficiency was further determined by qPCR.

ETA pretreatment

For ETA pretreatment, 1 mM ETA was added into the complete RPMI-1640 medium supplemented with 10 ng/mL IL-2 during OT-I T cell activation process. Cells were subsequently cultured in fresh medium containing 1 mM ETA for 2 days and washed twice before conducting experiment.

Generation of human CD19.28Z and MSLN.28Z CAR-T cells

Lentivirus particles were generated via 293FT transfection using lipofectamine 2000 (Cat# 11668019, Invitrogen) according to the manufacturer's protocol. The virus was either used immediately or stored at -80°C until required. Peripheral blood mononuclear cells (PBMCs) were isolated from healthy donor blood samples through density gradient centrifugation and stored at liquid nitrogen. Upon thawing, the PBMCs were rested for 12 hours in X-vivo medium prior to stimulation. Stimulation was performed using anti-CD3/CD28 dynabeads (Cat# 11161D, Thermo Fisher). The culture medium used for PBMCs comprised X-vivo 15 Serum-free Hematopoietic Cell Medium, supplemented with 5% human serum, 10 mM N-Acetyl-L-cysteine, 10 ng/mL IL-7, and 10 ng/mL IL-15. At 24-hour post-stimulation, concentrated lentivirus particles were added to the PBMC culture. Cells were mixed gently by pipetting. Three days post-stimulation, the anti-CD3/CD28 dynabeads were removed, and cells were cultured in fresh medium for further expansion. GFP$^+$ cells were sorted by FACS and used in subsequent experiments.

Manipulations of PE levels in human MSLN.28Z CAR-T cells

Pcyt2i meclizine pretreatment

MSLN.28Z CAR-T cells were pre-treated with 50 μM Pcyt2i Meclizine for 24 hours in X-vivo 15 Serum-free Hematopoietic Cell medium supplemented with 5% human serum, 10 mM N-Acetyl-L-cysteine, 10 ng/mL IL-2. After treatment, cells were washed twice with fresh medium and used for subsequent experiments.

ETA pretreatment

MSLN.28Z CAR-T cells were generated and cultured in X-vivo 15 Serum-free Hematopoietic Cell Medium, supplemented with 5% human serum, 10 mM N-Acetyl-L-cysteine, 10 ng/mL IL-2, and 1mM ETA to produce ETA-supplemented MSLN.28Z CAR-T cells.

T cell killing and cytokine production

Killing experiment

Tumor cells ($1x10^4$ cells/well) were labelled with CellTracker Deep Red dye (Invitrogen, Cat# A66433) and seeded in the flat-bottom 96-well plate overnight. On the following day, activated $CD8^+$ T cells or MSLN.28Z CAR-T cells were added into the plates at varying E:T ratios. After 8 hours or 24 hours of co-culture, the cell mixtures were collected by trypsinization, and live tumor cells were counted by flow cytometry.

Cytokine production

Activated $CD8^+$ T cells or MSLN.28Z CAR-T cells were stimulated with tumor cells at varying E:T ratios in a flat 96-well plate for 24 hours. For intracellular staining, Brefeldin A Solution (1:1000) was added four hours before harvesting to block cytokine secretion. Subsequently, cytokine production was measured using a standard intracellular staining procedure mentioned in the manufacturing protocol with the indicated antibodies.

Virus infection

HCV and VSV virus were propagated in huh7 cells. The viral supernatant was collected and filtered through a 0.45 μm syringe filter. Viral titers were determined by a focus-forming assay. For HCV infection, huh7 cells were inoculated with HCV at a multiplicity of infection (MOI) of 0.0125 and PE (18:0/20:4) at 37 ℃ for 72 hours. For VSV infection, huh7 cells were inoculated with VSV for 16 hours at 37 ℃ at a multiplicity of infection (MOI) of 0.25, and then treated with PE 18:0/20:4) for 24 hours at 37 ℃. For FluB infection, A549 cells were inoculated with FluB for 2 hours at 33 ℃ at a multiplicity of infection (MOI) of 1, and then treated with PE (18:0/20:4) for 48 hours at 33 ℃.

Imaging

Confocal and HIS-SIM imaging of intracellular/extracellular PE vesicles and other organelles

Activated OT-I $CD8^+$ T cells were loaded on poly-Lysine coated dishes and incubated for 30 minutes at 4℃. Incubation was extended to 4 hours at 37 ℃ for capturing PE-containing extracellular vesicles. To visualize intracellular Granzyme B, Granzyme B-mCherry fusion proteins were expressed in CTLL-2 cytotoxic T cell lines to trace Granzyme B localization. Cells were fixed with intracellular fixation buffer (Cat# 00-8222, Invitrogen) and stained with Duramycin-Cy3 (2-5 μM), anti-mLAMP1-Alexa Fluor 488 (5 μg/mL), anti-Reep3 (5 μg/mL), anti-Calnexin (5 μg/mL), anti-LC3b (1:200), anti-Tgoln1 (1:200), anti-Tomm20 (0.4

μg/mL), anti-IFNγ-APC (5 μg/mL) and either anti-mCD45-BV421 (0.12 μg/mL) or anti-mTCRb-BV421(2 μg/mL) in permeabilization buffer (Cat# 00-8333-56, Invitrogen) overnight at 4℃. For non-fluorescent antibodies staining, samples were washed twice on the following day and stained with Alexa Fluor 647-labeled secondary antibody (2.5 μg/mL) for 2-4 hours at room temperature. Unbound antibodies were washed away by PBS before imaging.

To image OT-I-tumor cellular conjugation, B16F10-OVA cells were seeded on the poly-Lysine coated dishes overnight. OT-I T cells were added to the dishes and co-incubated with tumor cells for 2 hours at 37 ℃. The cell mixtures were then gently fixed to preserve cell-cell contact. After staining and extensive washing, images were captured by Leica SP8 confocal microscope and High Sensitivity Structured Illumination Microscope (HIS-SIM). ImageJ software was used for analysis.

Confocal imaging of PE-treated tumor cells

B16F10 cells were seeded on the poly-Lysine coated dishes overnight. On the following day, cells were treated with 30 μg/ml PE (18:0/20:4) and fixed at different timepoints. Cells were fixed and stained with Duramycin-Cy3 (2-5 μM) and anti-Calnexin (5 μg/mL) in permeabilization buffer overnight at 4℃ followed by staining with Alexa flour 488-labeled secondary antibody (2.5 μg/mL) for 2-4 hours at room temperature. Unbound antibodies were washed away by PBS before imaging.

TIRFM imaging of immunological synapse and PE-loaded vesicle in T cells

Small unilamellar vesicles (SUVs) were prepared for the formation of supported lipid bilayers (SLBs). 86% PC (16:0/18:1), 4% 18:1 Biotinyl-PE, and 10% DGS-NTA-Ni were dissolved in chloroform in a round bottom flask. Chloroform was then removed via rotary evaporator and the lipid film was resuspended with PBS. The lipid solution was sonicated for 90 minutes, ultracentrifuged at 37000 rpm, 25°C for 1 hour and then at 43000 rpm, 4°C for 8 hours to remove large multilamellar vesicles (LMVs) and large unilamellar vesicles (LUVs). The supernatant was collected, diluted to the total lipid concentration of 5 mM and stored at 4°C with nitrogen protection.

To prepare SLBs coated with anti-CD3/CD28, glass-bottomed 96-well plates were firstly treated with isopropanol overnight and washed with H_2O (MilliQ). Then plates were treated with 5M NaOH at 50°C for 4 hours and thoroughly washed with H_2O. 0.1mM SUVs diluted in PBS were incubated in the well for 25 minutes to form SLBs, followed by wash with 0.1% BSA/PBS (m: v) to remove residual SUVs and treatment with 1% BSA/PBS (m: v) for 20 minutes to block the bottom. Then SLBs were then incubated with 20 nM streptavidin to provide binding site for biotinylated antibodies, followed by additional PBS washes to remove excessive streptavidin. Next, streptavidin-containing SLBs were incubated with 5 μg/ml biotinylated anti-mCD3ε/ biotinylated anti-mCD28 and 10 nM recombinant murine ICAM1 protein with His Tag (Sinobiological) for 30 minutes, with extensive PBS washes to remove unbound antibodies and proteins. All procedures except NaOH treatment were under room temperature.

Activated $CD8^+$ T cells were seeded on the SLBs, centrifuged at 100 g for 1 minute, and incubated at 37℃ for 20 minutes in PBS for re-stimulation. The cells were fixed with intracellular fixation buffer and stained with Duramycin-Cy3, anti-mLAMP1-Alexa flour 488 and anti-mTCRβ-BV421 in permeabilization buffer overnight at 4℃. Following PBS washes, TIRFM images were captured by HIS-SIM and analyzed by ImageJ software.

Transmission Electron Microscopy (TEM)

B16F10 cells were treated with 30 μg/mL Methanol or PE (18:0/20:4) for 48 hours. The cell pellets were

fixed in 2.5% glutaraldehyde for 1 hour at room temperature and stored at 4 °C overnight. Samples were then treated with 1% osmium tetroxide for 1 hour at room temperature, followed by dehydration through a graded ethanol series (from 30%, 50%, 70%, 80%, 95% to 100% ethanol). The dehydrated samples were embedded in Epon812: acetone for 2 hours. Ultrathin sections were prepared using an LKB-V ultramicrotome, stained with uranyl acetate and lead citrate, and imaged with a transmission electron microscope. ER length was quantified by Image J.

Animal experiments

Esyt1-manipulated B16F10 melanoma mouse models

For the xenograft model, B16F10 cells (control, Esyt1-knockdown or Esyt1-overexpression) were injected subcutaneously into the right flank of female C57BL/6 mice (8–10 weeks old). Tumor growth in the Esyt1-knockdown model was measured every two days starting from day 5 post-injection, whereas tumor growth in the Esyt1-overexpression model was measured every four days starting from day 8 post-injection. Tumor dimensions were determined using a vernier caliper and tumor size was calculated as (length × width^2)/2. Mice were euthanized if the tumor exceeded 17 mm along its longest axis for ethical consideration.

For the lung-metastatic melanoma model, B16F10 cells (5×10^5 cells per mouse) were administered via intravenous injection into female C57 BL/6 mice (8–10 weeks old). On day 20 post-injection, mice were euthanized, and metastatic nodules on the lung surface were counted to assess metastatic capability.

For the toxin-null xenograft model, 3.5×10^6 *Ifngr1*^{KO}*Tnfr1*^{KO} B16F10-OVA cells (Esyt1-knockdown or non-targeting control) were subcutaneously injected into *Prf1*$^{-/-}$ OT-I transgenic mice. Tumor progression was monitored every 2 days using a vernier caliper and tumor size was calculated as (length × width^2)/2.

B16F10 melanoma model and OT-I T cell therapy

WT B16F10-OVA cells (4×10^5 cells per mouse) were injected subcutaneously into the right flank of female C57BL/6 mice (8–10 weeks old). On day 5, mice with comparable tumor size were randomly allocated into three groups, receiving either PBS, untreated OT-I T cells, Pcyt2i-pretreated OT-I T cells, or ETA-pretreated OT-I T cells (1×10^6 cells per mouse) by intravenous injection.

Esyt1-depleted B16F10-OVA cells (8×10^5 cells per mouse) or Chop-depleted B16F10-OVA cells (4×10^5 cells per mouse) were injected subcutaneously into the right flank of female B-NDG mice (8–10 weeks old). On day 7, mice with comparable tumor size were randomly allocated into three groups, receiving untreated OT-I T cells or ETA-pretreated OT-I T cells (4×10^6 cells per mouse) by intravenous injection.

Tumor size was recorded every two days after adoptive T cell transfer. Tumor size was calculated as (length × width^2)/2. Mice were euthanized when the tumor exceeded 13 mm along its longest axis for ethical consideration, and endpoints were recorded for survival analysis.

HCT116 colorectal cancer model and human MSLN.28Z CAR-T cell therapy

HCT116 cells (1.5×10^6 cells per mouse) were injected subcutaneously into the right flank of female B-NDG mice (8–10 weeks old). On day 7, mice with comparable tumor size were randomly allocated into two groups, receiving either MSLN.28Z CAR-T cells or ETA-MSLN.28Z CAR-T cells (1.5×10^6) by intravenous injection. Tumor size was recorded every two days after CAR-T cell transfer. Tumor size was calculated as (length × width^2)/2. Mice were euthanized when the tumor exceeded 13 mm along its longest axis for ethical consideration, and endpoints were recorded for survival analysis.

RNA experiments

RNA preparation and real-time quantitative PCR (qPCR)

Total RNA was isolated using the TRIzol Reagent (Invitrogen). Extracted RNA was treated with DNase and subjected to reverse transcription using RT reagent Kit with gDNA Eraser (Cat# RR047A, Takara). qPCR was performed using SYBR supermix (Novorptein, E096-01B). qPCR primers are listed in Supplementary Table 9.

Bulk RNA sequencing

Total RNA was isolated using the Trizol Reagent (Invitrogen), after which the concentration, quality and integrity were determined using a NanoDrop spectrophotometer (Thermo Fisher Scientific). The sequencing libraries were generated and sequenced on NovaSeq 6000 platform (Illumina) by Novogene. Sequencing strategy was PE150. Samples are sequenced on the platform to get image files, which are transformed by the software of the sequencing platform, and the original data in FASTQ format (Raw Data) is generated. FastQC (v0.11.9) is applied to check data quality and filtered Clean Data is used for further analysis. Reads were aligned to an assembly of Mus Musculus (GRCm39) using STAR software (V2.7.10a) (https://github.com/alexdobin/STAR).

Gene counts were normalized by library size and differential expression analysis was performed using DESeq2 (V1.36.0). Gene Set Enrichment Analysis (GSEA) is completed by GSEA 4.3.3 (https://www.gsea-msigdb.org/gsea/downloads.jsp). Genesets of ER stress and ER-stress-induced apoptosis was provided in Supplementary Table 10 as lists.

Single cell RNA sequencing

Droplet-based scRNA-seq

Mock- or ETA-pretreated OT-I T cells were processed using the Chromium Single Cell 5′ Kit (10x Genomics) according to the manufacturer's instructions. Single-cell suspensions with >90% viability were loaded onto a 10x Chromium chip to generate Gel Beads-in-Emulsion (GEMs), where individual cells were lysed and mixed with barcoded beads in oil droplets. RNA was extracted, reverse-transcribed, amplified, and subjected to quality control. 5′ gene expression libraries were constructed from qualified cDNA using the 10x Library Construction Kit and sequenced on an Illumina NovaSeq 6000 platform (150-bp paired-end reads; Novogene Bioinformatics Technology Co., Ltd.). Sequencing data were processed with Cell Ranger (v7.1.0) for read filtering, alignment to the mouse reference genome (GRCm38), cell barcode assignment, and generation of UMI count matrices.

scRNA-seq data processing and analysis

All samples were converted and merged into a single Seurat object using the *merge* function in Seurat (v5.1.0) in R (v4.4.1). Cells expressing fewer than 200 genes, fewer than 1,000 UMI counts, or >10% mitochondrial UMIs were removed, yielding 15,215 cells (7,001 control and 8,214 ETA-treated). Data normalization, scaling, and identification of highly variable genes were performed using *SCTransform*. Harmony (v1.2.3) was applied to correct batch effects across samples, followed by principal component analysis (PCA), Uniform Manifold Approximation and Projection (UMAP), and graph-based clustering at a resolution of 0.7. Because the cultured mouse T cells exhibited high transcriptional similarity, cell-cycle correction was applied to reduce artificial variance before clustering. Visualization was performed using *ggplot2* (v3.5.1).

Processing of proteomics data from CPTAC Database

Multiple research cohort datasets of proteomics data were downloaded from the Proteomic Data Commons

(PDC, https://pdc.cancer.gov/pdc/), and analyzed via PCAS algorithm in R. Proteomics datasets based on the TMT method were performed to ensure consistency in data standardization.

Hepatocellular carcinoma (HCC): PDC000198; Breast cancer (BRCA): PDC000120; Clear cell renal cell carcinoma (CCRCC): PDC000127; Colorectal cancer (COAD): PDC000116; Glioblastoma (GBM): PDC000204; Head and neck squamous cell carcinoma (HNSCC): PDC000221; laryngeal squamous cell carcinoma (LSCC): PDC000234; Lung adenocarcinoma (LUAD): PDC000153; Ovary cancer (OV): PDC000118; Pancreatic adenocarcinoma (PDAC): PDC000270; Uterine corpus endometrial carcinoma (UCEC): PDC000125.

Statistics

Statistical analyses were performed using GraphPad Prism 9.0.0 (GraphPad Software). Statistical significance was defined as p-value < 0.05, with exact p values provided in the figures. Three-dimension plots were performed via OriginPro 2021 (Origin Software).

For unpaired samples, the distribution of data was assessed using the D'Agostino & Pearson normality test. If the data followed a normal distribution, a two-tailed unpaired t-test was used when the variances were similar. If the variances were unequal, a two-tailed unpaired t-test with Welch's correction was applied. If the data did not follow a normal distribution, the Mann–Whitney test was used. For datasets containing more than two groups, statistical significance between pairs of groups was determined using multiple comparisons. All measurements were taken from distinct samples.

Data availability

The processed lipidomics and proteomics data were shown in Supplementary Tables. RNA sequencing data will be deposited before publication. All raw data will be provided upon request and submitted to the journal before publication.

Supplementary Information Guide

Supplementary Table 1: Lipidomics analysis of antibody-stimulated CD8 ACM vs NCM.

Supplementary Table 2: Lipidomics analysis of Tumor-cell-stimulated CD8 ACM vs Tumor CM vs BM.

Supplementary Table 3: Lipidomics analysis of Human CAR-T ACM vs CAR-T NCM.

Supplementary Table 4: Enrichment rank of PE and PC species in CD8 ACM.

Supplementary Table 5: Unique proteins identified in PE^+ EVs.

Supplementary Table 6: Common PE-binding proteins identified in mouse $CD8^+$ T cells.

Supplementary Table 7: Common PE-binding proteins specifically in mouse $CD8^+$ T cells (exclusion of the shared hits between $CD8^+$ T cells and B16F10 cells).

Supplementary Table 8: Common PE-binding proteins identified in mouse B16F10 melanoma cells.

Supplementary Table 9: Primers for qPCR experiments.

Supplementary Table 10: Gene sets of ER stress and ER stress-induced apoptosis.

Supplementary Movie 1: Live imaging of NBD-PE transfer experiments.

Declaration of interests

The authors declare no conflict of interests.

Declaration of Generative AI and AI-assisted technologies in the writing process

During the preparation of this work the authors used ChatGPT 3.5 to polish the language. After using this tool, the authors reviewed and edited the content as needed and take full responsibility for the content of the publication.

Uncategorized References

1 Wang, W. *et al.* CD8(+) T cells regulate tumour ferroptosis during cancer immunotherapy. *Nature* **569**, 270-274 (2019). https://doi.org/10.1038/s41586-019-1170-y

2 Upadhyay, R. *et al.* A Critical Role for Fas-Mediated Off-Target Tumor Killing in T-cell Immunotherapy. *Cancer Discov* **11**, 599-613 (2021). https://doi.org/10.1158/2159-8290.Cd-20-0756

3 Ritter, A. T. *et al.* ESCRT-mediated membrane repair protects tumor-derived cells against T cell attack. *Science* **376**, 377-382 (2022). https://doi.org/10.1126/science.abl3855

4 Larson, R. C. *et al.* CAR T cell killing requires the IFNγR pathway in solid but not liquid tumours. *Nature* **604**, 563-570 (2022). https://doi.org/10.1038/s41586-022-04585-5

5 Balint, S. *et al.* Supramolecular attack particles are autonomous killing entities released from cytotoxic T cells. *Science* **368**, 897-901 (2020). https://doi.org/10.1126/science.aay9207

6 Golstein, P. & Griffiths, G. M. An early history of T cell-mediated cytotoxicity. *Nature Reviews Immunology* **18**, 527-535 (2018). https://doi.org/10.1038/s41577-018-0009-3

7 Tuzlak, S. *et al.* Repositioning TH cell polarization from single cytokines to complex help. *Nature Immunology* **22**, 1210-1217 (2021). https://doi.org/10.1038/s41590-021-01009-w

8 Zhou, Z. *et al.* Granzyme A from cytotoxic lymphocytes cleaves GSDMB to trigger pyroptosis in target cells. *Science* **368** (2020). https://doi.org/10.1126/science.aaz7548

9 Zhang, Z. *et al.* Gasdermin E suppresses tumour growth by activating anti-tumour immunity. *Nature* **579**, 415-420 (2020). https://doi.org/10.1038/s41586-020-2071-9

10 Voskoboinik, I., Whisstock, J. C. & Trapani, J. A. Perforin and granzymes: function, dysfunction and human pathology. *Nat Rev Immunol* **15**, 388-400 (2015). https://doi.org/10.1038/nri3839

11 Carneiro, B. A. & El-Deiry, W. S. Targeting apoptosis in cancer therapy. *Nat Rev Clin Oncol* **17**, 395-417 (2020). https://doi.org/10.1038/s41571-020-0341-y

12 Strasser, A., Jost, P. J. & Nagata, S. The many roles of FAS receptor signaling in the immune system. *Immunity* **30**, 180-192 (2009). https://doi.org/10.1016/j.immuni.2009.01.001

13 Gocher, A. M., Workman, C. J. & Vignali, D. A. A. Interferon-gamma: teammate or opponent in the tumour microenvironment? *Nat Rev Immunol* **22**, 158-172 (2022). https://doi.org/10.1038/s41577-021-00566-3

14 van Loo, G. & Bertrand, M. J. M. Death by TNF: a road to inflammation. *Nat Rev Immunol* **23**, 289-303 (2023). https://doi.org/10.1038/s41577-022-00792-3

15 Elia, I. *et al.* Tumor cells dictate anti-tumor immune responses by altering pyruvate utilization and succinate signaling in CD8(+) T cells. *Cell Metab* **34**, 1137-1150.e1136 (2022). https://doi.org/10.1016/j.cmet.2022.06.008

16 Notarangelo, G. *et al.* Oncometabolite d-2HG alters T cell metabolism to impair CD8(+) T cell function. *Science* **377**, 1519-1529 (2022). https://doi.org/10.1126/science.abj5104

17 Yan, C. *et al.* Exhaustion-associated cholesterol deficiency dampens the cytotoxic arm of antitumor immunity. *Cancer Cell* **41**, 1276-1293 e1211 (2023). https://doi.org/10.1016/j.ccell.2023.04.016

18 Fong, L. *et al.* Adenosine 2A Receptor Blockade as an Immunotherapy for Treatment-Refractory Renal Cell Cancer. *Cancer Discov* **10**, 40-53 (2020). https://doi.org/10.1158/2159-8290.CD-19-0980

19 Xu, S. *et al.* Uptake of oxidized lipids by the scavenger receptor CD36 promotes lipid peroxidation and dysfunction in CD8(+) T cells in tumors. *Immunity* **54**, 1561-1577.e1567 (2021). https://doi.org/10.1016/j.immuni.2021.05.003

20 Brovkovych, V., Aldrich, A., Li, N., Atilla-Gokcumen, G. E. & Frasor, J. Removal of Serum Lipids and Lipid-Derived Metabolites to Investigate Breast Cancer Cell Biology. *Proteomics* **19**, e1800370 (2019).

https://doi.org/10.1002/pmic.201800370

21 Hokazono, E., Tamezane, H., Hotta, T., Kayamori, Y. & Osawa, S. Enzymatic assay of phosphatidylethanolamine in serum using amine oxidase from Arthrobacter sp. *Clin Chim Acta* **412**, 1436-1440 (2011). https://doi.org/10.1016/j.cca.2011.04.023

22 Nilsson, A. & Duan, R. D. Absorption and lipoprotein transport of sphingomyelin. *J Lipid Res* **47**, 154-171 (2006). https://doi.org/10.1194/jlr.M500357-JLR200

23 Iwamoto, K. *et al.* Curvature-dependent recognition of ethanolamine phospholipids by duramycin and cinnamycin. *Biophys J* **93**, 1608-1619 (2007). https://doi.org/10.1529/biophysj.106.101584

24 Zhao, M. Lantibiotics as probes for phosphatidylethanolamine. *Amino Acids* **41**, 1071-1079 (2011). https://doi.org/10.1007/s00726-009-0386-9

25 Fu, G. *et al.* Metabolic control of T(FH) cells and humoral immunity by phosphatidylethanolamine. *Nature* **595**, 724-729 (2021). https://doi.org/10.1038/s41586-021-03692-z

26 Talleur, A. C. *et al.* Preferential expansion of CD8+ CD19-CAR T cells postinfusion and the role of disease burden on outcome in pediatric B-ALL. *Blood Adv* **6**, 5737-5749 (2022). https://doi.org/10.1182/bloodadvances.2021006293

27 Bergers, G. & Fendt, S. M. The metabolism of cancer cells during metastasis. *Nat Rev Cancer* **21**, 162-180 (2021). https://doi.org/10.1038/s41568-020-00320-2

28 Su, M. W. *et al.* Fratricide of CD8+ cytotoxic T lymphocytes is dependent on cellular activation and perforin-mediated killing. *Eur J Immunol* **34**, 2459-2470 (2004). https://doi.org/10.1002/eji.200425096

29 Grossman, W. J. *et al.* Human T regulatory cells can use the perforin pathway to cause autologous target cell death. *Immunity* **21**, 589-601 (2004). https://doi.org/10.1016/j.immuni.2004.09.002

30 Filion, M. C. & Phillips, N. C. Toxicity and immunomodulatory activity of liposomal vectors formulated with cationic lipids toward immune effector cells. *Biochim Biophys Acta* **1329**, 345-356 (1997). https://doi.org/10.1016/s0005-2736(97)00126-0

31 Contreras-Naranjo, J. C., Wu, H. J. & Ugaz, V. M. Microfluidics for exosome isolation and analysis: enabling liquid biopsy for personalized medicine. *Lab Chip* **17**, 3558-3577 (2017). https://doi.org/10.1039/c7lc00592j

32 Krauss, R. M. Small dense low-density lipoprotein particles: clinically relevant? *Curr Opin Lipidol* **33**, 160-166 (2022). https://doi.org/10.1097/MOL.0000000000000824

33 Zech, T. *et al.* Accumulation of raft lipids in T-cell plasma membrane domains engaged in TCR signalling. *Embo j* **28**, 466-476 (2009). https://doi.org/10.1038/emboj.2009.6

34 Quann, E. J., Merino, E., Furuta, T. & Huse, M. Localized diacylglycerol drives the polarization of the microtubule-organizing center in T cells. *Nat Immunol* **10**, 627-635 (2009). https://doi.org/10.1038/ni.1734

35 Rouquette-Jazdanian, A. K., Pelassy, C., Breittmayer, J. P., Cousin, J. L. & Aussel, C. Metabolic labelling of membrane microdomains/rafts in Jurkat cells indicates the presence of glycerophospholipids implicated in signal transduction by the CD3 T-cell receptor. *Biochem J* **363**, 645-655 (2002). https://doi.org/10.1042/0264-6021:3630645

36 Molano, A. *et al.* Age-dependent changes in the sphingolipid composition of mouse CD4+ T cell membranes and immune synapses implicate glucosylceramides in age-related T cell dysfunction. *PLoS One* **7**, e47650 (2012). https://doi.org/10.1371/journal.pone.0047650

37 Stinchcombe, J. C. *et al.* Ectocytosis renders T cell receptor signaling self-limiting at the immune synapse. *Science* **380**, 818-823 (2023). https://doi.org/10.1126/science.abp8933

38 Chang, H. F. *et al.* Identification of distinct cytotoxic granules as the origin of supramolecular attack

particles in T lymphocytes. *Nat Commun* **13**, 1029 (2022). https://doi.org/10.1038/s41467-022-28596-y

39 Jainarayanan, A. K. *et al.* Comparison of different methods for isolating CD8(+) T lymphocyte-derived extracellular vesicles and supramolecular attack particles. *J Extracell Biol* **2**, e74 (2023). https://doi.org/10.1002/jex2.74

40 Choudhuri, K., Wiseman, D., Brown, M. H., Gould, K. & van der Merwe, P. A. T-cell receptor triggering is critically dependent on the dimensions of its peptide-MHC ligand. *Nature* **436**, 578-582 (2005). https://doi.org/10.1038/nature03843

41 Jahn, R., Cafiso, D. C. & Tamm, L. K. Mechanisms of SNARE proteins in membrane fusion. *Nat Rev Mol Cell Biol* **25**, 101-118 (2024). https://doi.org/10.1038/s41580-023-00668-x

42 Papareddy, P. *et al.* The role of extracellular vesicle fusion with target cells in triggering systemic inflammation. *Nat Commun* **15**, 1150 (2024). https://doi.org/10.1038/s41467-024-45125-1

43 Gerard, A., Cope, A. P., Kemper, C., Alon, R. & Kochl, R. LFA-1 in T cell priming, differentiation, and effector functions. *Trends Immunol* **42**, 706-722 (2021). https://doi.org/10.1016/j.it.2021.06.004

44 Guerra-Espinosa, C., Jimenez-Fernandez, M., Sanchez-Madrid, F. & Serrador, J. M. ICAMs in Immunity, Intercellular Adhesion and Communication. *Cells* **13** (2024). https://doi.org/10.3390/cells13040339

45 Zhang, W. *et al.* ICAM-1-mediated adhesion is a prerequisite for exosome-induced T cell suppression. *Dev Cell* **57**, 329-343.e327 (2022). https://doi.org/10.1016/j.devcel.2022.01.002

46 Wang, C. L. *et al.* Radiotherapy enhances CXCR3(high)CD8(+) T cell activation through inducing IFNγ-mediated CXCL10 and ICAM-1 expression in lung cancer cells. *Cancer Immunol Immunother* **72**, 1865-1880 (2023). https://doi.org/10.1007/s00262-023-03379-6

47 Chen, X. *et al.* Quantitative profiling of lipid transport between organelles enabled by subcellular photocatalytic labelling. *Nat Chem* (2025). https://doi.org/10.1038/s41557-025-01886-w

48 Casas, J. *et al.* Ligand-engaged TCR is triggered by Lck not associated with CD8 coreceptor. *Nat Commun* **5**, 5624 (2014). https://doi.org/10.1038/ncomms6624

49 Al-Habsi, M. *et al.* Spermidine activates mitochondrial trifunctional protein and improves antitumor immunity in mice. *Science* **378**, eabj3510 (2022). https://doi.org/10.1126/science.abj3510

50 Shibata, Y. *et al.* The membrane curvature-inducing REEP1-4 proteins generate an ER-derived vesicular compartment. *Nat Commun* **15**, 8655 (2024). https://doi.org/10.1038/s41467-024-52901-6

51 de Saint Basile, G., Ménasché, G. & Fischer, A. Molecular mechanisms of biogenesis and exocytosis of cytotoxic granules. *Nature Reviews Immunology* **10**, 568-579 (2010). https://doi.org/10.1038/nri2803

52 Duong, V. T., Lee, D., Kim, Y. H. & Oh, S. O. Functional role of UNC13D in immune diseases and its therapeutic applications. *Front Immunol* **15**, 1460882 (2024). https://doi.org/10.3389/fimmu.2024.1460882

53 Bruinsma, S. *et al.* Small molecules that inhibit the late stage of Munc13-4-dependent secretory granule exocytosis in mast cells. *J Biol Chem* **293**, 8217-8229 (2018). https://doi.org/10.1074/jbc.RA117.001547

54 Elstak, E. D. *et al.* The munc13-4-rab27 complex is specifically required for tethering secretory lysosomes at the plasma membrane. *Blood* **118**, 1570-1578 (2011). https://doi.org/10.1182/blood-2011-02-339523

55 Saheki, Y. *et al.* Control of plasma membrane lipid homeostasis by the extended synaptotagmins. *Nat Cell Biol* **18**, 504-515 (2016). https://doi.org/10.1038/ncb3339

56 Yu, H. *et al.* Extended synaptotagmins are Ca2+-dependent lipid transfer proteins at membrane contact sites. *Proc Natl Acad Sci U S A* **113**, 4362-4367 (2016). https://doi.org/10.1073/pnas.1517259113

57 Luan, L., Liang, D., Chiu, D. C., Tei, R. & Baskin, J. M. Imaging Interorganelle Phospholipid Transport by Extended Synaptotagmins Using Bioorthogonally Tagged Lipids. *ACS Chem Biol* **19**, 1683-1694

(2024). https://doi.org/10.1021/acschembio.4c00345

58 Zou, Y. *et al.* Plasticity of ether lipids promotes ferroptosis susceptibility and evasion. *Nature* **585**, 603-608 (2020). https://doi.org/10.1038/s41586-020-2732-8

59 Liao, P. *et al.* CD8(+) T cells and fatty acids orchestrate tumor ferroptosis and immunity via ACSL4. *Cancer Cell* **40**, 365-378 e366 (2022). https://doi.org/10.1016/j.ccell.2022.02.003

60 Kagan, V. E. *et al.* Oxidized arachidonic and adrenic PEs navigate cells to ferroptosis. *Nat Chem Biol* **13**, 81-90 (2017). https://doi.org/10.1038/nchembio.2238

61 Yang, W. S. *et al.* Regulation of ferroptotic cancer cell death by GPX4. *Cell* **156**, 317-331 (2014). https://doi.org/10.1016/j.cell.2013.12.010

62 Dixon, S. J. *et al.* Ferroptosis: an iron-dependent form of nonapoptotic cell death. *Cell* **149**, 1060-1072 (2012). https://doi.org/10.1016/j.cell.2012.03.042

63 Dixon, S. J. & Olzmann, J. A. The cell biology of ferroptosis. *Nat Rev Mol Cell Biol* **25**, 424-442 (2024). https://doi.org/10.1038/s41580-024-00703-5

64 Taylor, R. C., Cullen, S. P. & Martin, S. J. Apoptosis: controlled demolition at the cellular level. *Nat Rev Mol Cell Biol* **9**, 231-241 (2008). https://doi.org/10.1038/nrm2312

65 van Meer, G., Voelker, D. R. & Feigenson, G. W. Membrane lipids: where they are and how they behave. *Nat Rev Mol Cell Biol* **9**, 112-124 (2008). https://doi.org/10.1038/nrm2330

66 Basu Ball, W., Neff, J. K. & Gohil, V. M. The role of nonbilayer phospholipids in mitochondrial structure and function. *FEBS Lett* **592**, 1273-1290 (2018). https://doi.org/10.1002/1873-3468.12887

67 Osorio, F. *et al.* The unfolded-protein-response sensor IRE-1alpha regulates the function of CD8alpha+ dendritic cells. *Nat Immunol* **15**, 248-257 (2014). https://doi.org/10.1038/ni.2808

68 Borradaile, N. M. *et al.* Disruption of endoplasmic reticulum structure and integrity in lipotoxic cell death. *J Lipid Res* **47**, 2726-2737 (2006). https://doi.org/10.1194/jlr.M600299-JLR200

69 Hetz, C., Zhang, K. & Kaufman, R. J. Mechanisms, regulation and functions of the unfolded protein response. *Nat Rev Mol Cell Biol* **21**, 421-438 (2020). https://doi.org/10.1038/s41580-020-0250-z

70 Chen, X. & Cubillos-Ruiz, J. R. Endoplasmic reticulum stress signals in the tumour and its microenvironment. *Nat Rev Cancer* **21**, 71-88 (2021). https://doi.org/10.1038/s41568-020-00312-2

71 Lee, Y. Y. *et al.* Tauroursodeoxycholate (TUDCA), chemical chaperone, enhances function of islets by reducing ER stress. *Biochem Biophys Res Commun* **397**, 735-739 (2010). https://doi.org/10.1016/j.bbrc.2010.06.022

72 Fang, C. *et al.* IFN-gamma-induced ER stress impairs autophagy and triggers apoptosis in lung cancer cells. *Oncoimmunology* **10**, 1962591 (2021). https://doi.org/10.1080/2162402X.2021.1962591

73 Ivashkiv, L. B. IFNgamma: signalling, epigenetics and roles in immunity, metabolism, disease and cancer immunotherapy. *Nat Rev Immunol* **18**, 545-558 (2018). https://doi.org/10.1038/s41577-018-0029-z

74 Han, J. *et al.* ER-stress-induced transcriptional regulation increases protein synthesis leading to cell death. *Nat Cell Biol* **15**, 481-490 (2013). https://doi.org/10.1038/ncb2738

75 Cubillos-Ruiz, J. R., Bettigole, S. E. & Glimcher, L. H. Tumorigenic and Immunosuppressive Effects of Endoplasmic Reticulum Stress in Cancer. *Cell* **168**, 692-706 (2017). https://doi.org/10.1016/j.cell.2016.12.004

76 Volmer, R. & Ron, D. Lipid-dependent regulation of the unfolded protein response. *Curr Opin Cell Biol* **33**, 67-73 (2015). https://doi.org/10.1016/j.ceb.2014.12.002

77 Volmer, R., van der Ploeg, K. & Ron, D. Membrane lipid saturation activates endoplasmic reticulum unfolded protein response transducers through their transmembrane domains. *Proc Natl Acad Sci U S A* **110**, 4628-4633 (2013). https://doi.org/10.1073/pnas.1217611110

78 Sassano, M. L. *et al.* PERK recruits E-Syt1 at ER-mitochondria contacts for mitochondrial lipid transport and respiration. *J Cell Biol* **222** (2023). https://doi.org/10.1083/jcb.202206008

79 Nghiem, T.-H. T. *et al.* The PERK-eIF2α-ATF4 Axis Is Involved in Mediating ER-Stress-Induced Ferroptosis via DDIT4-mTORC1 Inhibition and Acetaminophen-Induced Hepatotoxicity. *Antioxidants* **14**, 307 (2025).

80 Ding, H. *et al.* Endoplasmic reticulum stress-mediated ferroptosis in granulosa cells contributes to follicular dysfunction of polycystic ovary syndrome driven by hyperandrogenism. *Reprod Biomed Online* **49**, 104078 (2024). https://doi.org/10.1016/j.rbmo.2024.104078

81 Guo, Z. *et al.* The Role and Interactive Mechanism of Endoplasmic Reticulum Stress and Ferroptosis in Musculoskeletal Disorders. *Biomolecules* **14** (2024). https://doi.org/10.3390/biom14111369

82 Gohil, V. M. *et al.* Meclizine inhibits mitochondrial respiration through direct targeting of cytosolic phosphoethanolamine metabolism. *J Biol Chem* **288**, 35387-35395 (2013). https://doi.org/10.1074/jbc.M113.489237

83 Ping, Y. *et al.* PD-1 signaling limits expression of phospholipid phosphatase 1 and promotes intratumoral CD8(+) T cell ferroptosis. *Immunity* **57**, 2122-2139 e2129 (2024). https://doi.org/10.1016/j.immuni.2024.08.003

84 Harayama, T. & Riezman, H. Understanding the diversity of membrane lipid composition. *Nat Rev Mol Cell Biol* **19**, 281-296 (2018). https://doi.org/10.1038/nrm.2017.138

85 Lee, T. H. *et al.* The intricate link between membrane lipid structure and composition and membrane structural properties in bacterial membranes. *Chem Sci* **15**, 3408-3427 (2024). https://doi.org/10.1039/d3sc04523d

86 Osawa, T. *et al.* Phosphoethanolamine Accumulation Protects Cancer Cells under Glutamine Starvation through Downregulation of PCYT2. *Cell Rep* **29**, 89-103.e107 (2019). https://doi.org/10.1016/j.celrep.2019.08.087

87 Doll, S. *et al.* ACSL4 dictates ferroptosis sensitivity by shaping cellular lipid composition. *Nat Chem Biol* **13**, 91-98 (2017). https://doi.org/10.1038/nchembio.2239

88 Jiang, X., Stockwell, B. R. & Conrad, M. Ferroptosis: mechanisms, biology and role in disease. *Nat Rev Mol Cell Biol* **22**, 266-282 (2021). https://doi.org/10.1038/s41580-020-00324-8

89 Choudhuri, K. *et al.* Polarized release of T-cell-receptor-enriched microvesicles at the immunological synapse. *Nature* **507**, 118-123 (2014). https://doi.org/10.1038/nature12951

90 Saliba, D. G. *et al.* Composition and structure of synaptic ectosomes exporting antigen receptor linked to functional CD40 ligand from helper T cells. *Elife* **8** (2019). https://doi.org/10.7554/eLife.47528

91 Céspedes, P. F. *et al.* T-cell trans-synaptic vesicles are distinct and carry greater effector content than constitutive extracellular vesicles. *Nat Commun* **13**, 3460 (2022). https://doi.org/10.1038/s41467-022-31160-3

92 Kvalvaag, A. *et al.* Clathrin mediates both internalization and vesicular release of triggered T cell receptor at the immunological synapse. *Proc Natl Acad Sci U S A* **120**, e2211368120 (2023). https://doi.org/10.1073/pnas.2211368120

93 Bentley, M. *et al.* SNARE status regulates tether recruitment and function in homotypic COPII vesicle fusion. *J Biol Chem* **281**, 38825-38833 (2006). https://doi.org/10.1074/jbc.M606044200

94 Nichols, B. J., Ungermann, C., Pelham, H. R., Wickner, W. T. & Haas, A. Homotypic vacuolar fusion mediated by t- and v-SNAREs. *Nature* **387**, 199-202 (1997). https://doi.org/10.1038/387199a0

95 Connor, J., Yatvin, M. B. & Huang, L. pH-sensitive liposomes: acid-induced liposome fusion. *Proc Natl Acad Sci U S A* **81**, 1715-1718 (1984). https://doi.org/10.1073/pnas.81.6.1715

96 Joardar, A., Pattnaik, G. P. & Chakraborty, H. Effect of Phosphatidylethanolamine and Oleic Acid on Membrane Fusion: Phosphatidylethanolamine Circumvents the Classical Stalk Model. *J Phys Chem B* **125**, 13192-13202 (2021). https://doi.org/10.1021/acs.jpcb.1c08044

97 Mishra, S. & Chakraborty, H. Phosphatidylethanolamine and Cholesterol Promote Hemifusion Formation: A Tug of War between Membrane Interfacial Order and Intrinsic Negative Curvature of Lipids. *J Phys Chem B* **127**, 7721-7729 (2023). https://doi.org/10.1021/acs.jpcb.3c04489

98 Kreutzberger, A. J. B. *et al.* Asymmetric Phosphatidylethanolamine Distribution Controls Fusion Pore Lifetime and Probability. *Biophys J* **113**, 1912-1915 (2017). https://doi.org/10.1016/j.bpj.2017.09.014

99 Weigelin, B. & Friedl, P. T cell-mediated additive cytotoxicity - death by multiple bullets. *Trends Cancer* **8**, 980-987 (2022). https://doi.org/10.1016/j.trecan.2022.07.007

100 Li, G. *et al.* Intersection of immune and oncometabolic pathways drives cancer hyperprogression during immunotherapy. *Cancer Cell* **41**, 304-322 e307 (2023). https://doi.org/10.1016/j.ccell.2022.12.008

101 Bullani, R. R. *et al.* Frequent downregulation of Fas (CD95) expression and function in melanoma. *Melanoma Res* **12**, 263-270 (2002). https://doi.org/10.1097/00008390-200206000-00010

102 Young, T. M. *et al.* Autophagy protects tumors from T cell-mediated cytotoxicity via inhibition of TNFalpha-induced apoptosis. *Sci Immunol* **5** (2020). https://doi.org/10.1126/sciimmunol.abb9561

103 Chaudhry, M. Z. *et al.* Cytomegalovirus inhibition of extrinsic apoptosis determines fitness and resistance to cytotoxic CD8 T cells. *Proc Natl Acad Sci U S A* **117**, 12961-12968 (2020). https://doi.org/10.1073/pnas.1914667117

104 Tu, J., Yin, Y., Xu, M., Wang, R. & Zhu, Z. J. Absolute quantitative lipidomics reveals lipidome-wide alterations in aging brain. *Metabolomics* **14**, 5 (2017). https://doi.org/10.1007/s11306-017-1304-x

105 Chen, X. *et al.* Trapped ion mobility spectrometry-mass spectrometry improves the coverage and accuracy of four-dimensional untargeted lipidomics. *Anal Chim Acta* **1210**, 339886 (2022). https://doi.org/10.1016/j.aca.2022.339886

106 Chen, X., Yin, Y., Zhou, Z., Li, T. & Zhu, Z. J. Development of a combined strategy for accurate lipid structural identification and quantification in ion-mobility mass spectrometry based untargeted lipidomics. *Anal Chim Acta* **1136**, 115-124 (2020). https://doi.org/10.1016/j.aca.2020.08.048

Supplementary Files

This is a list of supplementary files associated with this preprint. Click to download.

- SupplementaryTable1antibodystimulatedCD8ACMlipidomics.xlsx
- SupplementaryTable2TumorcellstimulatedACMlipidomics.xlsx
- SupplementaryTable5UniqueproteinsidentifiedinPEEVs.xlsx
- SupplementaryTable8PEbindingproteininB16F10cell.xlsx
- SupplementaryTable10genelistinERstressrelatedgenesets.xlsx
- SupplementaryTable3CARTACMlipidomics.xlsx
- SupplementaryTable9primerlist.xlsx
- SupplementaryTable6PEbindingproteinsinCD8Tcell.xlsx
- SupplementaryMovie1LiveimagingofNBDPEtransferexperiments.mp4
- SupplementaryTable4EnrichmentrankofPEandPCspeciesinCD8ACM.xlsx
- SupplementaryTable7PEbindingproteinsspeciallyinCD8Tcell.xlsx
- SupplementaryTable10genelistinERstressrelatedgenesets.xlsx
- SupplementaryTable9primerlist.xlsx